UNIVERSITÀ DEGLI STUDI DI PADOVA

Dipartimento di Fisica e Astronomia "Galileo Galilei"

Master Degree in Astrophysics and Cosmology

FINAL DISSERTATION

Testing Gravity with Cross-Correlation of Cosmic Microwave Background and Large-Scale-Structures of the Universe

Thesis Supervisor

Prof. Nicola Bartolo

Thesis co-supervisor

Dr. Giampaolo Benevento

Candidate

Guglielmo Frittoli

Academic Year 2021/2022

Abstract

The aim of this Thesis is to test gravity models through the cross-correlation of the Cosmic Microwave Background (CMB) temperature anisotropies with tracers of the Large-Scale-Structure (LSS). This cross-correlation is sensitive to the Integrated Sachs-Wolfe (ISW) effect, which is a secondary contribution to the temperature anisotropies in the CMB and a powerful probe for gravity. The ISW effect is a way to test gravity since it arises when a photon of the CMB travels through gravitational potentials that evolve in time due to the accelerated expansion of the Universe. Thus, exploring the *late* ISW effect is a powerful method to test Dark Energy and gravity models. However, the ISW effect is faint compared to the other Cosmic Microwave Background temperature anisotropies and to cosmic variance at large angular scales. Cross-correlation of the CMB temperature with tracers of the Large-Scale-Structures ensures the detection of the ISW effect, making it a viable tool. As a tracer of LSS, we considered the galaxy number count with an Euclid-like number distribution. When considering the various Dark Energy/Modified Gravity models we adopted an Effective Field Theory (EFT) formalism. The EFT approach allows for more straightforward analytical and numerical results since it encompasses any model but it still can be mapped to specific cases. We computed the cross-correlations for some state-of-the-art models using CAMB and EFTCAMB codes. For each model, we computed the Signal-to-Noise ratio according to an Euclid-like prescription and explored the parameter space that affects cross-correlation amplitudes. The state-of-the-art models investigated are the K-mouflage, the Generalized Cubic Covariant Galileon (GCCG), the Galileon Ghost Condensate (GGC), and the Transitional Planck Mass (TPM) model, and all are reviewed in the work. All the cross-correlations found are compatible with the costraints set by theory and observations. The TPM cross-correlation proved to be the most interesting case, being quite different with respect to the ΛCDM one. In this regard, we further investigated this model finding and studying the key parameters affecting the cross-correlation amplitude.

Contents

Introduction

Among other sciences, Cosmology finds itself to study a peculiar object, the Universe. This is quite a task since the Universe is vast and complicated. However, when scientists want to describe general behaviors, statistical tools are an important contribution to simplifying things since statistical information on random fields in the universe provides vital knowledge on a broad range of issues. For instance, regarding the Large-Scale-Structure (LSS), statistical properties of the fields can help to put constraints on the primordial Universe (e.g. inflation models, Guth 1981) and also contain information about the evolution of the Universe. The structures we see in the Universe today originate from initial density fluctuations, which are believed to be generated by cosmic inflation in the very early universe. Different theories predict different statistical properties of the initial density field, so constraints become crucial. However, extracting statistical information from the observed fields is quite challenging (Verde 2009). The first challenge is to understand which kind of statistics is useful and which statistical description is better to adopt. One of the fundamental properties used within the standard cosmological model is that the Universe is statistically isotropic and homogeneous when smoothed over suitably large scales. So, it is possible to do statistics over different spatial regions of the Universe and we can expect the same results regardless of position and direction - barring cosmic variance. This fruitful result helped Cosmologists model a theory that could describe the observable Universe. While still do not have a complete perfect model, the most reliable we have so far is the so-called Λ Cold Dark Matter cosmological model (the ΛCDM model). Its name highlights the two most abundant components in our Universe at the present epoch, which are two among the most important questions in cosmology. The first is the so-called Dark Matter, the latter the Dark Energy, represented by the cosmological constant Λ. Regarding the latter, Dark Energy is considered the source of our late accelerated expansion of the Universe and it is still a mystery (Abdalla et al. 2022). Its nature is yet to be explained in detail while some of its features are known: accelerated expansion and cosmic structure growth. In the Standard Model of Cosmology, it is treated as a constant, the Λ constant, but such a description could not be satisfactory. This thesis moves from the boundaries and the limits of the ΛCDM to explore alternative theories that could alleviate some of the cosmic tensions that have appeared in recent years, and describe Dark Energy in a more detailed way. The methodology adopted to probe gravity is to exploit a temperature anisotropy effect (the so-called

Integrated Sachs-Wolfe effect) in the Cosmic Microwave Background which is sensitive to gravitational potentials and their evolution. Testing it directly in the CMB is nearly impossible and once again statistics come to our aid. The tools used to probe these models and their depiction of gravity are once again of statistical nature: cross-correlations (Crittenden and Turok 1996). Cross-correlating CMB temperature anisotropies to tracers of the LSS (hence the sources of gravitaional potentials) effectively showcases the Integrated Sachs–Wolfe effect. This is the main aim of the thesis: to obtain these cross-correlations for some of the state-of-the-art cosmological models. The methodology, however, is not bound to the model and it is a feat of strength of the investigation in this work. In fact, the various cosmological models (alternative to ΛCDM) considered in this Thesis are described within the so called Effective Field Theory approach. In this way, rather than using one single model each time, the most general EFT action (or Lagrangian) is employed (Gubitosi et al. 2013), reducing the computational cost and generalizing some of the results. Recovering the specific result for each case is still possible since from the EFT action each specific theory can be mapped. The EFT approach can be a very useful addition to the toolkit of a Cosmologist and it goes well hand in hand with the computation of correlations of cosmological perturbations. Investigating the Universe in this fashion is a powerhouse for the near future: forthcoming surveys and space missions (one above all, Euclid) will provide some new information and possibly help paint a better picture of these unanswered questions. In this sense, a Euclid-like distribution (Euclid Collaboration et al. 2020) of the tracers of the gravitational potential is implemented. This work is organized in a linear and sequential order: in the first Chapter, we will review the current most supported model, the ΛCDM. We will explore its fundamentals and its strenghts, but also its few limits with the well-known tensions (Abdalla et al. 2022) and the Λ problem (S. Weinberg 1989). In Chapter 2, adopting the ΛCDM we will recover the key effect that we want to investigate: the Integrated Sachs-Wolfe effect (Sachs and Wolfe 1967). Thus, we will describe the CMB and how anisotropies and inhomogeneities characterize our Universe and how they are described (see e.g. *Modern Cosmology* 2021). In Chapter 3 we will introduce the basics of Dark Energy and Modifief Gravity models (w.r.t to General Relativity) as alternative to the standard ΛCDM model (see e.g. Clifton et al. 2012). In addition, we will review the formalism of the EFT approach and its results (see e.g. Frusciante, Peirone, et al. 2020). Finally, we will briefly summarize the models used for our computations (Kable et al. 2021, Benevento, Kable, et al. 2022). In Chapter 4 we will introduce the cross-correlation formalism and relate it to Dark Energy/Modified Gravity theories (Nakamura et al. 2019). There we will present the results obtained. In the last chapter, Chapter 5, we will summarize the main features of the work and make considerations on what can be built upon the results and the method of investigation we used.

CHAPTER 1

The Standard ΛCDM Cosmological Model

The most comprehensive and well-supported model of our Universe is the so-called Λ-Cold-Dark-Matter (ΛCDM) cosmological model (see *Modern Cosmology* (2021) for a general review on its building blocks). Supported by years of observations, it is considered the standard cosmological model to which cosmologists refer when making computations. The model itself is built on the validity of the *Cosmological Principle* and the Friedmann-Robertson-Walker metric (Ellis and van Elst 2008). Upon this, the description of the components of our Universe is based on General Relativity and Einstein Equations (Einstein 1917). In this picture, the most abundant component of the Universe at the present epoch is the so-called Dark Energy (DE), a contribution that is expressed by the *cosmological constant* Λ. Following, the most abundant component is Dark Matter, which is a (pressureless) matter that does not interact with the electromagnetic field, making it sensible only to gravitational interaction. While the ΛCDM model proved to be valid and still results in the one that best fits a variety of cosmological data, the premise of the model itself leaves the door open for alternatives that could better describe the Universe. Obtaining the equations of the ΛCDM and its key quantities prove to be the best example of how to approach a cosmological model. In this light, we will review the ΛCDM and its discontents in this chapter.

1.1 The Homogenous and Isotropic Friedmann Universe

It is useful here to summarize some basic concepts about the homogeneous and isotropic Friedmann Universe. These concepts are the basis for our understanding and description of the Universe in its present structure and evolution. While highly structured on scales smaller than a few to several tens of Mpc, all observations show excellent evidence for isotropy and homogeneity of the Universe on larger scales, and particularly almost perfect homogeneity on scales larger than a few hundred Mpc. The above is the first fundamental evidence about the global properties of the Universe, and makes the content of the *Cosmological Principle*: "Viewed on a suffi-

ciently large scale, the properties of the universe are the same for all observers". The two testable structural consequences of the cosmological principle are homogeneity and isotropy. Homogeneity means that the same observational evidence is available to observers at different locations in the universe. Isotropy means that the same observational evidence is available by looking in any direction in the universe. The principles are distinct but closely related because a universe that appears isotropic from any two (for spherical geometry, three) locations must also be homogeneous. In fact, it looks to share the same properties as any fundamental observer at a given cosmic time. This is key to any attempt to describe the general properties of the Universe based on what we observe in our past light cone. This behavior can be effectively formalized into a metric, called the *Friedmann-Lemaître- Robertson-Walker* (FLRW) metric. This is the general cosmological metric and our description of the Universe at large scales:

$$\mathrm{d}s^2 = -\mathrm{d}t^2 + a^2(t)\left[\frac{\mathrm{d}r^2}{1-kr^2} + r^2\left(\mathrm{d}\theta^2 + \sin^2\theta \mathrm{d}\phi^2\right)\right] \tag{1.1}$$

with the adopted signature $(-,+,+,+)$. $a(t)$ is the scale factor detailing the uniform expansion of the Universe. This metric involves only the symmetry properties of space and nothing else, in particular, it does not require any precise law of gravitation (like General Relativity). The parameter k is the curvature constant, it does not vary with time and it can be set to either $0, -1, +1$ (corresponding to flat Euclidean, open hyperbolic, and closed spherical models). Inflation results (Guth 1981) will allow us to set $k = 0$. The radial r and angular coordinates θ and ϕ are expressed in the so-called *comoving units*, that is they make a time-invariant coordinate grid to identify cosmic objects at a given time, typically the present time t_0. Proper (or physical) coordinates (those that would be measured in a reference frame at time t) are simply scaled from the comoving ones as

$$d(t) = a(t)\int_0^r \frac{d\tilde{r}}{\sqrt{1-k\tilde{r}^2}}. \tag{1.2}$$

This distance cannot be physically measured, and in cosmology we define and measure luminosity and angular distances. A first application of the FLRW metric is the fundamental generalization of the Hubble law $cz \sim v = H_0 r$ which linked the recession velocities of galaxies to their distances (Hubble 1937). The proportionality constant is the so-called Hubble constant $H_0 = \dot{a}(t_0)/a(t_0)$. This generalization is the computation of the redshifting of light rays due to the expansion of the universe. In terms of the frequency of a light ray emitted at time t_e and observed at t_0, we have

$$\frac{a(t_e)}{a(t_0)} = \frac{\nu_0}{\nu_e} \tag{1.3}$$

and because of the definition of redshift, we have $(1+z)^{-1} = a(t_e)$, a relation generalizing the concept of redshift (cosmological redshift) to sources at any distance in space-time. The conclusion is that the cosmological redshift z is a measure of how much the scale factor has changed from the epoch when the signal has been sent to that it has been received. This introduces a substantial modification of the standard Doppler redshift. For large distances, the redshift is a very fundamental measure of

distance and expresses the ratio of the scale factor at the time the photon is emitted to that when it is received.

1.2 General Relativity and Friedmann Equations

1.2.1 General Relativity

In 1915 A. Einstein presented to the scientific community field equations that related spacetime curvature to the stress-energy tensor. The result was obtained thanks to the results obtained in differential geometry given by Bianchi and the known applications and solutions regarding curvature, obtained by Gauss and Riemann. Einstein's approach was to link the geometry of the spacetime to the matter distribution, imposing the weak-field limit to be consistent with Newtonian Gravity. Later on, as a description of Dark Energy, the Λ constant was introduced to compensate for the presence of such unknown energy (Einstein 1917). The nature of Λ will be discussed later. This is the historical approach, later formalized through the introduction of the Einstein-Hilbert action with the Λ constant (Hilbert 2007):

$$S = \int d^4x\sqrt{-g}\left(\frac{M_{pl}^2}{2}R - 2\Lambda\right) \tag{1.4}$$

which yields the Einstein field equations through the stationary-action principle. Deriving equations of motion from an action has several advantages. First, it allows for easy unification of General Relativity with other classical field theories (such as Maxwell's theory), which are also formulated in terms of an action. In the process, the derivation identifies a natural candidate for the source term coupling the metric to matter fields. Moreover, symmetries of the action allow for easy identification of conserved quantities through Noether's theorem. In General Relativity, the action is usually assumed to be a functional of the metric (and matter fields), and the connection is given by the Levi-Civita connection. The Palatini formulation of General Relativity (Palatini 1919) assumes the metric and connection to be independent and varies with respect to both independently, which makes it possible to include fermionic matter fields with non-integer spin. The Einstein equations in the presence of matter are given by adding the matter action ($S_m(\psi_m, g_{\mu\nu})$) to the Einstein-Hilbert action. To obtain Einstein's equations we have to vary with respect to the metric. Let's consider the previous action with $S_m(\psi_m, g_{\mu\nu})$ more compactly:

$$S = \int \left[\frac{1}{2\kappa}(R - 2\Lambda) + \mathcal{L}_{\mathrm{M}}\right]\sqrt{-g}\ \mathrm{d}^4x \tag{1.5}$$

where $\mathcal{L}_{\mathrm{M}}$ is the Lagrangian density associated with the S_m. Taking variations with respect to the inverse metric:

$$\begin{aligned}\delta S &= \int \left[\frac{\sqrt{-g}}{2\kappa}\frac{\delta R}{\delta g^{\mu\nu}} + \frac{R}{2\kappa}\frac{\delta\sqrt{-g}}{\delta g^{\mu\nu}} - \frac{\Lambda}{\kappa}\frac{\delta\sqrt{-g}}{\delta g^{\mu\nu}} + \sqrt{-g}\frac{\delta\mathcal{L}_{\mathrm{M}}}{\delta g^{\mu\nu}} + \mathcal{L}_{\mathrm{M}}\frac{\delta\sqrt{-g}}{\delta g^{\mu\nu}}\right]\delta g^{\mu\nu}\mathrm{d}^4x \\ &= \int \left[\frac{1}{2\kappa}\frac{\delta R}{\delta g^{\mu\nu}} + \frac{R}{2\kappa}\frac{1}{\sqrt{-g}}\frac{\delta\sqrt{-g}}{\delta g^{\mu\nu}} - \frac{\Lambda}{\kappa}\frac{1}{\sqrt{-g}}\frac{\delta\sqrt{-g}}{\delta g^{\mu\nu}} + \frac{\delta\mathcal{L}_{\mathrm{M}}}{\delta g^{\mu\nu}} + \frac{\mathcal{L}_{\mathrm{M}}}{\sqrt{-g}}\frac{\delta\sqrt{-g}}{\delta g^{\mu\nu}}\right]\delta g^{\mu\nu}\sqrt{-g}\ \mathrm{d}^4x.\end{aligned} \tag{1.6}$$

The variation of action is zero:

$$0 = \delta S = \frac{1}{2\kappa}\frac{\delta R}{\delta g^{\mu\nu}} + \frac{R}{2\kappa}\frac{1}{\sqrt{-g}}\frac{\delta\sqrt{-g}}{\delta g^{\mu\nu}} - \frac{\Lambda}{\kappa}\frac{1}{\sqrt{-g}}\frac{\delta\sqrt{-g}}{\delta g^{\mu\nu}} + \frac{\delta\mathcal{L}_{\mathrm{M}}}{\delta g^{\mu\nu}} + \frac{\mathcal{L}_{\mathrm{M}}}{\sqrt{-g}}\frac{\delta\sqrt{-g}}{\delta g^{\mu\nu}} \quad (1.7)$$

and we insert some known results:

$$\begin{aligned} \frac{\delta R}{\delta g^{\mu\nu}} &= R_{\mu\nu} \\ \frac{1}{\sqrt{-g}}\frac{\delta\sqrt{-g}}{\delta g^{\mu\nu}} &= \frac{-g_{\mu\nu}}{2} \\ T_{\mu\nu} &= \mathcal{L}_{\mathrm{M}} g_{\mu\nu} - 2\frac{\delta\mathcal{L}_{\mathrm{M}}}{\delta g^{\mu\nu}}. \end{aligned} \quad (1.8)$$

Finally, we obtain:

$$\begin{aligned} \frac{1}{2\kappa}R_{\mu\nu} + \frac{R}{2\kappa}\frac{-g_{\mu\nu}}{2} - \frac{\Lambda}{\kappa}\frac{-g_{\mu\nu}}{2} + \left(\frac{\delta\mathcal{L}_{\mathrm{M}}}{\delta g^{\mu\nu}} + \mathcal{L}_{\mathrm{M}}\frac{-g_{\mu\nu}}{2}\right) &= 0 \\ R_{\mu\nu} - \frac{R}{2}g_{\mu\nu} + \Lambda g_{\mu\nu} + \kappa\left(2\frac{\delta\mathcal{L}_{\mathrm{M}}}{\delta g^{\mu\nu}} - \mathcal{L}_{\mathrm{M}} g_{\mu\nu}\right) &= 0 \\ R_{\mu\nu} - \frac{R}{2}g_{\mu\nu} + \Lambda g_{\mu\nu} - \kappa T_{\mu\nu} &= 0, \end{aligned} \quad (1.9)$$

with the final result:

$$G_{\mu\nu} = R_{\mu\nu} - \frac{1}{2}g_{\mu\nu}R + \Lambda g_{\mu\nu} = \frac{1}{M_{pl}^2}T_{\mu\nu}. \quad (1.10)$$

Varying the action is the standard procedure to obtain the equations of motion from a given action. This is an important example since the methodology used is general and not specific to the case of General Relativity. Thus, the same procedure has to be applied to any Modified Gravity action to obtain the respective equations of motion.

1.2.2 Friedmann equations

Given the Einstein Equations, the set of equations that drive the Universe on large scales can be obtained by inserting the FRLW metric into the gravitational equations (Friedman 1999). Let us consider $k = 0$. In computing the stress-energy tensor, the assumption made is that the cosmological expansion is driven by a perfect fluid:

$$T^{\mu\nu} = (\rho + p)u^\mu u^\nu + p g^{\mu\nu} \quad (1.11)$$

where ρ is the density; p is pressure, u^μ is the 4-velocity. Computing the Einstein tensor components and the energy tensor yields:

$$\begin{aligned} \frac{\dot{a}^2}{a^2} &= \frac{\rho}{3M_{pl}^2} + \frac{\Lambda}{3} \\ \frac{2\ddot{a}}{a} + \frac{\dot{a}^2}{a^2} &= \frac{-p}{M_{pl}^2}. \end{aligned} \quad (1.12)$$

If we consider Bianchi Identities ($\nabla_\mu G^{\mu\nu} = 0$), which assure local conservation of energy-momentum, we obtain a third equation that is, however, not independent:

$$\dot{\rho} + \frac{3\dot{a}}{a}(\rho + p) = 0. \tag{1.13}$$

To obtain solutions for the scale factor and ρ we have to add a relation between ρ and p. If we consider an equation of state $w = \frac{p}{\rho}$, it is different according to different fluids. The three cases known are:

- Vacuum energy $w = -1$: in this case $\dot{\rho} = const.$ thus it does not dilute as the space expands. It is associated with the space itself. this is the case of the cosmological constant which behaves as a source with $\omega = -1$. Solving in this case gives:
$$\rho = const. \quad , \quad a = a_{\text{in}} e^{\frac{\rho^{1/2}}{\sqrt{3}M_{pl}}(t-t_{in})} \tag{1.14}$$
- Radiation $w = \frac{1}{3}$: it is given by the radiation pressure. The result can be obtained by observing a photon in a metallic box and the pressure of such photons on the wall of the box. Solving for radiation gives:
$$\rho = \rho_{in}\left(\frac{a_{in}}{a}\right)^4 \quad , \quad a = a_{in}\left(\frac{t}{t_{in}}\right)^{\frac{1}{2}} \tag{1.15}$$
- Matter $w = 0$. It is obtained with the same reasoning as the radiation, but with massive particles. In the case of the matter:
$$\rho = \rho_{in}\left(\frac{a_{in}}{a}\right)^3 \quad , \quad a = a_{in}\left(\frac{t}{t_{in}}\right)^{\frac{2}{3}} \tag{1.16}$$

1.2.3 Cosmic Inventory

We can now express quantitatively the amount and which components are in the Universe. A constituent can be made up of several particle species but each has to have the same equation of state. It is useful to define the *density parameters*

$$\Omega_s = \frac{\rho_s(t_0)}{\rho_{crit}} \tag{1.17}$$

where s is a generic constituent. It could be Cold Dark Matter (c), Baryons (b), photons (r), and a cosmological constant Λ or dark energy.

- **Photons**: The majority of radiation contribution to the cosmic energy budget is in the form of the Cosmic Microwave Background (CMB). They are characterized by a Bose-Einstein distribution. Photons make up a very small fraction of the universe's energy budget today. Using the zeroth-order Bose-Einstein distribution function for the photons we find that ρ_γ depends only on time. In fact, there are small perturbations around this zeroth-order distribution function. These do have a spatial and momentum dependence and correspond to the anisotropies in the Cosmic Microwave Background (CMB), which we will see next Chapter.

- **Baryons**: we refer to all ordinary matter, i.e. nuclei and electrons, as baryons, even though this is technically incorrect as electrons are leptons. However, nuclei are so much more massive than electrons that virtually all of the mass is in the baryons. Unlike the CMB, baryons cannot be simply described with an equilibrium distribution function. This is because baryons come in many different phases: diffuse neutral gas and ionized plasma, stars and planets, compact objects, and so on. This makes a baryonic inventory much more difficult.

- **Dark Matter**: The anisotropies in the CMB provide a measurement of the physical matter density parameter. The sensitivity of the CMB to the matter density is both due to the effect of matter on the expansion history in the early universe, as well as the fact that dark matter dominates the gravitational potential wells which also leave their imprint in the CMB anisotropies. The large-scale structure provides two beautiful ways to probe gravitational potential wells and hence the amount of matter: galaxy velocities and gravitational lensing (Fermi-LAT Collaboration et al. 2014). Velocities are probed through the characteristic distortion they imprint on the three-dimensional statistics of galaxy number counts. Gravitational lensing is detected through the statistics of galaxy shapes. Finally, another way of measuring the total mass density is to pick out observations sensitive to $\Omega_b/(\Omega_b + \Omega_c)$ and use the value of Ω_b, determined through either Big Bang Nucleosynthesis or CMB, to infer the matter density. Massive galaxy clusters are perhaps the most promising target (Bleem et al. 2015) since most of the baryonic mass in a galaxy cluster is in the form of hot gas which is observable through its thermal X-ray emission or the so-called Sunyaev-Zel'dovich (SZ) effect (Sunyaev and Zeldovich 1980). There is now agreement among a wide variety of probes (Abdalla et al. 2022) that the total matter density in the universe is about 30% of the critical density, with 80% of that being in the form of non-baryonic dark matter.

- **Dark Energy**: We now know that there is an additional ingredient in the universe's energy budget, dark energy, a substance whose equation of state w is neither 0 (as it would be if the substance was nonrelativistic) nor 1/3 (ultra-relativistic), but rather close to -1. A multitude of independent pieces of evidence has accumulated for the existence of dark energy, a substance that has this negative equation of state and does not participate in gravitational collapse. For one, we have strong evidence that the universe is Euclidean, with a total density parameter close to 1. Since $\Omega_b+\Omega_c \sim 0.3$ is very far from 1 (and radiation is negligible today), something that does not clump as does matter has to make up this budgetary shortfall. Second, the expansion of the universe is accelerating, as measured by standard candles and rulers (Riess, Filippenko, et al. 1998). Accelerated expansion occurs only if the dominant constituent in the universe has a negative equation of state, i.e. negative pressure. Observing supernovae reported direct evidence for an accelerating universe, one that is best explained by postulating the existence of dark energy. The evidence is based on measurements of the luminosity distance. Moreover, we now have yet another piece of independent evidence for dark energy: the Baryon Acoustic

Oscillation (BAO) standard ruler provides both a measurement of the angular diameter distance to a given redshift and the distance interval corresponding to a certain redshift interval (Alam et al. 2017). The existence of dark energy can be inferred not only using probes that measure the expansion history directly (sometimes called geometric probes). Accelerated expansion also directly affects the evolution of structure in the universe. The growth of structure probes independently supports the Euclidean concordance cosmology. A compelling argument for the existence of dark energy is that both geometric (background) and dynamic (structure) probes agree on the same cosmological model.

Figure 1.1: Evidence for dark energy from SN-only constraints. Here we show confidence contours at 68% and 95% for the Ω_Λ, Ω_m (where $\Omega_m = \Omega_b + \Omega_c$) cosmological parameters for both the Riess, Filippenko, et al. (1998) discovery sample and the *Pantheon* sample (a combination of several datasets, see Scolnic et al. (2018)). The Pantheon constrains with systematic uncertainties are shown in red and with only statistical uncertainties are shown in gray (line) quantifying the contribution of matter and cosmological constant to the cosmic energy budget from the Type Ia supernovae. Image from Scolnic et al. (2018)

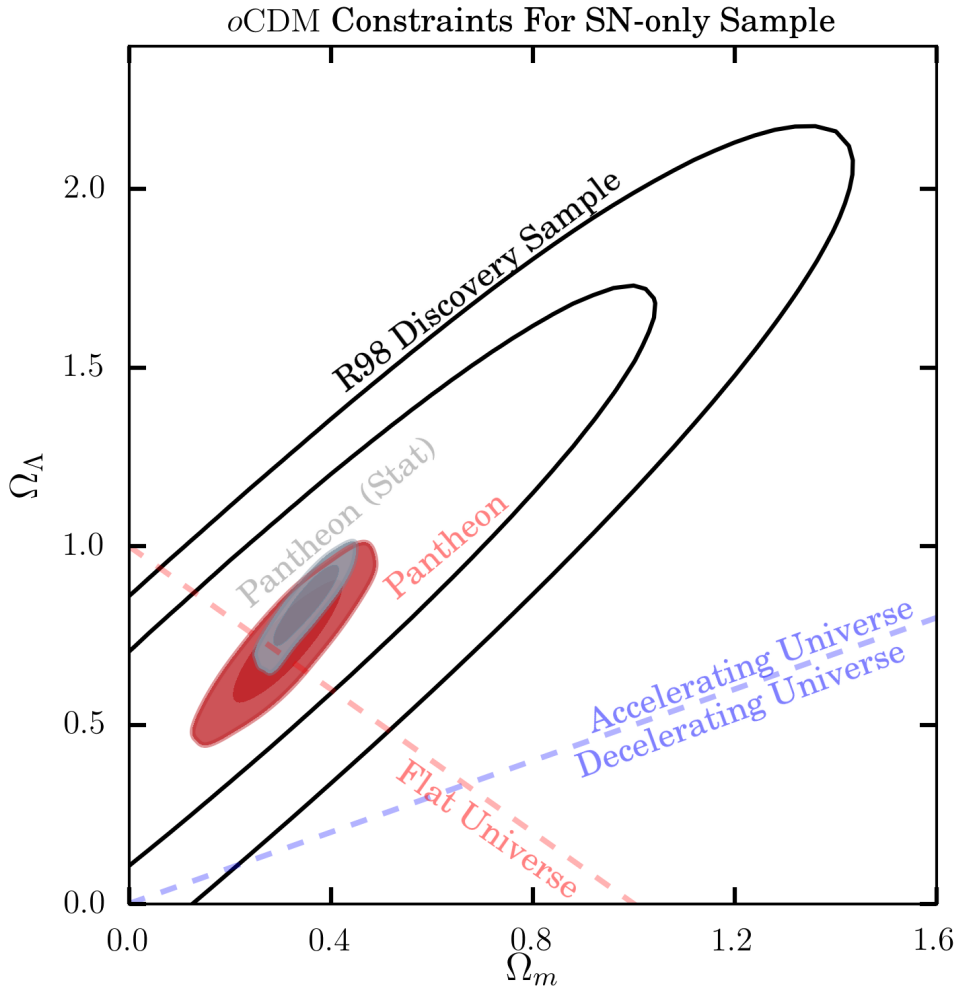

1.3 Cosmological parameters

The ΛCDM is fully described by a set of fundamental parameters. Five parameters determine the background homogeneous spacetime (matter density Ω_m, radiation density Ω_r, vacuum energy density Ω_Λ, baryon density Ω_b, and Hubble parameter H), four parameters determine the spectrum of primordial perturbations (scalar and tensor amplitudes A_S and A_T of the primordial power spectrum and power law indices n_s and $_T$), and a single parameter τ describing the total optical depth since reionization. Obtaining their measurement is no easy task and nowadays the Cosmic Microwave Background (CMB) is currently the strongest probe of precision cosmology. It was first detected in 1965 by Penzias and Wilson during an investigation of the sources of atmospheric noise in telecommunication (Penzias and Wilson 1965). The Cosmic Microwave Background consists of photons that last interacted with matter, leading to information about the hot primordial Universe and its subsequent evolution. Thus, it is a rich footprint with which to test any cosmological model. The power spectrum of CMB anisotropies has a rich structure, and its shape depends on cosmological parameters. By measuring it precisely, we can constrain the various parameters that describe the ingredients that enter the calculation. The price of this multidimensional parameter space is that there are partial degeneracies: the effect of varying one parameter can be mimicked by varying, in general, several other parameters in specific ways. CMB anisotropies are widely recognized as one of the most powerful probes of cosmology and early-Universe physics. Given a set of initial conditions and assumptions concerning the background cosmology, the angular power spectrum of the CMB anisotropies can be computed numerically to high precision using linear perturbation theory. The combination of precise experimental measurements and accurate theoretical predictions can be used to set tight constraints on cosmological parameters. *Planck* is the third-generation space mission, following Cosmic Background Explorer (COBE) and Wilkinson Microwave Anisotropy Probe (WMAP), dedicated to measurements of the CMB anisotropies (Smoot 1999, Bennett et al. 2013). The primary aim of Planck is to measure the temperature and polarization anisotropies with micro-Kelvin sensitivity per resolution element over the entire sky. The wide frequency coverage of Planck (30-857 GHz) was chosen to provide accurate discrimination of Galactic emission from the primordial anisotropies and to enable a broad range of ancillary science, such as detections of galaxy clusters, extragalactic point sources, and the properties of Galactic dust emission. We report in Table 1.1 the latest cosmological parameters measurements from *Planck* (P. Collaboration, Aghanim, Akrami, Ashdown, Aumont, Baccigalupi, M. Ballardini, Banday, Barreiro, N. Bartolo, Basak, Benabed, et al. 2020). The results were first presented in P. Collaboration, Ade, et al. (2014). These were based on temperature (TT) power spectra and CMB lensing measurements from the first 15.5 months of Planck data combined with the WMAP polarization likelihood at multipoles $l \leq 23$ to constrain the reionization optical depth τ. Since then, multiple instances of Planck Collaboration presented finer and finer values of the cosmological parameters, as the data gathering went on. In the analysis, the baseline assumption is the ΛCDM model with purely adiabatic scalar primordial perturbations with a power-law spectrum. They assumed three neutrinos species, approximated as two

massless states and a single massive neutrino of mass $m_\nu = 0.06ev$. They put flat priors on the baryon density $\Omega_b h^2$, cold dark matter density $\Omega_c h^2$, an approximation to the observed angular size of the sound horizon at recombination θ_{MC}, the reionization optical depth τ, the initial super-horizon amplitude of curvature perturbations A_s at $k = 0.05Mpc^{-1}$, and the primordial spectral index n_s. The baseline likelihood is a hybrid, patching together a low-multipole likelihood at $l \leq 30$ with a Gaussian likelihood constructed from pseudo-cross-spectrum estimates at higher multipoles. Correlations between the low and high multipoles are neglected. In the paper, they used two independent high-multipole TT, TE, and EE likelihoods. The Plik high-multipole likelihood (described in detail in P. Collaboration, Aghanim, Akrami, Ashdown, Aumont, Baccigalupi, M. Ballardini, Banday, Barreiro, N. Bartolo, Basak, Benabed, et al. (2020)) is a Gaussian approximation to the probability distributions of the TT, EE, and TE angular power spectra, with semi-analytic covariance matrices calculated assuming a fiducial cosmology. The CamSpec likelihood has been used to analyze Planck temperature and polarization maps of the cosmic microwave background since the first Planck data release. These two likelihoods are in very good agreement in TT but show small differences in TE and EE. A detailed description of CamSpec can be found in G. Efstathiou and Gratton (2021).

Table 1.1: Best fit parameters of Planck experiment. Taken from P. Collaboration, Aghanim, Akrami, Ashdown, Aumont, Baccigalupi, M. Ballardini, Banday, Barreiro, N. Bartolo, Basak, Battye, et al. (2020)

Parameter	Plik Best Fit Value	Plik	CamSpec	Combined
$\Omega_b h^2$	0.022383	0.02237 ± 0.00015	0.02229 ± 0.00015	0.02233 ± 0.00015
$\Omega_c h^2$	0.12011	0.1200 ± 0.0012	0.1197 ± 0.0012	0.1198 ± 0.0012
$100\theta_{MC}$	1.040909	1.04092 ± 0.00031	1.04087 ± 0.00031	1.04089 ± 0.00031
τ	0.0543	0.0544 ± 0.0073	$0.0536^{+0.0069}_{-0.0077}$	0.0540 ± 0.0074
$\ln(10^9 A_s)$	3.0448	3.044 ± 0.014	3.041 ± 0.015	3.043 ± 0.014
n_s	0.96605	0.9649 ± 0.0042	0.9656 ± 0.0042	0.9652 ± 0.0042
H_0	67.32	67.36 ± 0.54	67.39 ± 0.54	67.37 ± 0.54
S_8	0.8331	0.832 ± 0.013	0.828 ± 0.013	0.830 ± 0.013

In the table are presented the latest Planck results for the parameter best fits, marginalized means, and 68 % errors from our default analysis using the Plik likelihood are given in the first two numerical columns. The CamSpec likelihood results give some idea of the remaining modeling uncertainty in the high-temperature polarization, though parts of the small shifts are due to slightly different sky areas in polarization. The "Combined" column gives the average of the Plik and CamSpec results, assuming equal weight. The last two parameters are derived values on the Hubble value today and the S_8 parameter. This parameter is another way to express σ_8 and to be specific:

$$S_8 = \sigma_8 (\frac{\Omega_m}{0.3})^{0.5} \tag{1.18}$$

The parameter σ_8 is the variance of the density fluctuation field calculated by averaging on the spatial scale of $8h^{-1}Mpc$.

1.3.1 Cosmological tensions

The preponderance of different cosmological probes allows the cosmological model to be tested in various ways, and a situation may arise when the different probes appear to give incompatible results (Abdalla et al. 2022). There is currently a debate about the compatibility of results from probes of the Hubble constant H_0 and to a lesser extent from the degree of clustering of matter, often measured by the quantity S_8. "Tension" is the term used to describe results that appear to be discrepant, the interesting question being whether such tensions are indications of the need for a revision to the standard cosmological model, or whether they are due to statistical fluctuations, errors, or approximations in analysis, or unmodelled systematic effects in the data. Finding the reasons for the apparent discrepancies is a major driver of cosmological research soon. The 2018 legacy release from the Planck satellite of the Cosmic Microwave Background (CMB) anisotropies, together with the latest Atacama Cosmology Telescope (ACT-DR4, Aiola et al. (2020)) and South Pole Telescope (SPT-3G, Balkenhol et al. (2021)) measurements, have confirmed the standard ΛCDM cosmological model. However, the improvement of the methods and the reduction of the uncertainties on the estimated cosmological parameters have seen the emergence of statistically significant tensions in the measurement of various quantities between the CMB data and late-time cosmological model independent probes. While some proportion of these discrepancies may eventually be due to the systematic errors in the experiments, their magnitude and persistence across probes strongly hint at a possible failure in the standard cosmological scenario and the necessity for new physics.

1.3.1.1 H_0 tension

The most statistically significant and long-standing tension is in the estimation of the Hubble constant H_0 between the CMB data, which are cosmological model dependent and are obtained assuming a vanilla ΛCDM model, and the direct local distance ladder measurements. In particular, we refer to the Hubble tension as the disagreement at 5.0σ between the Planck collaboration value, and the latest 2021 SH0ES collaboration (R21, Riess, Yuan, et al. (2022)) constraint, $H_0 = (73.04 \pm 1.04) kms^{-1}Mpc{-}1$ at 68% CL, based on the Supernovae calibrated by Cepheids. However, there are not only these two values, but actually, two sets of measurements and all of the indirect model dependent estimates at early times agree between them, such as CMB and BAO experiments, and the same happens for all of the direct late time ΛCDM-independent measurements, such as distance ladders and strong lensing. We can see a collection of these measurements in fig.1.2.

1.3.1.2 S_8 tension

Recent observations of probes of the large-scale structure have allowed us to constrain the strength with which matter is clustered in the Universe. These constraints on the strength of matter clustering differ from that inferred by probes of the early Universe. In particular, the primary anisotropies of the CMB as measured by the Planck satellite exhibit a tension in the matter clustering strength at the level of

2-3σ when compared to lower redshift probes such as weak gravitational lensing and galaxy clustering. This tension is often quantified using the S_8 parameter, which modulates the amplitude of the weak lensing measurements. The S_8 parameter is closely related to $f\sigma_8(z = 0)$ measured by redshift space distortions (RSD) , where $f = [\Omega_m(z)]0.55$ approximates the growth rate in GR as a function of the matter density parameter, $\Omega_m(z)$, at redshift z. The lower redshift probes generally prefer a lower value of S_8 compared to the high redshift CMB estimates. Measuring S_8 is model dependent and in all cases where the underlying model is the standard flat ΛCDM model. This model provides a good fit to the data from all probes but predicts a lower level of structure formation compared to what is expected from the CMB observations. We can see a collection of these measurements in Fig. 1.3.

Figure 1.2: H_0 measurements, image from Abdalla et al. (2022)

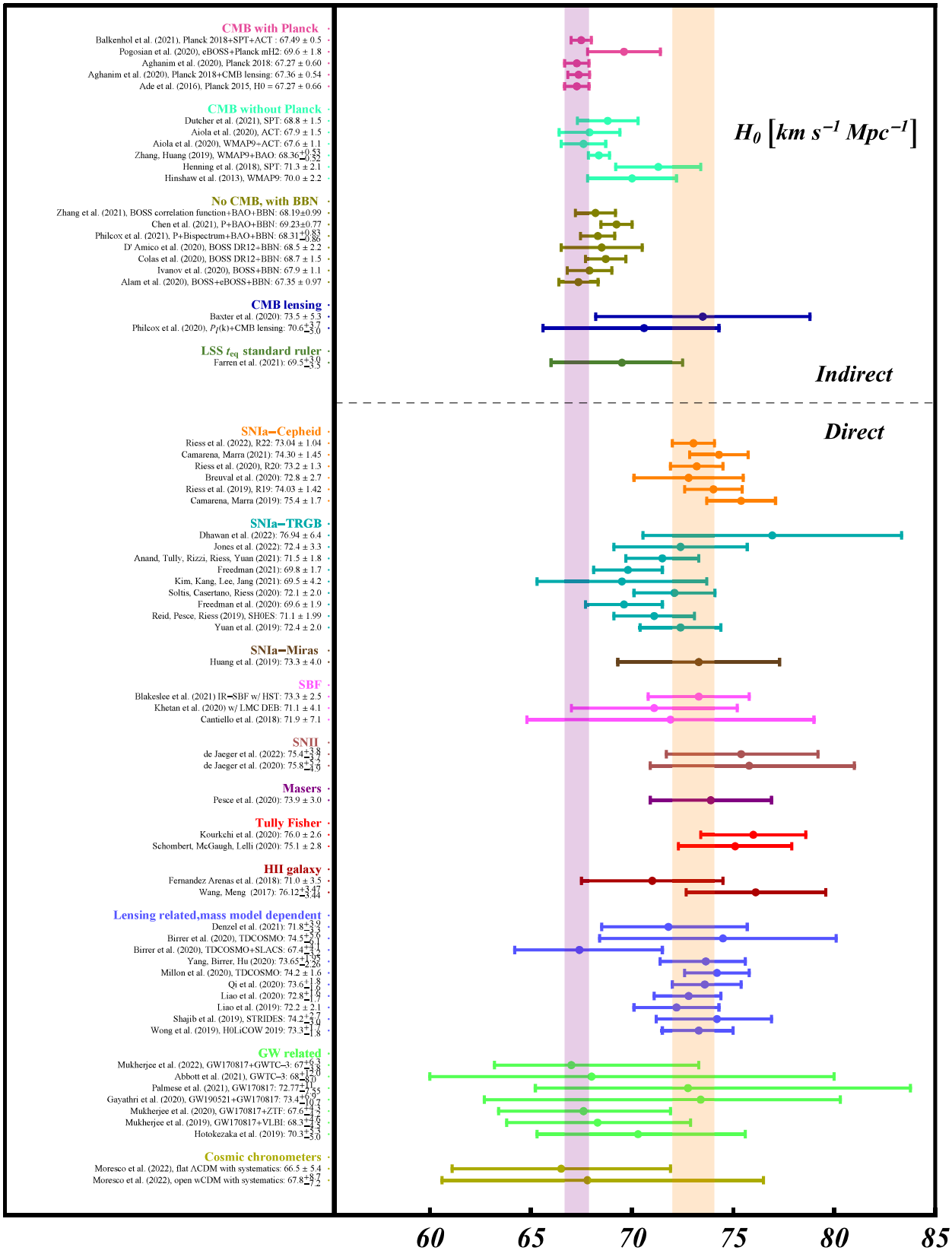

Figure 1.3: S_8 measurements, image from Abdalla et al. (2022)

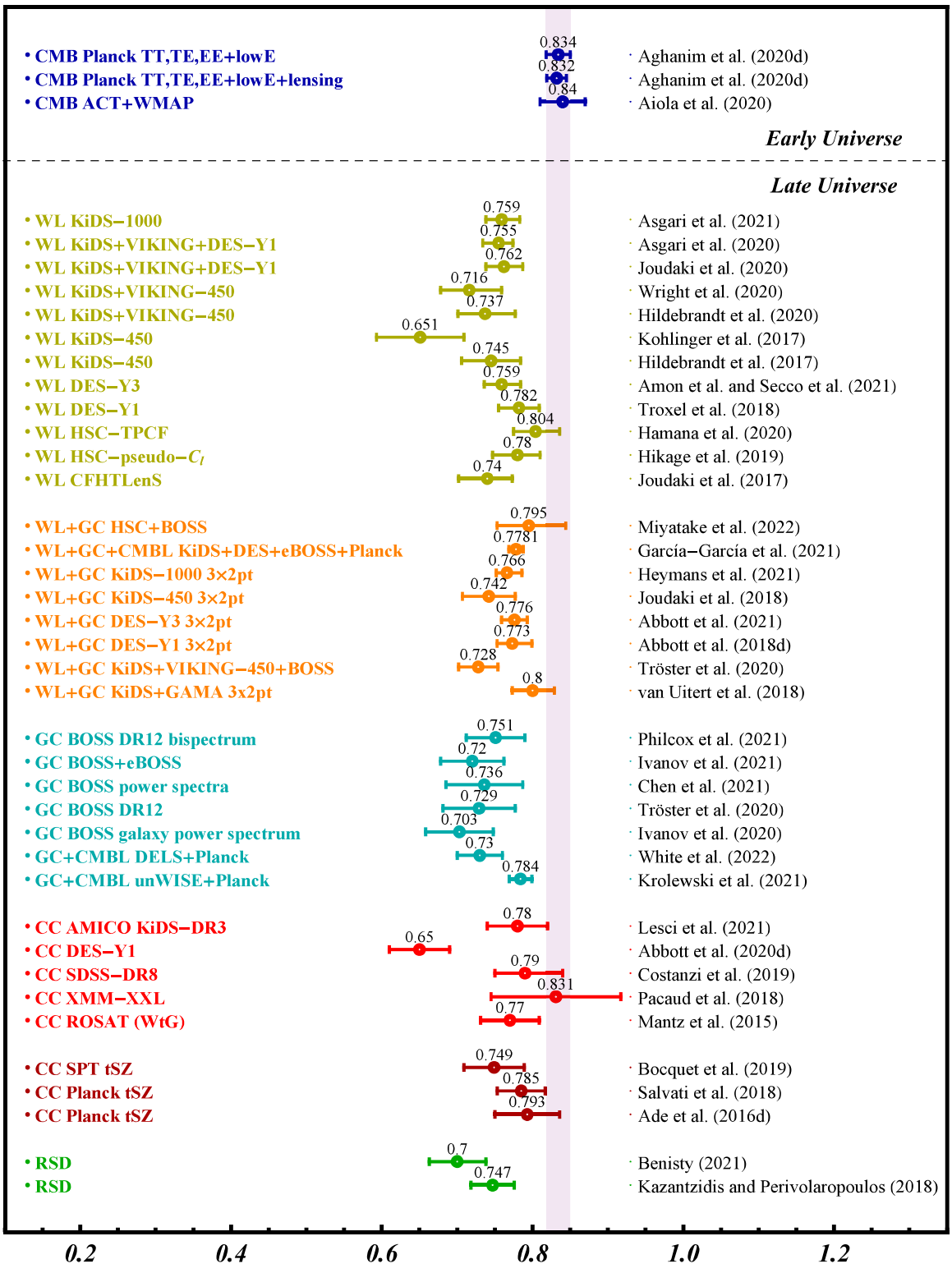

1.3.2 The Λ problem

In addition to cosmological tensions, there is one flaw in the ΛCDM which resides in the Λ parameter itself. While we have seen that there are some tensions, there is overwhelming observational evidence that the universe is undergoing accelerated expansions: from observations of type Ia supernovae, CMB measurements, and detailed studies of LSS. All of them are in agreement for a value of an observed cosmological constant of about:

$$\Lambda_{obs} \approx (10^{-3} eV)^4 \tag{1.19}$$

This value is absurdly small and it is clear if we recast it in units of Planck mass:

$$\Lambda_{obs} \approx (10^{-30} M_{pl})^4 \tag{1.20}$$

This value represents the *cosmological constant problem* when compared to the theoretical value that should arise from quantum fluctuations (S. Weinberg 1989). Such a small, value, by itself, is nothing extraordinary in physics, since small values appear all the time. However, if we consider the field theory language and the Standard Model particles, the contributions to the cosmological constant are ludicrously big. These contributions arise from:

$$\langle T_{\mu\nu} \rangle \approx -\langle \rho \rangle g_{\mu\nu} \tag{1.21}$$

and the form of this contribution may be deduced by noting that on flat space, Lorentz invariance forces $\langle T_{\mu\nu} \rangle \propto \eta_{\mu\nu}$. Then, we invoke the equivalence principle to promote $\eta_{\mu\nu} \to g_{\mu\nu}$. As a first approximation, we can estimate the size of these contributions by modeling the Standard Model fields as a collection of independent harmonic oscillators at each point in space and then summing over their zero-point energies

$$\langle \rho \rangle \sim \int_0^{\Lambda_{\rm UV}} \frac{\mathrm{d}^3 k}{(2\pi)^3} \frac{1}{2} \hbar E_k \sim \int_0^{\Lambda_{\rm UV}} \mathrm{d}k k^2 \sqrt{k^2 + m^2} \sim \Lambda_{\rm UV}^4 \tag{1.22}$$

with Λ_{UV} the cutoff. One could argue that in this case the leading divergence in the integral could be kept. If we then focus on the logarithmically divergent piece, which is the most optimistic assumption about ultraviolet physics, it leads to a logarithmic dependent $\langle \rho \rangle$ which however does not appreciably change the results. If we consider $\Lambda_{UV} \sim 1$Tev, then

$$\Lambda_{th} \approx (TeV)^4 \approx 10^{-60} M_{pl}^4. \tag{1.23}$$

This discrepancy of 60 orders of magnitude is the cause of disconcerting. In this sense, the cosmological constant is not *technically natural*. Let's consider for instance the electron mass $m_e \sim 10^{-7}$Tev, which is a small value. It is, however, stable under quantum corrections which in technical terms is technically natural. This means that the theory enjoys enhanced symmetry in the limit where the electron mass goes to zero (chiral symmetry), which tells us that quantum corrections to the electron mass must be proportional to the mass itself. So if we set the electron mass to be small, it stays small. No such symmetry is known for the cosmological constant. Given this problem, it is only natural to ponder if Λ could be better modeled.

CHAPTER 2

Einstein-Boltzmann Equations

The linear Einstein–Boltzmann equations describe the evolution of perturbations in the Universe and its numerical solutions play a central role in Cosmology. We revisit this system of differential equations and present a detailed investigation of its mathematical properties. For this purpose, we focus on a simplified set of equations aimed at describing the broad features of the matter power spectrum. We will follow the methodology used in *Modern Cosmology* (2021) and W. Hu and Sugiyama (1995) for the description of the matter inhomogeneities and the Cosmic Microwave Background (CMB) temperature anisotropies. The scope of this chapter is to provide the derivation and characterization of the Integrated Sachs-Wolfe Effect (ISW) and the distribution of matter and galaxies which we will cross-correlate. While doing so, we will introduce all the relevant tools that we will use for the explanation of the cross-correlation in Chapter 4, such for instance the *power spectrum*.

Perturbed metric

To derive the equations, we need to specify the form of the metric which should account for perturbations around the smooth universe. While the smooth universe is characterized by a single scale function $a(t)$, the perturbed universe requires two functions, Ψ and Φ, both of which depend on both space and time. These are the perturbations to the metric which correspond to the Newtonian potential, and the perturbation to the scalar curvature. Since we consider small perturbations, we will consider Ψ and Φ as small quantities. The line element in conformal time η is:

$$ds^2 = a^2(\eta)\left[-(1+2\Psi(\vec{x},\eta))d\eta^2 + (1-2\Phi(\vec{x},\eta))\delta_{ij}dx^i dx^j\right] \tag{2.1}$$

This is the case of a particular gauge choice, the *conformal Newtonian gauge*. This is necessary due to the fact that even if only scalar perturbations are considered, there is still considerable freedom in the variables one chooses to describe the fluctuations. Although any physical result must be insensitive to the gauge choice, it is possible to use a gauge quite different from this and still describe the same physics.

2.1 Boltzmann equations

The Boltzmann equations describe the statistical behavior of a thermodynamic system even out of equilibrium. This is the perfect candidate to investigate the universe, as we know that non-equilibrium conditions have contributed to the formation of the present Universe, from the baryonic asymmetry to the production of Dark Matter, and many more. To put it simply, it tells us how the distribution in the phase space of every component of the Universe (photons, neutrinos, electrons, baryons, dark matter, and dark energy) changes due to their interactions. Schematically, the unintegrated Boltzmann equation is:

$$\frac{df}{dt} = L[f] = C[f] \tag{2.2}$$

where the left hand is the Liouville operator, representing the total derivative of the distribution function f of a given specie, and the right-hand side contains all the information regarding the collision terms. These can be complicated functions of the distribution function. In the absence of collision terms the right-hand side vanishes, and in this case, the equation says that the number of particles in a given element of phase space does not change with time. Taking into account the previous metric, f, in a relativistic environment, is dependent on the space-time point and also on the 4-momentum vector. The Liouville operator with the geodesic equation, in a relativistic environment, can be expressed as

$$L = P^\mu \frac{\partial}{\partial x^\nu} - \Gamma^\mu_{\nu\gamma} P^\mu P\nu \frac{\partial}{\partial P^\mu} \tag{2.3}$$

where $P^\mu = \frac{dx^\mu}{d\lambda}$ is the 4-momentum with λ an affine parameter. Let's briefly review the Boltzmann equations for photons, baryonic matter, and dark matter. The main idea is to "unwrap" the Boltzmann Equation by considering piece by piece the total derivative of the equation. The main tools to do so lay in the quantities related to the 4-momentum:

$$P^2 = g_{\mu\nu} P^\mu P^\nu, \qquad p^2 = g_{ij} P^i P^j, \qquad \vec{p} = p^i = p\frac{P^i}{|P|}. \tag{2.4}$$

$$\tag{2.5}$$

2.1.1 The case for the photons

In principle f is a function defined in a 8-dimensional space. However, not all components of the momentum are independent due to the fact that the photon is massless. The independent components, then, are only three which can be constrained if we take into account the previous metric.

$$P^2 = 0 = -1(1+2\Psi)(P^0)^2 + g_{ij} P^i P^j \tag{2.6}$$

thus we find a constraint equation to the time component P^0. Now, unwrapping the total derivative, the calculation relies on the magnitude p of the momentum and the angular direction $\hat{p}$.

$$\frac{df}{dt} = \frac{\partial f}{\partial t} + \frac{\partial f}{\partial x^i}\frac{\partial x^i}{\partial t} + \frac{\partial f}{\partial p}\frac{\partial p}{\partial t} + \frac{\partial f}{\partial \hat{p}^i}\frac{\partial \hat{p}^i}{\partial t} \tag{2.7}$$

Immediately we can simplify the equation by neglecting the last term since it is a product of two terms that are necessarily non-zero or since they depend on the direction $\hat{p}$. Now all the remaining terms are computed considering the useful relations of the four-momentum and the fact that the potentials in the metric are small quantities. In particular, after churning some math, we have the relation:

$$\frac{\partial x^i}{\partial t} = \frac{\hat{p}^i}{a}(1 + \Psi + \Phi) \tag{2.8}$$

An overdense region has $\Psi < 0$ and $\Phi > 0$, meaning that the parenthesis becomes less than 1 and so photons slow down while traveling through such regions. If we insert this expression in (2.7), it is multiplied with $\frac{\partial f}{\partial x^i}$ which is the first-order term, so we can neglect the potentials. The next term computed is:

$$\frac{\partial p}{\partial t} = p\left[-H + \frac{\partial \Phi}{\partial t} - \frac{\hat{p}^i}{a}\frac{\partial \Psi}{\partial x^i}\right] \tag{2.9}$$

This equation describes the photon momentum as it moves through a perturbed FRW Universe. The first term accounts for the expansion of the Universe. The second and the third terms relate to the overdense regions and how photons lose energy while exiting gravitational wells. We can now recast (2.7):

$$\frac{df}{dt} = \frac{\partial f}{\partial t} + \frac{\hat{p}^i}{a}\frac{\partial f}{\partial x^i} - p\frac{\partial f}{\partial p}\left[H - \frac{\partial \Phi}{\partial t} + \frac{\hat{p}^i}{a}\frac{\partial \Psi}{\partial x^i}\right] \tag{2.10}$$

Now what we are missing is the distribution function f. In a situation of equilibrium, the photon distribution is the Bose-Einstein distribution. We have now to expand the distribution:

$$f(\vec{x}, p, \hat{p}, t) = \left[\exp\left(\frac{p}{T(t)(1 + \Theta((\vec{x}, \hat{p}, t))}\right) - 1\right]^{-1} \tag{2.11}$$

where T is the zero-order temperature as a function of time only, and $\Theta = \frac{\delta T}{T}$ is the perturbation. If we consider the zero-order distribution, $T(t)$ must depend only on time, due to the anisotropy and homogeneity. Now that we introduce perturbations, Θ must include inhomogeneities (thus the dependence on $\vec{x}$) and anisotropies (thus the dependence on $\hat{p}$). Inserting the perturbed distribution in (2.7) we can get the zero-order and first-order perturbed equation. For future reference and the sake of generalization, it is useful to consider quantities in conformal time η and expand the temperature perturbation field in multipoles:

$$\Theta_l = \frac{1}{(-i)^l}\int_{-1}^{1}\frac{d\mu}{2}\mathcal{P}_l(\mu)\Theta(\mu) \tag{2.12}$$

where $\mathcal{P}_l$ is the Legendre polynomial of order l. This multipole expansion is necessary since relativistic particles such as photons require more information to characterize. The monopole and dipole perturbations (which are equivalent to an overdensity δ and a velocity for matter particles) are not enough to fully characterize the photon distribution since it has quadrupole and higher moments too. The distribution, then, depends not only on $\hat{x}$ and time but also on $\hat{p}$, the direction of propagation. If we

switch to Fourier space, which custom, the photon perturbations would depend on k, η, and $\mu = \hat{p} \cdot k$. Thus, the perturbation variable is $\tilde{\Theta} = \Theta(k, \mu, \eta)$ where we dropped the tilde for simplicity. Given the multipole expansion, the photon perturbations can be described by a whole hierarchy of moments, $\Theta_l(k, \eta)$. Until now, we focused on the Liouville operator acting on the distribution and we neglected any collision term. To get the full extension of Boltzmann Equations we need to take into account Compton scattering too.

$$e^-(\vec{q}) + \gamma(\vec{p}) \leftrightarrow e^-(\vec{q}') + \gamma(\vec{p}') \tag{2.13}$$

While considering the scattering, we need to take into account the amplitude dependence on the polarization. The dependence means that a small portion of the CMB will be polarized due to Compton scattering so that the temperature anisotropies are coupled with the polarization field. Taking this contribution into account requires some lengthy calculations and for the specifics we refer to *Modern Cosmology* (2021). Just to put it simply, we can incorporate the polarization effects in what we can call *strenght of polarization* Θ_P. It describes the change in the polarization fields and it can be expanded in multipoles, $\Theta_P l$. If it is Fourier transformed, it will depend on k, η, and μ as well. We can now write the equations for photons:

$$\begin{aligned} \dot{\Theta} + ik\mu\Theta &= +\dot{\Phi} - ik\mu\Psi - \dot{\tau}\left[\Theta_0 - \Theta + \mu v_\mathrm{b} - \frac{1}{2}\mathcal{P}_2(\mu)\Pi\right] \\ \Pi &= \Theta_2 + \Theta_{P2} + \Theta_{P0} \\ \dot{\Theta}_P + ik\mu\Theta_P &= -\dot{\tau}\left[-\Theta_P + \frac{1}{2}\left(1 - \mathcal{P}_2(\mu)\right)\Pi\right] \end{aligned} \tag{2.14}$$

where we introduced the optical depth with σ_T the Thomson cross-section.

$$\tau(\eta) = \int_\eta^{\eta_0} d\eta' n_e \sigma_T a(\eta') \tag{2.15}$$

2.1.2 The case for matter

The same line of reasoning can be applied to matter and cold dark matter, with the appropriate caveats: these are non-relativistic particles and we have to remember that dark matter does not have a collision term. It should be reminded that often in cosmology "matter" is constituted of electrons and protons, both commonly grouped under the label "baryonic matter" even if technically electrons are leptons. In both cases it is useful to express the equations in terms of number density and velocity:

$$n = \int \frac{d^3p}{(2\pi)^3} f v^i = \frac{1}{n}\int \frac{d^3p}{(2\pi)^3} f \frac{p\hat{p}^i}{P^0} \tag{2.16}$$

As we perturbed Temperature in the case of photons, here the perturbations are fluctuations of density, expressed as overdensities $\delta = \frac{\delta\rho}{\rho}$. So by expanding after the first order:

$$n = n_0(1 + \delta(\vec{x}, t)) \tag{2.17}$$

In the case of baryonic matter, electrons and protons are coupled through Coulomb scattering, whose rate is much larger than the expansion rate at all epochs of interest. The coupling forces electrons and protons to have the same overdensity δ_b. Eventually, the equations for matter, in Fourier space, are:

$$\begin{aligned} \dot{\delta}_{dm} + ikv &= +3\dot{\Phi} \\ \dot{v}_{dm} + \frac{\dot{a}}{a} v_{dm} &= -ik\Psi \\ \dot{\delta}_{\mathrm{b}} + ikv_{\mathrm{b}} &= +3\dot{\Phi} \\ \dot{v}_{\mathrm{b}} + \frac{\dot{a}}{a} v_{\mathrm{b}} &= -ik\Psi + \frac{\dot{\tau}}{R}\left[v_{\mathrm{b}} + 3i\Theta_1\right] \end{aligned} \tag{2.18}$$

where the subscripts dm and b refer to dark matter and baryonic matter respectively.

2.2 Einstein Equations perturbed

In the previous section, we described how perturbations in the gravitational field affect particle distribution. However, this is not the full picture, since perturbations in the distributions affect the gravitational field too. When studying the Boltzmann Equations, what effectively has been done is to consider how the universe components are determined by the gravitational potential Ψ and Φ introduced in the metric. Now, in order to see the effect of the distributions on the metric, the natural thing to do is to consider Einstein Equations. In these, the distributions are sources for the energy tensor, while the gravitational potential will play a role in the metric. Coupling the Boltzmann equations and the Einstein equations will give the exact and complete picture. Practically, we can expand the Einstein equations around a zero-order homogeneous solution and extract information. We will sketch only the steps for the calculation, given that it is lengthy and without any tricky passages. The fundamental equation in this case is

$$G_{\mu\nu} = R_{\mu\nu} - \frac{1}{2} g_{\mu\nu} R = 8\pi G T_{\mu\nu}. \tag{2.19}$$

In principle, we should also include a term for the perturbation of the dark energy. In practice, though, most models of dark energy predict that it should be important only very recently. Therefore, we are justified in neglecting dark energy as a source of perturbations to the metric in this case. Considering then the tensorial equation, there should be 16 different equations but due to the symmetric nature of the tensors involved, just 10 equations appear. When the metric is considered too, we are only interested in only 2 equations, focusing on the two independent functions Ψ and Φ. If we proceed with the calculations, let's look first at the left-hand side of the equation. Firstly, the Christoffel symbols are computed according to the metric involved.

$$\Gamma^{\sigma}_{\mu\nu} = \frac{1}{2} g^{\alpha\sigma} (g_{\alpha\mu,\nu} + g_{\alpha\nu,\mu} - g_{\mu\nu,\alpha}) \tag{2.20}$$

As we know the Christoffel symbols are the building blocks for the Riemann tensor

$$R^{\rho}_{\sigma\mu\nu} = \Gamma^{\rho}_{\nu\sigma,\mu} - \Gamma^{\rho}_{\sigma\mu,\nu} + \Gamma^{\rho}_{\mu\lambda}\Gamma^{\lambda}_{\nu\sigma} - \Gamma^{\rho}_{\nu\lambda}\Gamma^{\lambda}_{\mu\sigma}. \tag{2.21}$$

From the Riemann tensor, we are interested in the Ricci tensor $R^{\rho}_{\sigma\rho\nu} = R_{\sigma\nu}$, which is given by contracting the first and third indices. Going further, the Ricci scalar is obtain by contracting the Ricci tensor with the metric $R = R_{\sigma\nu}g^{\sigma\nu}$.
Let's now look at the right-hand side and how to derive the evolution equations for Ψ and Φ, the perturbations to the metric. As we said before, in

$$G^{\mu}_{\nu} = 8\pi G T^{\mu}_{\nu} \tag{2.22}$$

there are 10 equations and we need only two. The others will be zero at first order or redundant. When considering the stress energy-momentum tensor, the general formulation would be:

$$T^{\mu}_{\nu} = -\sum_{allspeciesi} g_i \int \frac{d^3p_{(i)}}{(2\pi)^3} \frac{(P^{\mu})_{(i)}(P_{\nu})_{(i)}}{P^0_{(i)}} \sqrt{-g} f_{(i)} \tag{2.23}$$

which is straightforward for the T^{00} component but tricky for the T^i_j. When considering the spatial part of G^{μ}_{ν}:

$$G^i_j = C\delta^i_j + \frac{k^i k_j(-\Phi + \Psi)}{a^2} \tag{2.24}$$

where C contains numerous terms that come from the spatial part of the Ricci tensor. To avoid dealing with these terms, a projection only on the longitudinal traceless part of G^i_j can be performed, so that:

$$(\hat{k}_i\hat{k}^j - \frac{1}{3}\delta^j_i)G^i_j = \frac{2}{3a^2}k^2(\Psi - \Phi). \tag{2.25}$$

Likewise, this projection should be performed on the spatial part of the energy tensor. Finally, it is now just a matter of inserting the results in the equations and expressing the final equations in Fourier space and conformal time, which is custom:

$$\begin{aligned} k^2\Phi + 3\frac{\dot{a}}{a}(\dot{\Phi} + \Psi\frac{\dot{a}}{a}) &= -4\pi G a^2(\rho_{dm}\delta_{dm} + \rho_b\delta_b + 4\rho_\gamma\Theta_0 + \rho_\nu\mathcal{N}_0) \\ k^2(\Psi - \Phi) &= -32\pi G a^2[\rho_\gamma\Theta_2 + \rho_\nu\mathcal{N}a_2]. \end{aligned} \tag{2.26}$$

We have now the full set to study perturbations: inhomogeneities and anisotropies. In particular, we are interested in a source of anisotropy known as the Integrated Sachs Wolfe effect. The solution of these coupled equations is only allowed due to initial conditions given by the Inflation, which "started" the primordial perturbations. These, we will see in the next section.

2.3 Eintein-Boltzmann equations at early times

The system of equations obtain describes the evolution and growth of matter and radiation. However, if we want to solve it we need to set initial conditions, which are given by inflation (Guth 1981). The theory of inflation lets us understand how

scales that should be uncorrelated today are observed to have the same temperature; it explains some cosmological concordance problems, like the flatness problem, and it is also the fundamental mechanism for generating primordial perturbations. In the case of our interest, inflationary conditions set the conditions on matter and radiation equations. Let's consider the Boltzmann equations first. If we impose that we consider times so early that for any k-mode $k/aH \ll 1$, then we have simplifications in all the equations: all the terms containing k can be neglected at early times. We obtain:

$$\begin{aligned} \dot{\Theta} &= \dot{\Phi} \\ \dot{\delta}_{dm} + ikv &= +3\dot{\Phi}. \\ \dot{\delta}_{\mathrm{b}} + ikv_{\mathrm{b}} &= +3\dot{\Phi} \end{aligned} \tag{2.27}$$

If we consider the Einstein equations (2.26), from the first we obtain

$$\ddot{\Phi}\eta + \dot{\Phi} + \dot{\Psi} = -2\dot{\Phi} \tag{2.28}$$

by neglecting once again k terms, considering that at early times radiation dominates the universe (so that $\dot{a}/a = 1/\eta$), and implementing the just found results. If we consider now the second equation in (2.26) and neglect the higher modes for photons and neutrinos, we get the condition: $\Psi = \Phi$. This can be inserted in the previous relation:

$$\ddot{\Phi}\eta = -4\dot{\Phi}. \tag{2.29}$$

From this equation, we can obtain a solution for adiabatic perturbations for some early-times η_i

$$\Phi(k, \eta_i) = 2\Theta_0(k, \eta_i) \tag{2.30}$$

from which we obtain

$$\delta_b = \delta_{dm} = 3\Theta_0. \tag{2.31}$$

In this equation, there should be an integration constant which however can be set to zero when considering adiabatic perturbations. It can be shown that for velocities and dipole moments of matter and radiation, the initial condition is

$$\Theta_1(k, \eta) = \mathcal{N}_1(k, \eta) = \frac{iv_b(k, \eta)_{b,dm}}{3} = -\frac{k}{6aH}\Phi(k, \eta). \tag{2.32}$$

We have now the full set of coupled Einstein-Boltzmann equations with inflationary initial conditions. While here we computed the analytical form of the coupled equations, in the thesis the computation has been conducted through numerical solvers. They are much more precise due to the accuracy and the higher degree of expansion that they can have, compared to the first-order expansion presented here. Nevertheless, it shows to be useful when trying to understand the computations underlying CAMB, the main numerical tool used for this thesis. In the next section, we will see how inhomogeneities and anisotropies arise since both play a pivotal role in our task.

2.4 Matter Perturbations

With the coupled equations we have obtained so far we can describe both the case for matter and radiation. In this section, we will focus on the former, while in the next we will compute the effect our thesis is focused on: the Integrated Sachs-Wolfe effect. The ultimate goal of this section is to introduce the matter's power spectrum and its features since it will be a key ingredient in the scope of the thesis. Firstly, it is necessary to give a panoramic view of inhomogeneities at early and late times, since perturbations have different behaviors when considering small or large scales and the epoch of the universe. Since our task is to relate galaxies to the temperature of the CMB, it is fundamental to describe matter inhomogeneities, which gave life to the galaxies that we know today.

2.4.1 Primordial power spectrum

On the largest scale, the Universe is considered homogeneous, however, one can recognize that inhomogeneities arise when *zooming in*. Two surveys broke new ground: the Sloan Digital Survey (Abdurro'uf et al. 2022) and the Two Degree Field Galaxy Redshift Survey (G. P. Efstathiou et al. 1999), which comprehends over a million galaxies. They highlighted that the galaxies are not randomically distributed, rather there is a large-scale structure. To understand this structure one has to introduce new tools. The most important statistic used when studying the LSS and the CMB is certainly the two-point correlation function, which translates into the so-called power spectrum when moving to the Fourier space. If we consider the number density of galaxies n_g of a survey, we can define an overdensity over the mean of the whole survey:

$$\delta_g = \frac{n_g - \bar{n}_g}{\bar{n}_g}. \tag{2.33}$$

We can define the Power Spectrum $P_g(k)$ as:

$$\langle \tilde{\delta}_g(k')^* \tilde{\delta}_g(k) \rangle = (2\pi)^3 \delta_D^{(3)}(k - k') P_g(k) \tag{2.34}$$

where on the left we have the ensemble average over the overdensities and on the left δ_D is the Dirac delta over the momenta. Intuitively, we can understand the power spectrum as the variance in the distribution: if the distribution is smooth then the power spectrum will be small, otherwise big in the presence of under- or overdensities. Once again, if we want to compute the power spectrum related to matter perturbations, we have to take into account primordial perturbations given by inflation. The scalar perturbations generated during inflation can be parametrized in terms of the power spectrum of the gauge-invariant curvature perturbation $\mathcal{R}$. This has the great advantage of being conserved on super-horizon scales, regardless of whether matter or radiation dominated, making it a good starting point:

$$P_{\mathcal{R}}(k) = \frac{2\pi}{k^3} \frac{H^2}{M_{pl}^2 \epsilon_{sr}} \bigg|_{k=aH} = 2\pi^2 \mathcal{A}_s k^{-3} \left(\frac{k}{k_p} \right)^{n_s - 1} \tag{2.35}$$

where $\mathcal{A}_s$ is the variance of curvature perturbations in a logarithmic wavenumber interval centered around the pivot scale k_p, and n_s is the scalar spectral index. From

this expression, we can start taking into account the evolution of perturbations. Let's see how perturbations behave differently according to the scale and epoch.

2.4.2 Matter Power Spectrum

To find the power spectrum at later times and relate it to the primordial power spectrum, we have to understand how matter perturbations evolve over time. Consequently, the initial task is to consider the evolution of the gravitational potential as a function of the scale factor for different wave modes. The behavior changes accordingly to when the modes enter the horizon, and schematically it is possible to sum it up as:

- At early times, all the modes are outside the horizon and the potential is constant
- At intermediate times, the wavelength can enter the horizon and the Universe evolves from radiation domination to matter domination.
- At late times, during matter domination the potential is constant and starts decaying when dark energy becomes relevant

Figure 2.1: The linear evolution of the gravitational potential Φ for modes of different wavenumber in the fiducial ΛCDM cosmology., Image from *Modern Cosmology* (2021).

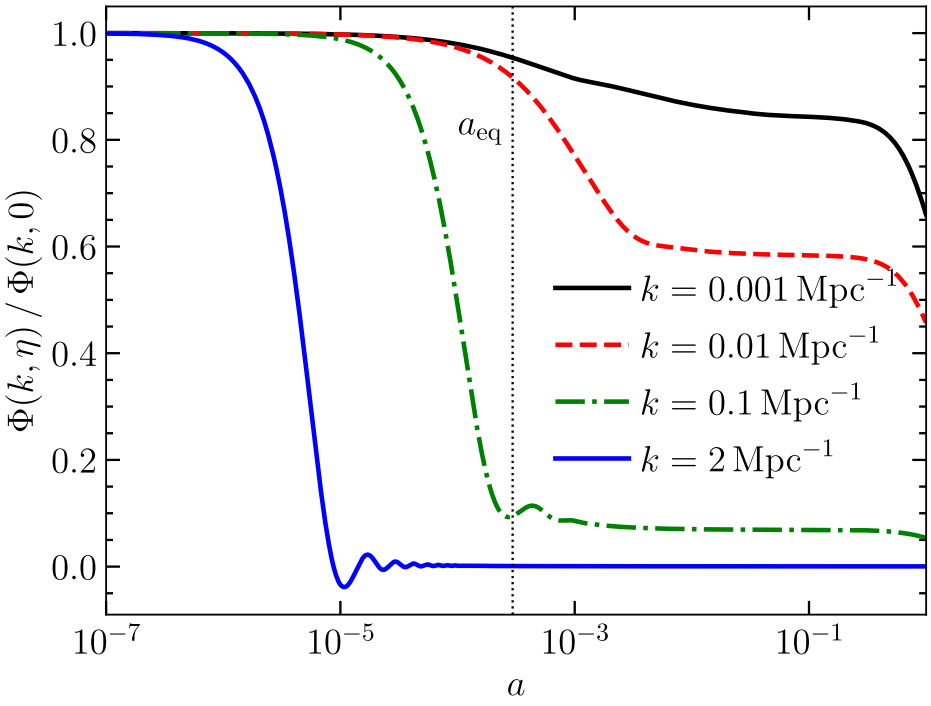

We can see that if the perturbation enters the horizon during the radiation-dominated phase, the potential is greatly suppressed, contrary to the case if enters after the

equivalence time. In addition, we can see that the smaller the mode is (conversely the bigger the length scale), the later it enters the horizon. The behavior is neatly understandable by the Fig. 2.1 The different behaviors can be taken into account by introducing a *transfer function* and a *growth factor*. The transfer function is defined as:

$$T(k) = \frac{\Phi(k, a_{matter})}{\Phi_{large-scale}(k, a_{matter})} \tag{2.36}$$

and it describes the evolution of perturbations through the epochs of horizon crossing and radiation/matter transition. The conventional normalization is set to the largest scales since it is constant during matter domination. The growth factor describes the wavelength-independent growth at late times after the transfer function has come into play (so at $a > a_{matter}$). This defines analytically the growth function as:

$$\frac{\Phi(k, a)}{\Phi(k, a_{matter})} = \frac{D_+(a)}{a} \tag{2.37}$$

where D_+ is the growth function. Thus, during matter domination $D_+ = a$. Given these two functions, we can write the potential as:

$$\Phi(k, a) = \frac{3}{5}\mathcal{R}(k)T(k)\frac{D_+(a)}{a}. \tag{2.38}$$

This parametrization neatly decouples early-universe physics (contained in $T(k)$) from late-universe physics (expressed in D_+), since after decoupling structure growth becomes scale-free.

Figure 2.2: The evolution of dark matter density perturbations in the fiducial ΛCDM cosmology. The amplitude of each mode starts to grow upon horizon entry. Well after a_{eq}, all sub-horizon modes evolve identically, and scale as the growth factor. At the very latest times, we can see a slight suppression from this linear trend due to the onset of accelerated expansion. Image from *Modern Cosmology* (2021).

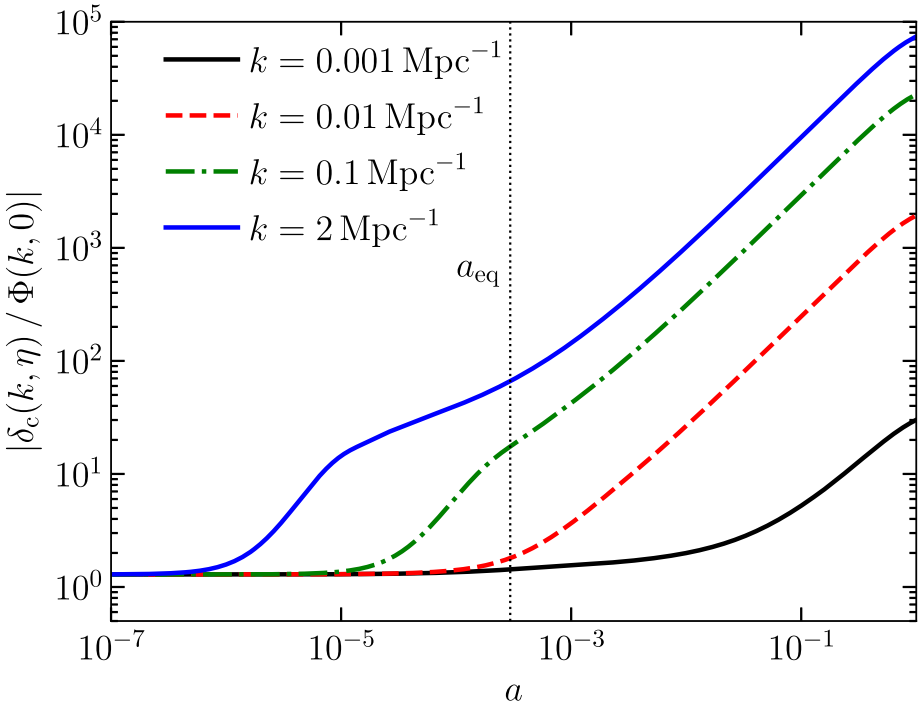

Using the Poisson equation we can relate the matter density at late times to the gravitational potential and the conserved curvature perturbation generated via inflation:

$$\delta_m(k,a) = \frac{2}{5}\frac{k^2}{\Omega_m H_0^2}\mathcal{R}(k)T(k)D_+(a) \qquad (a > a_{matter}, k \geq aH) \tag{2.39}$$

and thus, considering the primordial power spectrum, we obtain the matter power spectrum

$$P_L(k,a) = \frac{8\pi^2}{25}\frac{\mathcal{A}_f}{\Omega_m^2}D_+^2(a)T^2(k)\frac{k^{n_s}}{H_0^4 k_p^{n_s-1}}. \tag{2.40}$$

In Figure 2.3 we can see the power spectrum for the ΛCDM today and higher redshifts with the predicted behaviors for the scales.

Figure 2.3: The linear matter power spectrum in the fiducial ΛCDM cosmology at different redshifts. Scales to the left of the vertical lines, which indicate non-linear regime $k_{NL}(z)$ for each of the redshifts shown, are still evolving approximately linearly at each redshift. Image from *Modern Cosmology* (2021)

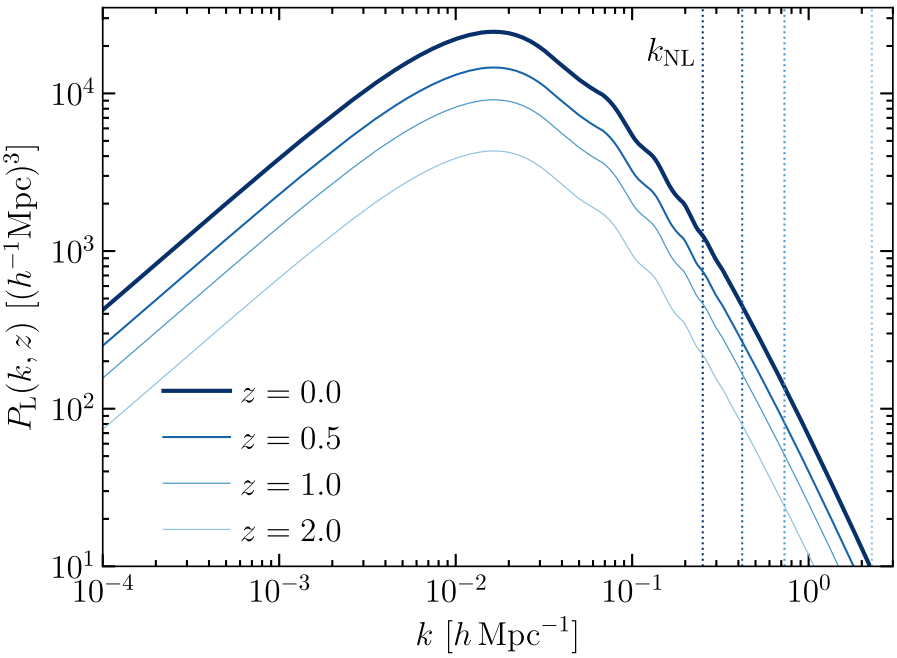

.

2.5 CMB anisotropies

Of the various epochs of the universe, Big Bang Nucleosynthesis (BBN) is of particular importance, as it produced the light elements of our universe. The BBN happened when the Universe cooled to 1 Mev and after it is complete the ordinary matter consists of protons, electrons, photons helium nuclei, and traces of heavier nuclei. The next important event (and the center of attention of the section) is when the Compton scattering between photons and electrons is not efficient enough to keep the photons tightly coupled to the baryons. This decoupling happens when the temperature drops to $\approx eV$ and the relic electromagnetic radiation that free-streams to us is the so-called Cosmic Microwave Background. Therefore, perturbations to the photons evolved completely different before and after the epoch of recombination at $z_* = 1100$. Before recombination, photons are tightly coupled to electrons and protons, and after they free-stream to us. Thus, the observed anisotropy spectrum is based on the anisotropies at recombination, computed accordingly to the constraints imposed by the fact that the photons are coupled. When considering anisotropies, on the largest scales we find them unaltered from the conditions imposed by inflation, since there is no causal physics. On smaller scales, causal physics comes into play and for the primordial fluid, the anisotropy moments can only be the monopole and dipole, since we are in fact in a fluid approximation.

2.5.1 CMB anisotropies today

We want to derive a solution for the photon moments today $\Theta_0(k, \eta_0)$ in the terms of monopole and dipole at recombination. Starting from the Boltzmann equation for photons (2.14) and subtract $\dot{\tau}\Theta$:

$$\dot{\Theta} + (ik\mu - \dot{\tau})\Theta = +\dot{\Phi} - ik\mu\Psi - \dot{\tau}\left[\Theta_0 + \mu v_{\rm b} - \frac{1}{2}\mathcal{P}_2(\mu)\Pi\right]. \tag{2.41}$$

The left-hand side can be rewritten as:

$$\dot{\Theta} + (ik\mu - \dot{\tau})\Theta = e^{-ik\mu\eta + \tau}\frac{d}{d\eta}\left[\Theta e^{ik\mu\eta - \tau}\right]. \tag{2.42}$$

Once we recast the left-hand side in this fashion, we can multiply both sides of (2.41) by $e^{ik\mu\eta-\tau}$ and then integrate for η. In this way we obtain:

$$\Theta(\eta_0) - \Theta(\eta_{init})e^{ik\mu\eta_{init} - ik\mu\eta_0 - \tau(\eta_{init})} = \int_{\eta_{init}}^{\eta^0} d\eta \mathcal{S} e^{ik\mu(\eta-\eta_0)-\tau(\eta)} \tag{2.43}$$

where we have defined the source function as $\mathcal{S} = \left(\dot{\Phi} - ik\mu\Psi - \dot{\tau}\left[\Theta_0 + \mu v_{\rm b} - \frac{1}{2}\mathcal{P}_2(\mu)\Pi\right]\right)$. Now some simplifications apply so that the second term vanishes and we can set the lower limit of the integral to zero. Since τ is defined as the scattering optical depth-integrated from today, the value $\tau(\eta_0) = 0$. On the other hand, $\tau(\eta_{init})$ will be large. Thus the solution is

$$\Theta(k, \mu, \eta_0) = \int_0^{\eta_0} d\eta \mathcal{S}(k, \mu, \eta) e^{ik\mu(\eta-\eta_0)-\tau(\eta)}. \tag{2.44}$$

Given that the integrand is given by a source function and an exponential, we can integrate by parts the terms containing μ so that $\mathcal{S}$ does not depend on μ anymore. In this way we obtain

$$\Theta(k, \mu, \eta_0) = \int_0^{\eta_0} d\eta S(k, \eta) e^{ik\mu(\eta-\eta_0)-\tau(\eta)}. \tag{2.45}$$

with now S a source function that does not depend on μ. Given the expression of the temperature anisotropy, we wish to expand in Θ_l moments. To do so we expand using Legendre Polynomials $\mathcal{P}_l(\mu)$ and integrate over μ. Remembering that

$$\int_{-1}^{1} \frac{d\mu}{2}\mathcal{P}_l(\mu)e^{ik\mu(\eta-\eta_o)} = \frac{1}{(-1)^l} j_l[k(\eta - \eta_0)] \tag{2.46}$$

with j_l a spherical Bessel function, we obtain an expansion of Θ_l in terms of Bessel functions. To weigh the contribution of the terms, it is important to introduce the so-called *visibility function*

$$g(\eta) = -\dot{\tau}e^{-\tau(\eta)} \qquad\qquad \int_0^{\eta_0} d\eta g(\eta) = 1 \tag{2.47}$$

which accounts for the probability of a photon last scattering at a time η. Introducing this function in the source function, we obtain:

$$S(k,\eta) \approx g(\eta)[\Theta_0(k,\eta) + \Psi(k,\eta)] + \frac{i}{k}\frac{d}{d\eta}[v_b(k,\eta)g(\eta)] + e^{-\tau[\dot{\Psi}(k,\eta)+\dot{\Phi}(k,\eta)]} \quad (2.48)$$

With the strength of this function, we can integrate over η. When integrating, we can see that the first two terms are dominant and the third is only weighted by $e^{-\tau}$, so that the terms contribute only to the case $\tau \leq 1$, so after recombination. Given that the visibility function is sharply peaked we can treat it as a δ-function and evaluate the first two terms at the time of recombination. However, this approximation is made only to show a more concise analytical result: the full computation is considered in the thesis for the numerical computations. Anyway we obtain the final expression:

$$\begin{aligned}\Theta_l(k,\eta_0) \simeq &[\Theta_0(k,\eta_*) + \Psi(k,\eta_*)]\, j_l[k(\eta_0-\eta_*)] \\ &+ 3\Theta_1(k,\eta_*)\left(j_{l-1}[k(\eta_0-\eta_*)] - (l+1)\frac{j_l[k(\eta_0-\eta_*)]}{k(\eta_0-\eta_*)}\right) \\ &+ \int_0^{\eta_0} d\eta e^{-\tau}\left[\dot{\Psi}(k,\eta) + \dot{\Phi}(k,\eta)\right] j_l[k(\eta_0-\eta)]\end{aligned} \quad (2.49)$$

The second term is obtained through the exploitation of spherical Bessel functions properties and by the fact that $v_b \approx -3i\Theta_1$. The expression obtained is the fundamental equation to study CMB anisotropies. We can see that contributions are given by monopole and dipole terms at recombination and a term integrated along the path of photons from recombination to today.

- The monopole term is given by the combination of $\Theta_0 + \Psi$ of the temperature anisotropy and gravitational redshift. Intuitively, the contribution of the potential is given by the fact that the photons that we see today had to emerge from potential wells at recombination. This contribution shows acoustic oscillations (which will see later in detail), whose behavior is at first order described by a tight-coupling solution.

- The Doppler-shift contribution $3\Theta_1$ shows the same acoustic oscillations but out of phase. In addition, this contribution is negligible on the larger scales

- These last corrections, encoded in the last line, are called *integrated Sachs-Wolfe* effects. These are due to the time evolution of gravitational potentials around recombination and at late times. Unlike the first two, it is an integrated contribution.

At this point, it is useful to introduce the power spectrum for the CMB. Anisotropies in the CMB can also be distinguished according to the scale, specifically on large scales and on smaller scales where causal physics comes into play. The anisotropy terms that we have found will have different effects according to the scale, but it is useful to recast them in terms of the angular power spectrum.

2.5.2 The angular power spectrum

The generic temperature perturbation we have introduced when considering the CMB radiation field

$$T(x,\hat{p},\eta) = T(\eta)(1+\Theta(x,\hat{p},\eta)) \tag{2.50}$$

has to be related to the anisotropy pattern we observe today (x_0,η_0). Thus, the temperature change is set by $\hat{p}$ and hence we have to map the direction of the incoming photons. The standard procedure is to use polar coordinates when describing incoming directions on the sky map. Specifically, the temperature perturbation is expanded in spherical harmonics:

$$\Theta(x,\hat{p},\eta) = \sum_{l=1}^{\infty}\sum_{m=-l}^{l} a_{lm}(x,\eta)Y_{lm}(\hat{p}) \tag{2.51}$$

All the information is contained in the $(\vec{x},\eta)$-dependent amplitudes a_{lm}. We can exploit the orthogonality property of spherical harmonics to recover such amplitudes:

$$\int d\Omega Y_{lm}(\hat{p})Y^*_{l'm'}(\hat{p}) = \delta_{ll'}\delta_{mm'} \tag{2.52}$$

thus obtaining

$$a_{lm}(x,\hat{p}) = \int \frac{d^3k}{(2\pi)^3}e^{ikx}\int d\Omega Y^*_{lm}(\hat{p})\Theta(x,\hat{p},\eta). \tag{2.53}$$

As initially stated we are interested in the $\Theta(x,\hat{p},\eta)$. The amplitudes a_{lm} provide us the link we need if we consider its square and the expectation value since they can be related to their counterpart in Θs. However $\langle\Theta(k,\hat{p})\Theta^*(k',\hat{p}')\rangle$ accounts for two phenomena: the initial values of the perturbation (which is randomly given via inflation from a Gaussian field) and the deterministic evolution into anisotropies. To take into account this fact, we can introduce the ratio:

$$\mathcal{T}(k,\hat{p}) = \frac{\Theta(k,\hat{p},\eta)}{\mathcal{R}(k)} \tag{2.54}$$

where $\mathcal{R}$ is the primordial curvature perturbation that does not depend on $\hat{p}$. Now,

$$\begin{aligned}\langle\Theta(k,\hat{p})\Theta^*(k',\hat{p}')\rangle &= \langle\mathcal{R}(k)\mathcal{R}^*(k')\rangle\mathcal{T}(k,\hat{p})\mathcal{T}^*(k',\hat{p})\\ &= (2\pi)^3\delta^{(3)}_D(k-k')P_{\mathcal{R}}(k)\mathcal{T}(k,\hat{p})\mathcal{T}^*(k',\hat{p})\end{aligned} \tag{2.55}$$

where we used the definition of the power spectrum of curvature perturbations. We can now define the variance of the a_{lm}

$$C_l\delta_{ll'}\delta_{mm'} = \langle a_{lm}a^*_{l'm'}\rangle \tag{2.56}$$

and inserting (2.53) we can exploit the deltas:

$$C_l = \int \frac{d^3k}{(2\pi)^3}P_{\mathcal{R}}(k)\int d\Omega\int d\Omega' Y^*_{lm}(\hat{p})Y_{lm}(\hat{p}')\mathcal{T}(k,\mu)\mathcal{T}^*(k,\mu') \tag{2.57}$$

which we can relate to the Θ_l moments by expanding in terms of Legendre Polynomials, leaving:

$$C_l = \int \frac{d^3k}{(2\pi)^3} P_{\mathcal{R}}(k) \int d\Omega \int d\Omega' Y^*_{lm}(\hat{p}) Y_{lm}(\hat{p}') \\ \times \sum_{l'l''} (-i)^{l'} (i)^{l''} (2l'+1)(2l''+1) \mathcal{P}_{l'}(\mu) \mathcal{P}_{l''}(\mu') \mathcal{T}(k,\mu) \mathcal{T}^*(k,\mu'). \tag{2.58}$$

We can now simplify the expression since the two angular integrals can be shown to be identical and nonzero only if $l = l' = l''$. In such case:

$$\int d\Omega Y_{lm}(\hat{p}) \mathcal{P}_{l'}(\mu) = \frac{4\pi}{2l+1} Y_{lm}(\hat{k}) \delta_{ll'} \tag{2.59}$$

then the integration over the angular part of d^3k is simply over $|Y_{lm}|^2$ which is 1. Thus leaving:

$$C_l = \frac{2}{\pi} \int_0^{\inf} dk k^2 \mathcal{P}_{\mathcal{R}}(k) |\mathcal{T}_l(k)|^2. \tag{2.60}$$

Then, this expression shows how C_l is the integral over all the Fourier modes of the variance of Θ_l. We can obtain the anisotropy spectrum today by combining Eq. (2.60) with Eq. (2.49). Let's use the power spectrum to describe anisotropies.

2.5.3 Large-scale anisotropies

The large-angle CMB anisotropies are determined by extremely large-scale modes that have enetered our horizon only recently. Therefore, on the largest scales we can consider the super-horizon regime ($k\eta << 1$) so that $\dot{\Theta} = \dot{\Phi}$ is valid and neglect the dipole contribution. When integrating, the constant is set by the initial conditions given by the inflationary scenario for which $2\Theta_0(\eta_{ini}) = \Phi(\eta_{ini})$. Since recombination takes place long after the epoch of equality, the observed anisotropy $(\Theta_0 + \Psi)$ can be expressed in terms of Φ or the curvature perturbation.

$$(\Theta_0 + \Psi)(k, \eta_*) = \frac{1}{3}\Phi(k, \eta_*) = \frac{1}{5}\mathcal{R}(k) \tag{2.61}$$

which expression in terms of $\mathcal{R}$ is useful when computing the anisotropy spectrum. This is the so-called *Sachs Wolfe effect* (Sachs and Wolfe 1967). To get the anisotropy spectrum we have to plug this expression in the monopole term and integrate (2.60), leaving

$$C_l^{SW} \approx \frac{2}{25} \sum_0^{\infty} dk k^2 P_{\mathcal{R}}(k) |j_l[k(\eta_0 - \eta_*)]|^2. \tag{2.62}$$

We can plug Eq. (2.35) into the expression and compute it analytically in terms of the gamma function. If the spectrum is invariant, $n_s = 1$, simplifications occur, resulting in

$$l(l+1)C_l^{SW} = \frac{8}{25}\mathcal{A}_s \tag{2.63}$$

which is a constant. Intuitively, the C_l is related to the three-dimensional power spectrum which is a constant itself if $n_s = 1$. We can see in Fig. 2.4 that the

deviation from a constant is due to the ISW effect and the dipole term, the latter being nonnegligible at higher l.

Figure 2.4: Large-scale CMB power spectrum as measured by Planck (P. Collaboration, Aghanim, Akrami, Ashdown, Aumont, Baccigalupi, M. Ballardini, Banday, Barreiro, N. Bartolo, Basak, Battye, et al. 2020), and fiducial ΛCDM prediction (solid). The dotted line shows the scale-invariant Sachs–Wolfe plateau predicted by (2.63). Image from *Modern Cosmology* (2021).

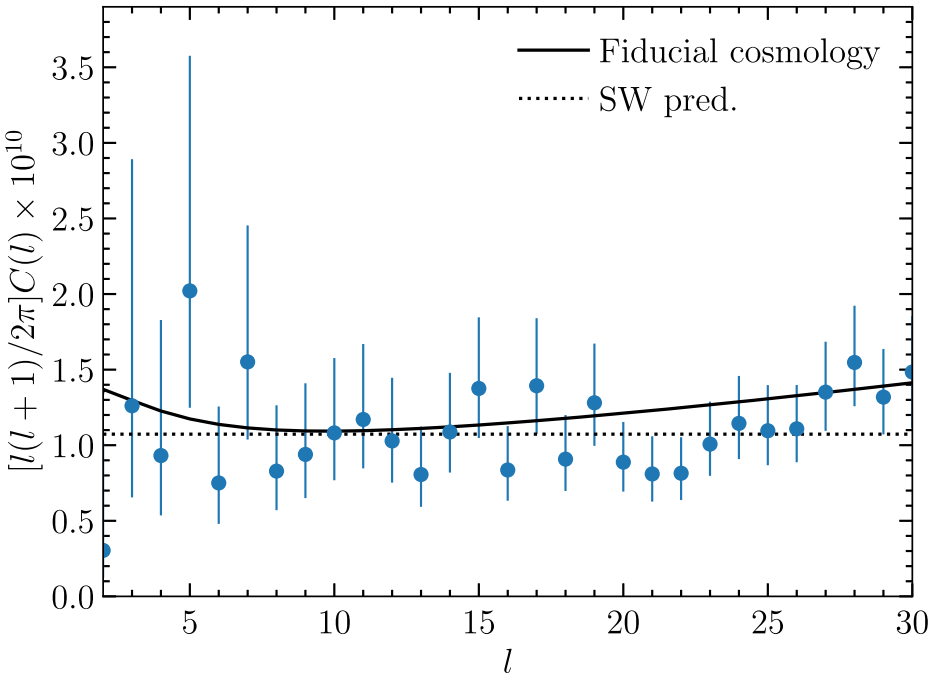

2.5.4 Small scales anisotropies

On small scales, where causal physics comes into play, all terms in Eq. (2.49) contribute to the anisotropies spectrum. Specifically, we can distinguish two phases in which the terms play a role. Before the photon decoupling, the primordial fluid has an established equilibrium when the gravitational potential is balanced by radiation pressure. The result of this effect is acoustic oscillations and diffusion damping. After recombination, the ISW contribution has to be taken into account, since it is an anisotropy that arises during the path from recombination to us. In fact, it is an integrated contribution.

Acoustic Peaks

Before recombination, the tightly coupled limit applies ($\tau \gg 1$) and the only non-negligible moments are the monopole and dipole. In this sense, the photons behave like a fluid, characterized by density and velocity. It is possible to find a first-order differential equation, one for each moment. If combined, the result is a second-order

differential equation, governing the soundwaves in the primordial fluid.

$$\Theta_0'' + + \frac{a'}{a}\frac{R}{1+R}\Theta_0' + k^2 c_s^2 \Theta_0 = -\frac{k^2}{3}\Psi + \frac{a'}{a}\frac{R}{1+R}\Phi' + \Phi'' \tag{2.64}$$

where we define the baryon-to-photon energy ratio R and the sound speed of the fluid c_s

$$R = \frac{r\rho_b}{4\rho_\gamma} \qquad\qquad c_s(\eta) = \sqrt{\frac{1}{3(1+R)}}. \tag{2.65}$$

We can see that the sound speed is lower due to the presence of baryons and determines the period of oscillations. We will skip the procedure in solving the differential equation, but it is necessary to point out that the solutions of monopole and dipole are out of phase from each other and this mismatch has important implications in the anisotropy spectrum: the dipole contributions lower the prominence of the peaks by making the roughs less pronounced. Another feature is that they add incoherently, implying the less importance of the dipole term.

Diffusion Damping

Diffusion damping is due to the finiteness of the mean free path of the photons before scattering, and it is relevant on very small scales. In such a case, higher multiple moments, like the quadrupole, have to be considered. We can see it as a correction to the treatment of baryons and photons as a fluid.

Integrated Sachs-Wolfe effect

The last term in (2.49) is the so-called *integrated Sachs-Wolfe* and it arises after the last scattering when the photons free stream toward the observer.

$$\Theta_l^{ISW}(k,\eta_0) \simeq \int_{\eta_{rec}}^{\eta_0} d\eta e^{-\tau} \left[\Phi'(k,\eta) + \Psi'(k,\eta)\right] j_l\left[k\left(\eta_0 - \eta\right)\right] \tag{2.66}$$

where the lower limit of the integration can be set to the time of recombination, which we assume to be instantaneous. It is important to point out that Θ_l^{ISW} depends on the derivatives of the gravitational potential. Therefore if these do not vary in time, the anisotropy effect vanishes. This is a peculiar case during a matter-dominated Universe but we can identify two periods of the Universe evolution during which the ISW contribution is nonnegligible:

- **early ISW**: The transition from radiation dominated to matter dominated is not abrupt and an ISW effect occurs right after recombination. In this case, the largest effect is typically on scales of the horizon at the time at which the potential evolves. The early ISW effect adds coherently to the monopole.
- **late ISW**: the effect occurs when potentials decay during the dark energy epoch at recent times. This effect is restricted to the largest scales and barely visible. The most direct way to detect the effect is to cross-correlate the CMB temperature anisotropies with angular galaxy correlations, as did in this thesis and which we will se in detail later.

CHAPTER 3

Alternative theories of gravity

As we have seen in the previous chapters, the ΛCDM model provides a strong description of the Universe but might be deemed to have some flaws. The Λ value is yet to be explained and the H_0 and σ_8 tensions still make cosmologists scratch their heads. So far, we have always talked about the cosmological constant Λ, with the one free parameter being the energy density associated with it. However, this is only the simplest possibility for what dark energy could be, and introducing a constant carries its own set of problems. However, there are other models that can come to our aid which include cases where gravity is not strictly described by Einstein's General Relativity in the ΛCDM. In this particular work we consider an Effective Field Theory (EFT) approach (Bloomfield et al. 2013) to the description of modified gravity (MG) and DE, since the EFT framework has proved to be able to establish a robust and economic way to connect data to fundamental theory. Being succesful in many other areas of physics, such as in particle physics and condensed matter systems, this particular line of work found its first application in cosmology to both inflation and late-time acceleration. In this chapter we introduce the principles behind building alternative cosmological models, we review the EFT approach to Modified Gravity and Dark Energy, and finally describe the models considered in this thesis.

3.1 Dark Energy and Modified Gravity models

The ΛCDM is remarkably robust and Einstein's description of gravity (Einstein 1917) is unique where the gravitational force is mediated by a single rank-2 tensor field. The simplest scenario to consider when one wants to describe gravity differently, is to add an extra scalar field. Of course, the effects of additional fields need to be suppressed at scales where GR is accurately tested, like in the Solar System. This is achieved through the so called screening mechanisms, like chameleon or Vainshtein mechanisms (see D. H. Weinberg et al. (2013) or see Joyce et al. (2015) for a DE/MG review structured around screening mechanisms). We see now the simplest

examples of how another theory of gravity can be considered. The principles driving the examples are the fundamental basics for the models we are going to consider. Firstly we consider models where Dark Energy is not a simple constant anymore (see reviews Copeland et al. (2006), Mortonson et al. (2013)) and then a simple example of modification of gravity (Clifton et al. 2012).

3.1.1 Dynamical Dark Energy

The Λ-constant corresponds to a fluid with a constant equation of state $w = -1$. We can broaden our comprehension by considering a situation in which the equation of state of DE changes with time. One possibility is to consider the cosmological constant to be zero, and the cosmic acceleration to be due to the potential of a scalar field. We thus introduce a new degree of freedom to model the dark energy, similarly to what has been done when modeling the inflationary period. These dynamical dark energy models are the simplest modifications of ΛCDM and are called *quintessence* models (Tsujikawa 2013). Quintessence is, then, described by a scalar field ϕ minimally coupled to gravity and with a potential $V(\phi)$ that leads to late time acceleration. The action for Quintessence is:

$$S = \int d^4x\sqrt{-g}\left(\frac{R}{16\pi G} - \frac{1}{2}g^{\mu\nu}\partial_\mu\partial_\nu\phi - V(\phi)\right) + S_m(\psi_m, g_{\mu\nu}), \tag{3.1}$$

where S_m is the action for the matter fields. In a FRW spatially flat spacetime we can vary the action with repspect to ϕ or the metric, obtaining respectively the equation of motion for the scalar field and the energy tensor:

$$\ddot{\phi} + 3H\dot{\phi} + \frac{dV}{d\phi} = 0 \qquad T_{\mu\nu} = \partial_\mu\phi\partial_\nu\phi - g_{\mu\nu}\left[\frac{1}{2}g^{\alpha\beta}\partial_\alpha\phi\partial_\beta\phi + V(\phi)\right] \tag{3.2}$$

Then, considering the stress-energy tensor components[1]:

$$\rho = -T^0_0 = \frac{1}{2}\dot{\phi}^2 + V(\phi) \qquad\qquad p = T^i_i = \frac{1}{2}\dot{\phi}^2 - V(\phi) \tag{3.3}$$

which we can insert in the bacgrkound equations and obtain:

$$H^2 = \frac{8\pi G}{3}\left[\frac{1}{2}\dot{\phi}^2 + V(\phi) + \rho_m\right] \tag{3.4}$$

$$\dot{H} = -\frac{8\pi G}{3}\left[\dot{\phi}^2 + (1 + w_m)\rho_m\right] \tag{3.5}$$

from which we can see that the Universe accelerates for a flat potential $\dot{\phi} < V(\phi)$. We also recover the equation of state for the field

$$w_\phi(t) = \frac{P_\phi}{\rho_\phi} = \frac{\frac{1}{2}\dot{\phi} - V(\phi)}{\frac{1}{2}\dot{\phi} + V(\phi)} \tag{3.6}$$

and we can now see the dependence on time. The scenario obtained is similar to the inflationary scenario, with the single field slow-roll condition. Importantly,

[1] The indeces of the Tensor T are not summed

quintessence fields must be weakly coupled to matter, otherwise the scalar field would mediate a fifth force. Precisely, for generic potentials the requisite flatness implies that excitations of the field are nearly massless, $m_\phi \approx \sqrt{V''(\phi)/2} \leq H_0 \sim 10^{-33} eV$. To provide the necessary energy density, the present value of the potential must be approximately $V(\phi) \sim (10^{-3} eV)^4$, so the field itself will typically be of order $\phi_0 \sim M_{pl}$. The exchange of very light fields gives rise to forces of very long range, so it is interesting to consider the direct interaction of the quintessence field to ordinary matter (Carroll 1998). However, the absence of observable interactions of quintessence with the fields of the standard model implies the existence of a symmetry which suppresses such couplings. Unless there is an underlying symmetry that suppresses these couplings, their values shall be very small, in order to satisfy tests of gravity; this leads to another fine-tuning requirement apart from that necessary to make the cosmological constant itself small. A different approach is to describe gravity in a different way, leading to modified gravity models.

3.1.2 Modified Gravity

On cosmological scales, gravity is the dominant force, driving the evolution of the Universe. It is natural to ask oneself if the gravitational interaction at the relevant scales is sufficiently adequate or if a modification of it would describe the physics better. (Jain et al. 2013, Joyce et al. 2015, Brax, Casas, et al. 2021) In order to achieve a new theory of gravity, we introduce a modification of the Einstein-Hilbert term (for instance introducing $f(R)$ like in Sotiriou and Faraoni (2010)) or a new coupling with, for instance, a scalar field. Introducing a scalar field is the example we will adopt since it is the foundation for the models we are going to consider. Specifically, we introduce now scalar-tensor theories, which are one among the most established and well studied alternative theories of gravity. Let us consider the action:

$$S = \int d^4x\sqrt{-g}\left(f(\phi)M_{pl}R - A(\phi)g^{\mu\nu}\nabla_\mu\phi\nabla_\nu\phi - 2\Lambda(\phi)\right) + S_m(\psi_m, A(\phi)g_{\mu\nu}) \quad (3.7)$$

where f, Λ, A are functions of the scalar field. The A function defines two different confromal frames in which one can work. If we consider the conformal transformation

$$A(\phi)g_{\mu\nu} \to g_{\mu\nu} \quad (3.8)$$

the resulting frame is characterized by no direct interaction between the scalar field and matter fields. This frame is referred to as the Jordan frame, while its counterpart is called Einstein frame. In the Jordan frame test particles follow geodesics of the metric to which they are coupled. If we then move to the Jordan frame, the resulting Lagrangian is:

$$S = \int d^4x\sqrt{-g}\left(\phi M_{pl}R - \frac{\omega(\phi)}{\phi}g^{\mu\nu}\nabla_\mu\phi\nabla_\nu\phi - 2\Lambda(\phi)\right) + S_m(\psi_m, g_{\mu\nu}) \quad (3.9)$$

where we have set $f(\phi) \to \phi$ without loss of generality and introduced ω as another generic function. $\omega(\phi)$ is an arbitrary function and studying its limits it is possible to reduce the theory to General Relativity. Varying the action with respect to

the metric and the scalar field we obtain the equation of motion for this particular theory. While being very different from Einstein equations, we have to apply the costraints that on smaller scales, like in the Solar System, it is necessary to recover General Relativity. Therefore, different so called *screening mechanisms* can be introduced (for a review: Joyce et al. 2015), according to the theory involved. For instance, screening could be provided by regions with strong Newtonian potentials. In this case, matter density contribution appears in the effective potential to which the scalar field responds. Thus, a careful choice of the gravitational potential can allow for screening. Two realizations of this kind of screening are the *chameleon* (Khoury and Weltman 2004b, Khoury and Weltman 2004a) and *symmetron* mechanisms (Hinterbichler and Khoury 2010). Another kind of screening can be identified in the derivatives of the scalar field. An example of a theory of this type is K-mouflage (Babichev et al. 2009), but it can also be present in generic models with kinetic interactions (Brax, Burrage, et al. 2013). These are mechanisms which shut off the fifth force when the local gravitational acceleration, $\vec{a} = -\vec{\nabla}\Phi$, exceeds some critical value. *kinetic screening* Armendariz-Picon et al. 2001 relies on the first derivatives, while the *Vainshtein effect* (Vainshtein 1972) involves higher order derivatives.

3.2 The Effective Field Theory approach

As a matter of fact, Nature comes in all kind of sizes. Galaxies, planets, molecules, atoms and nuclei have all different sizes, all held togheter by different binding energies. Luckily, we do not need to have a all-comprehensive description to understand how Nature works in a particular scale. The mathematical framework we can use shares the same pecularity of Nature: it automatically limits the role which smaller scales come into play when describing larger objects. This property has many practical applications as it let us oversee and neglect certain contributions when compared to the scale at hand. It is possible to find a systematic identification when different scales enter into calculations, providing a remarkable tool when analysing two different scales, $l << L$. In these cases it is usually profitable to expand quantities in the powers of the small parameter, l/L. This is the general gist but eventually the building blocks of an Effective Field Theory can be boiled down to a few and simple rules: specify the symmetries of the theory, identify the low energy fields, and write down all the different operators in the action consistent within the symmetry. As we said, the power of the EFT lies in the fact that there's some systematic expansion over some small parameter (often by derivatives) which tells us what terms we can ignore to a given order of accuracy. As the name suggests, EFTs are only *effective* descriptions, valid only in the range prescribed, usually identified by a specific scale called *cutoff*. While in the vailidity range, it is called *infrared theory*, and beyond this energy scale, the theory stops being predictive and new elements need to be introduced. Such high-energy parent theory is called *ultraviolet (UV) theory*.
This approach was firstly introduced in condensed matter physics and in particle physics theory but over the last decade the theoretical cosmology community has increasingly shifted towards the viewpoint that the effective field theory (EFT) framework offers the most promising and robust arena in which to explore extensions

of ΛCDM. When exploring outside the range of General Relativity we get to what we call *modified gravity*, but we are forced to face the fact that any infrared theory departing from GR implies additional degrees of freedom, as a consequence of Lovelock's theorem (Lovelock 1971, Lovelock 1972). To put it simply, Lovelock's theorem says that from a local gravitational action which contains only second derivatives of the four-dimensional spacetime metric, then the only possible equations of motion are the Einstein field equations. Therefore, the simplest modification is to introduce an extra scalar degree of freedom to General Relativity, and this degree can be thought as a Goldstone field of broken time translations in an expanding Universe. On the other hand spatial diffemorphisms are preserved. This peculiar situation, of an expanding Universe, works well with the choice of the so called unitary gauge (i.e. the guage where the fluctuations of the scalar field $\delta\phi = 0$, see below for details) since it allows us to write down the most general action for cosmological perturbations, without relying on any specific model, and thus being e good description of modified gravity. This procedure was first applied to inflation (Cheung et al. 2008) but eventually spread to DE/MG models (Gubitosi et al. 2013, Jérôme Gleyzes, Langlois, and Vernizzi 2014, Frusciante and Perenon 2020). Considering the latter, not only a vast amount of DE/MG models can be recovered from the general action, but also it is possible to recover the so called "Hordenski theories" (Horndeski 1974), by requiring that the linear perturbation equations contain derivatives up to second order. In addition, from this general EFT, new scalar-tensor theories have sparked (GLVP for instance in Jérôme Gleyzes, Langlois, and Vernizzi 2014); moreover, the EFT approach encodes theories such as Horava's gravity (Horava 2009), degenerate higher-order scalar-tensor (DHOST) theories (Langlois and Noui 2016, Jérôme Gleyzes, Langlois, Piazza, et al. 2015b), massive bi-gravity (Hassan and Rosen 2012), up to the point that there's been progress even in extending the framework to include non-linear perturbative effects (Bellini, Jimenez, et al. 2015, Bellini, Nicola Bartolo, et al. 2012). The idea behind building an EFT for cosmological models is to apply this EFT directly to cosmological perturbations, by treating them as Goldstone bosons of spontaneously broken time-translations. The analogy is with the spontaneous breaking of the $SU(2) \times U(1)$ gauge symmetry in the Standard Model. In the unitary gauge the would-be Goldston bosons are "eaten" by the longitudinal degrees of freedom of $W_{\pm}$ and Z. While loosing manifest gauge invariance, one can deal directly, at the EFT level, with the observable low energy degrees of freedom: three massive vector bosons and the Higgs particle. The use of unitary gauge brings into cosmology similar advantages. Historically, the approach to EFT for DE/MG (from now on simply DE), followed to basic steps:

- It was assumed the validity of the weak equivalence principle (WEP) and therefore the existence of a metric $g_{\mu\nu}$ coupled to a matter field ψ through the action $S[g_{\mu\nu}, \psi]$;
- The action was written in the unitary gauge, so that the most general gravitational action for a metric compatible with the symmetries of unbroken spatial diffeomorphisms is recovered.

The first assumption makes it natural to work in the Jordan frame since it is univocally defined by the coupling to matter, once WEP is postulated, and it is more

directly connected to observations. While the Jordan frame is still the standard frame where the interpretation of cosmological meausrements are performed, the WEP assumption can be relaxed considering a frame where the gravitational interaction between the new DoF and the matter fields is explicit. However, since the aim of this section is to introduce the EFT, it is convenient to keep the WEP assumption and treat the direct couplings later on. The EFT action is constructed in the unitary gauge and written in terms of relevant operators compatible with residual symmetries. These operators are expressed in powers of the number of perturbations and spatial derivatives. Let's start by describing the background and the unitary gauge.

3.2.1 The Background and the Unitary gauge

In this framework, the background is assumed to be homogeneous and isotropic, so the Friedmann-Lemaitre-Robertson-Walker (FLRW) line element is considered:

$$ds^2 = -dt^2 + a(t)^2 \left(\frac{dr^2}{1 - kr^2} + r^2 d\Omega^2 \right) \tag{3.10}$$

where $a(t)$ is the sacale factor, t is the cosmic time, k is the spatial curvature constant and $d\Omega^2$ is the solid angle.
Given this background, let's see what are the rules for writing down the most general Lagrangian in the unitary gauge. The unitary gauge is also known as the velocity orthogonal gauge. It corresponds to the choice of gauge in which the perturbation of the extra scalar DoF, responsible of the spontaneous symmetry breaking, vanishes. Consider a scalar field $\phi(t, x)$ and its decomposition in a perturbed FLRW metric as follows:

$$\phi(t, \vec{x}) = \tilde{\phi(t)} + \delta\phi(t, \vec{x}) \tag{3.11}$$

where $\vec{x}$ are the spatial coordinates, $\tilde{\phi(t)}$ is the homogeneus background value of the scalar field, and $\delta\phi$ is the perturbation. The unitary gauge is the one in which the time coordinate t is chosen so that the perturbation vanishes, so the additional DoF does not explicitly appear in the action. The choice is then to set $t = t(\phi)$. With this choice ϕ defines a preferred time slicing where $\phi = const$ and constant time hypersurfaces coincide with constant scalar field hypersurfaces. We can now understand the name *velocity orthogonal gauge*: the gradient of the scalar field is orthogonal to the constant time hypersurfaces. The choice of the unitary gauge implies that the action that we will recover will not show any explicit dependence on the scalar field, so that the EFT actions will be built on geometrical quantities and the metric only. In addition, the unitary gauge breaks the full diffeomorphisms invariance leaving unbroken the subgroup of time-dependent spatial diffeomorphisms. One can therefore build various terms:

- terms which are invariant under unbroken diffeomorphisms (such as polynomials of the Riemann tensor and of its covariant derivatives, contracred to give a scalar)
- The gradient $\partial_\mu \phi$ becomes δ^0_μ in the unitary gauge.

- It is useful to define a unit vector perpendicular to surfaces of constant $\tilde{t}$

$$n_\mu = \frac{\partial_\mu \phi}{\sqrt{-g^{\mu\nu}\partial_\mu\phi\partial_\nu\phi}} = -\frac{\partial_\mu\phi}{\sqrt{-(\partial_\mu\phi)^2}} = \frac{\delta^0_\mu}{\sqrt{-g^{00}}} \tag{3.12}$$

  This allows to define the induced spatial metric on sufaces of contant ϕ. Every tensor can be projected on these surfaces using $h_{\mu\nu} = g_{\mu\nu} + n_\mu n_\nu$.

- Additional possibilities will come from the covariant derivatives of $\partial_\mu\phi$ or equivalently from the covariant derivatives of n_μ: the derivative acting on the normalization factor just gives terms which are covariant on their own and can be used in the unitary gauge Lagrangian. The covariant derivative of n_ν projected on the surfaces of constant ϕ gives the extrinsic curvature of these surfaces

$$K_{\mu\nu} = h^\sigma_\mu \nabla_\sigma n_\nu. \tag{3.13}$$

  The index ν is already projected on the surface because $n^\nu\nabla_\sigma n_\nu = \frac{1}{2}\nabla_\sigma(n^\nu n_\nu) = 0$. The covariant derivative of n_ν perpendicular to the surface can be rewritten as

$$n^\sigma\nabla_\sigma n_\nu = -\frac{1}{2}(-g_{00})^{-1}h^\mu_\nu\partial_\mu(-g^{00}). \tag{3.14}$$

  Therefore all covariant derivatives can be rewritten in terms of $K_{\mu\nu}$ and g^{00}.

- A generic function of ϕ becomes $f(t)$ in the unitary gauge so that we can use generic functions of time in front of any terms of the action.

Considering in particular this last point, the symmetry of the action is still satisfied if each operator is accompanied by a time dependent function. These functions of time which scale with the perturbations on the FRLW background are called *EFT functions*. Unlike standard covariant approaches, the EFT action is built on a perturbative fashion. Thus, operators, let's call one B, will be written as $B(t, x_i) = \tilde{B}(t) + \delta B(t, x_i)$. This perturbation scheme enables us to write an action up to any order. In a cosmological context one usually stops at linear order perturbations. We can conclude that the most generic action in the unitary gauge is given by

$$S = \int d^4x\sqrt{-g}F(R_{\mu\nu\rho\sigma}, g^{00}, K_{\mu\nu}, \nabla_\mu, t), \tag{3.15}$$

where all the free indices inside the function F must be upper 0's. Before presenting the full actions, it is better to spend few words on the validity and shortcomings of this EFT framework. If we consider the regime of applicability of such action, it spans from the largest cosmological scales up to the ultraviolet cut-off. If we consider a linear regime, the cut-off, shall it be M_{cut}, must be larger than the Hubble parameter at present day, H_0, so that the cosmological background and observable perturbation modes can be described. However the linear framework can be expanded to mildly non-linear scales by including appropriate operators and EFT functions. Both the linear and non-linear regimes are regulated by strong coupling scale of dark energy and the screening effect. The former corresponds to the scale at which non-linear interactions of the EFT exit perturbative unitarity, thus setting a

cut-off for predictability and where UV completition becomes necessary. The latter is associated to the non-linear scale of the extra scalar field, but if the screening is weak, the linear EFT is still valid.
Of the full action there are several versions and notations (Gubitosi et al. 2013, Bloomfield et al. 2013, Jerome Gleyzes et al. 2013, Piazza et al. 2014, B. Hu et al. 2017, Tsujikawa 2015). We report here the action up to second order in perturbations, using the notation as presented for the first time. This EFT actions reads (Gubitosi et al. 2013):

$$\begin{aligned} S = \frac{1}{2}\int d^4x\sqrt{-g}\,\big[&M_{\rm pl}^2 \mathrm{f}(t)R - 2\Lambda(t) - 2c(t)g^{00} \\ &+ M_2^4(t)\left(\delta g^{00}\right)^2 - \bar{M}_1^3(t)\delta g^{00}\delta K - \bar{M}_2^2(t)\delta K^2 \\ &- M_3^2(t)\delta K^\nu_\mu \delta K^\mu_\nu + \mu_1^2(t)\delta g^{00}\delta R + m_2^2(t)h^{\mu\nu}\partial_\mu g^{00}\partial_\nu g^{00} \\ &+ \ldots] + S_m\left[g_{\mu\nu}, \chi_m\right] \end{aligned} \tag{3.16}$$

In this equation: M_{pl} is the Planck Mass; g is the determinant of the metric; $g^{00} = -1 + \delta g^{00}$; δR and $\delta R_{\mu\nu}$ are the perturbations of the Ricci scalar and tensor; S_m is the matter action for all the matter fields χ_m; $f, \Lambda, c, M_i, \bar{M}_i, \bar{m}_i, m_i, \mu_i$ are the so called EFT functions (Gubitosi et al. 2013). In the first line of the equations we read the operators contributing both to the background evolution of the Universe and the linear perturbation equations, as we will see later. Therefore, the functions f, Λ, c are known as *background* EFT functions, while operators in the second and third line enter only in the perturbation equations. The EFT function M_2^4 is sourced by a non-standard kinetic term of the scalar field, $\bar{M}_1^3$ is sourced by the mixing between the metric and the scalar field, $\bar{M}_2^2$ is related to a non-standard speed of gravitational waves, while all the other functions describe deviations from Hordenski models. We omitt second order operators or higher order terms, which are hinted in the ellipsis in the third line. The advantage of this action is that it can be used both independently, without assuming any model, or it can be reshaped so that specific models can be recovered (for a review:Frusciante, Peirone, et al. 2020). The first approach is called *pure* EFT approach and it consists in selecting all the EFT functions or a sub-set of them to identify general features of gravity without assuming any specific model. On the other hand, it is possible to encode specific models in the EFT through a mapping procedure, which will be explained later. Other than the possibility of studying one specific model in detail, the advantage of this procedure can be exploited on the computational side too. We will see it better later on, but the idea is that it is faster to compute results for the general EFT action and then map them to specific models, rather then set up different computations, one for each model considered. The EFT action obtained is written in the unitary gauge which is useful from a theoretical standopoint if we want to identify the relevant operators at large scales. In addition, as said, it allows to select sub-classes of models to study, yet it is not convenient if we want to look at the evolution of the extra scalar field and the metric perturbations separately. In the unitary gauge, the extra degree of freedom is hidden in the metric and it is possible to make such field appear through the *Stuckelber trick* (Gubitosi et al. 2013). Without going into detail, the idea is to restore the full diffeomorphism invariance forcing

back the broken gauge transformation, imposing

$$t \to t + \pi(x^\mu) \tag{3.17}$$

where π is the perturbation of the scalar field. Time translation is restored and induces time dependent functions in the action. Recasting the action while keeping this restored transformation in mind, it is possible to obtain the dynamical equation for the extra degree of freedom. Considering once again the unitary gauge action, it is interesting now to see what background solutions can be obtained from a model independent EFT.

3.2.2 Modified Friedmann Equations

In order to obtain the modified background Friedmann equations for MG/DE models we vary the action with respect to g^{00}. We can intuitively predict that these equations will depend on the EFT characterizing the background evolution (f, Λ, c). We get:

$$c = M_{pl}^2 f \left(-\dot{H} + \frac{k}{a^2} - \frac{1}{2}\frac{\ddot{f}}{f} + \frac{H}{2}\frac{\dot{f}}{f} \right) - \frac{1}{2}(\rho_m + p_m) \tag{3.18}$$

$$\Lambda = M_{pl}^2 f \left(\dot{H} + 2\frac{k}{a^2} + \frac{1}{2}\frac{\ddot{f}}{f} + \frac{5H}{2}\frac{\dot{f}}{f} + 3H^2 \right) - \frac{1}{2}(\rho_m - p_m) \tag{3.19}$$

As we know, the set of equations is complete only if we include the the matter continuity equation, here assumed to be a perfect fluid:

$$\dot{\rho}_m + 3H(\rho_m + p_m) = 0. \tag{3.20}$$

We can rewrite ρ_{DE} and p_{DE} in terms of f, Λ, c:
The modified Friedmann equations can be rewritten following the fluid description:

$$H^2 + \frac{k}{a^2} = \frac{1}{3M_{pl}f}(\rho_m + \rho_{DE}) \tag{3.21}$$

$$\dot{H} - \frac{k}{a^2} = -\frac{1}{2M_{pl}f}(\rho_m + p_m + \rho_{DE} + p_{DE}), \tag{3.22}$$

If we now include a "dark fluid" $(\rho_{DE} + p_{DE})$ with

$$\rho_{DE} = c + \Lambda - 3H\dot{f}M_{pl}^2 \tag{3.23}$$

$$p_{DE} = c - \Lambda + 2H\dot{f}M_{pl}^2 + \ddot{f}M_{pl}^2, \tag{3.24}$$

we can recover an equation governing the behaviour of ρ_{DE}:

$$\dot{\rho}_{DE} + 3H(\rho_{DE} + p_{DE}) = 3M_{pl}^2\dot{f}(H^2 + \frac{k}{a^2}) \tag{3.25}$$

These results are completely general and not related to a specific model. The equations have 4 unknowns: the background EFT functions and the expansion history H. Therefore 2 of these must be fixed and the remaining can be obtained through the equations. Which to fix have non trivial repercussions: for instance it is possible to fix H to that of ΛCDM but this aslo fixes strong hypotheses on the behaviour of the underlying gravity model.

3.2.3 Stability conditions

We have built the general framework in MG models can be embedded. Now we need to set the theoretical boundaries that such a general approach can have, specifically pathological instabilities, such as ghosts (Gumrukcuoglu et al. 2016,Carroll et al. 2003,Cline et al. 2004, Sbisà 2015), gradient and tachyionic instabilities (De Felice, Frusciante, et al. 2017). It is important to assess these possible problems since they can help constraining the parameter space of specific models while testing gravity with statistical tools. It could happen that these instabilities could even dominate over the constraining power of data. Since instabilities are related to the extra scalar and the matter fields, the latter can contribute to the instability condition. Hence, there raises the need for a consistent expression for the matter action and the most appropriate choice until now is the Sorokin-Schutz action (Schutz and Sorkin 1977), which we mention for completeness. With this matter action, combined with the EFT action, it is possible to construct an action for scalar modes and one for tensor modes (i.e. gravitational waves). One can then construct this action S made by the EFT action (3.16) (S_{EFT}) and the Sorkin-Schutz one (S_m), $S = S_{EFT} + S_m$. The action S then includes one DoF for the gravity sector, namely ζ, defined as the scalar perturbation of ${h_{ij}}^2$, as many DoFs, $\delta_{m,i}$, as matter fluids considered and the tensor modes h^t_{ij}. As a result one obtain an action for scalar modes (S_s) and one for tensor modes (S_T). In Fourier space they have the following compact forms:

$$\begin{aligned} S^s &= \frac{1}{(2\pi)^3}\int d^3k dt a^3 \left(\dot{\vec{\chi}}^t \mathbf{A}\dot{\vec{\chi}} - k^2\vec{\chi}^t\mathbf{G}\vec{\chi} - \dot{\vec{\chi}}^t\mathbf{B}\vec{\chi} - \vec{\chi}^t\mathbf{M}\vec{\chi}\right), \\ S^T &= \frac{1}{(2\pi)^3}\int d^3k dt a^3 \frac{M^2(t)}{8}\left[\left(\dot{h}^T_{ij}\right)^2 - c_t(t)^2\frac{k^2}{a^2}\left(h^T_{ij}\right)^2\right], \end{aligned} \tag{3.26}$$

where $\vec{\chi}^t = (\zeta, \delta_i)$ is a dimensionless vector and A, G, B, M are matrices whose coefficients are combinations of EFT functions and some matrices also manifest a k dependence. We refer the reader to De Felice, Frusciante, et al. 2017 for further details and the complete expressions of the matrices. Finally, $M^2(t)$ and $c^2(t)$ are respectively the effective Planck mass and the speed of propagations of tensor modes. In section 3.4 we provide their expressions in terms of EFT functions. Let us see the three main sources of instability:

- The *Ghost instability* corresponds to having modes with negative kinetic energy. In this case the high energy vacuum is unstable to the spontaneous production of particles(Cline et al. 2004, Carroll et al. 2003). Such a pathology is regulated by demanding for a positive kinetic term if only one field is involved, or a positive kinetic matrix if more fields define the system. In the scalar modes action such condition corresponds to requiring A to be positive definite, i.e. all eigenvalues must be strictly positive. The condition is imposed only in the high energy regime because the ghost instability generated

[2]The Anowitt-Deser-Misne (ADM) metric (which we will describe better later) perturbations for the scalar and tensor components reads: $ds^2 = -(1+2\delta N)dt^2 + 2\partial_i\psi dt dx^i + a^2\left[(1+2\zeta)\delta_{ij} + h^T_{ij}\right]dx^i dx^j$, where $\delta N(t,\vec{x})$ is the perturbation of the lapse function, $\partial\psi(t,\vec{x})$ is the scalar perturbation of the shift function, $\zeta(t,\vec{x})$ of the three dimensional metric and $h^T_{ij}(t,\vec{x})$ are the perturbed metric components which contribute to tensor modes.

in the infrared regime corresponds to the physical phenomenon of the Jeans/tachyonic instability (Gumrukcuoglu et al. 2016), which can be controlled demanding for specific conditions, as we will discuss in the following. Let us note that in the case of the EFT framework, one has to consider that such approach is valid up to a certain cutoff scale.

- The *Gradient or Laplacian instability* corresponds when there is a degree of freedom characterized by a negative squared speed of its fluctuations. This means exponentially growing modes and it is manifest in the high-modes regime. The prescription is to require positive speeds.

- The *Tachyonic and Jeans instabilities* are the less severe instabilities and they appear when the DoF has a negative mass squared. In particular, they arises when the perturbations are not computed about the true vacuum of the theory (Joyce et al. 2015). In order to account for this pathology, one can look at the boundedness of the Hamiltonian at low momenta. These conditions are less explored with respect to the no-ghost/nogradient conditions and a full and general derivation in the context of the EFT framework is done in De Felice, Frusciante, et al. 2017. Starting from the above action (3.26), it is possible to obtain the associated Hamiltonian, namely $\mathcal{H}(\Phi_i, \dot{\Phi}_i)$ of canonical fields Φ_i, which in the case of one fluid assumes the form

$$\mathscr{H}\left(\Phi_i, \dot{\Phi}_i\right) = \frac{a^3}{2}\left[\dot{\Phi}_1^2 + \dot{\Phi}_2^2 + \mu_1(t,k)\Phi_1^2 + \mu_2(t,k)\Phi_2^2\right] \tag{3.27}$$

  where μ_1 and μ_2 are the mass eigenvalues. The Hamiltonian is unbounded from below if the mass eigenvalues are negative, i.e. $\mu_i(t,0) < 0$. Requiring $\mu_i > 0$ would result in a too stringent condition. A less severe request, if the μ_i are negative, is to demand they satisfy the condition $|\mu_i(t,0)| \lesssim H^2$. In this case the time scale of evolution of the instability is larger than the Hubble time so that it will not affect the stability of the system. Such condition will allow to have μ_i negative at some times. This behavior is known as Jeans instability and it is necessary in order for structures to form.

3.2.4 Gravitational couplings

Considering linear scalar perturbations around a FLRW background in the Newtonian gauge, it can be shown that the Newtonian potential, and intrinsic spatial curvature, on sub-horizon scales and with the *quasi-static approximation* (QS)[3], are related to gauge-invariant comoving matter density fluctuations through a modified Poisson equation and a modified lensing equation (Amendola et al. 2007, Pogosian, Silvestri, et al. 2010, Bertschinger and Zukin 2008). In scalar-tensor theories, two new phenomenological functions appear and will play a pivotal role when considering cosmological probes (Pogosian and Silvestri 2016). The *effective gravitational coupling* or the effective Newton constant $\mu(t,k)$ characterizes the modifications of gravity on the clustering of matter. The *light deflection parameter* $\Sigma(t,k)$ describes

[3]The quasi-static approximation prescribes to neglect terms with time derivatives in the Einstein equations for linear perturbations.

the modifications of gravity on null geodesics. The mathemtical definition of these functions comes from the line element in Newtonian gauge (2.1) and are defined in Fourier space as:

$$-\frac{k^2}{a^2}\Psi = 4\pi G_N \mu(t,k)\rho_m \Delta_m, \qquad -\frac{k^2}{a^2}(\Psi+\Phi) = 8\pi G_N \Sigma(t,k)\rho_m \Delta_m \tag{3.28}$$

where G_N is the Newtonian gravitational constant, $\Delta_m = \delta_m + 3\frac{Hv}{k}$ is the comoving density contrast, being v the irrotational component of the peculiar velocity. Galaxy number counts and Redshift Space Distortion data are direct probes of μ, while Σ measures the deviation in the potential $\frac{\Psi+\Phi}{2}$ and can be probed through the lensing of light. (Amendola et al. 2007) We can define a combination of the two functions, called *gravitational slip parameter*:

$$\eta(t,k) = \frac{\Phi}{\Psi} \tag{3.29}$$

and it is linked to the other two functions through:

$$\Sigma(t,k) = \frac{\mu(t,k)}{2}(1+\eta(t,k)). \tag{3.30}$$

We can see that for $\Sigma = \mu = \eta = 1$ we recover General Relativity. It is necessary to stress that Σ and μ being different from 1 can actually quantify the discrepancy from General Relativity, thus making these functions optimal probes. Usually the values of the functions are obtained through numerical computantions, specifically because analytical forms is generally not possible. However, it is possible to link them to specific theories in the QS approximation. Numerical computation consider the full linear perturbative equations of the EFT formulation, making the EFT approach advantageous. In addition, if we consider the QS limit, algebraic expressions in terms of EFT functions can be found for these phenomenological functions.

3.2.5 Mapping Procedure

The power of the EFT approach relies on its capability to encompass DE/MG models with a single additional DoF. However, it is still possible to *map* specific theories in the EFT language and match the operators with the general EFT action. In this subsection we will sketch the methodology for a general recipe of mapping and we will comment on how the procedure allows for writing numerical codes for solving the coupled Boltzmann-Equations of gravity in a perturbative fashion.
In order to map a theory we can use two paths: one more related to the theory considered and one totally general. The first consists in starting from the covariant action of a specific model and impose the unitary gauge. This is the usual procedure when trying to find the EFT equivalent of the ultraviolet model at play. For instance, if we consider the simple Quintessence model introduced at the beginning,

$$\mathcal{L}_{\mathcal{Q}} \sim -\frac{1}{2}(\partial\phi)^2 - V(\phi) \to -\frac{1}{2}\dot{\bar{\phi}}^2 g^{00} - V(\bar{\phi}) \tag{3.31}$$

where we applied the unitary gauge ($\delta\phi = 0$). When comparing to Eq. (3.16), we can see the correspondence of

$$c(t) = -\frac{1}{2}\dot{\bar{\phi}}^2, \qquad \Lambda(t) = V(\bar{\phi}). \tag{3.32}$$

While the steps are applicable to any theory, the actual computation is specific and computations can become convoluted in more complicated cases. Nevertheless it is a widespread approach and the results are useful from a computational point of view, which we will explain later. For an in-dept computation, we refer to Kase and Tsujikawa 2014. The general procedure involves the Anowitt-Deser-Misner (ADM) formalism (Arnowitt et al. 1959), for which the line element can be written as:

$$ds^2 = -N^2dt^2 + h_{ij}(dx^i + N^i dt)(dx^j + N^j dt) \tag{3.33}$$

where $N(t, x^i)$ is the lapse function, $N^i(t, x^i)$ the shift and $h_{ij}(t, x^i)$ is the three dimensional spatial metric. Using the ADM formalism, a general Lagrangian can be written as function of operators that depend on geometrical quantities

$$L(N, \mathcal{R}, \mathcal{S}, K, \mathcal{Z}, \mathcal{U}, \mathcal{Z}_1, \mathcal{Z}_2, \alpha_1, \alpha_2, \alpha_3, \alpha_4, \alpha_5; t) \tag{3.34}$$

where:

$$\begin{aligned} &\mathcal{S} = K_{\mu\nu}K^{\mu\nu}, \mathcal{Z} = \mathcal{R}_{\mu\nu}\mathcal{R}^{\mu\nu}, \mathcal{U} = \mathcal{R}_{\mu\nu}K^{\mu\nu} \\ &\mathcal{Z}_1 = \nabla_i\mathcal{R}\nabla^i\mathcal{R}, \mathcal{Z}_2 = \nabla_i\mathcal{R}_{jk}\nabla^i\mathcal{R}^{jk}, \alpha_1 = a^i a_i \\ &\alpha_2 = a^i\Delta a_i, \alpha_3 = \mathcal{R}\nabla_i a^i, \alpha_4 = a_i\Delta^2 a^i, \alpha_5 = \Delta\mathcal{R}\nabla_i a^i \end{aligned} \tag{3.35}$$

where specifically a_ν is the acceleration of the normal vector and $\Delta = \nabla\nabla$. The operators considered describe gravity up to sixth order spatial derivatives. Since we want to refer to the EFT action (3.16), we only need $\mathcal{L}(N, \mathcal{R}, \mathcal{S}, K, \alpha_1; t)$. The next step is to expand the Lagrangian up to quadratic order when perturbing the operators and match it with the EFT action written in the ADM formalism. Expanding the operators, we obtain

$$\begin{aligned} S_{ADM} = \int d^4x\sqrt{-g}\Big[&\bar{L} + \dot{\mathcal{F}} + 3H\mathcal{F} + \left(L_N - \dot{\mathcal{F}}\right)\delta N \\ &+ \left(\dot{\mathcal{F}} + \frac{1}{2}L_{NN}\right)(\delta N)^2 + L_{\mathcal{S}}\delta K^\nu_\mu\delta K^\mu_\nu + \frac{1}{2}\mathcal{A}(\delta K)^2 \\ &+ \mathcal{B}\delta N\delta K + \mathcal{C}\delta K\delta\mathcal{R} + L_{N\mathcal{R}}\delta N\delta\mathcal{R} + L_{\mathcal{R}}\delta\mathcal{R} \\ &+ \frac{1}{2}L_{\mathcal{R}\mathcal{R}}\delta\mathcal{R}^2 + L_{\alpha_1}\partial_i\delta N\partial^i\delta N\Big], \end{aligned} \tag{3.36}$$

where $\bar{L}$ is the background expressions, $L_{\mathcal{S}}$ the derivative of L with respect to $\mathcal{S}$ and so on. For the others:

$$\begin{aligned} &\mathcal{A} = L_{KK} + 4H^2L_{\mathcal{S}\mathcal{S}} + 4HL\mathcal{S}K, \qquad \mathcal{B} = L_{KN} + 2HL_{\mathcal{S}N} \\ &C = L_{KR} + 2HL_{\mathcal{S}R}, \qquad \mathcal{F} = L_K + 2HL\mathcal{S}, \end{aligned} \tag{3.37}$$

ff we write the EFT action in the ADM formalism. We skip the manipulations which are based on the application of the Gauss-Codazzi relations (Gourgoulhon

2007). These are geometrical relations that relate to the extrinsic and intrinsic curvature:

$$\begin{aligned} S_{EFT} = \int d^4x\sqrt{-g}\Bigg\{ & \frac{M_{\rm pl}^2}{2}\mathfrak{f}\mathcal{R} + 3H^2M_{\rm pl}^2\mathfrak{f} + 2\dot{H}M_{\rm pl}^2\mathfrak{f} + 2M_{\rm pl}^2H\dot{\mathfrak{f}} + M_{\rm pl}^2\ddot{\mathfrak{f}} \\ & + c - \Lambda + \left[H\dot{\mathfrak{f}}M_{\rm pl}^2 - 2\dot{H}M_{\rm pl}^2\mathfrak{f} - M_{\rm pl}^2\ddot{\mathfrak{f}} - 2c\right]\delta N - \left(M_{\rm pl}^2\dot{\mathfrak{f}} + \bar{m}_1^3\right)\delta K\delta N \\ & + \frac{1}{2}\left[M_{\rm pl}^2\mathfrak{f} - \bar{M}_3^2\right]\delta K_\nu^\mu\delta K_\mu^\nu - \frac{1}{2}\left[M_{\rm pl}^2\mathfrak{f} + \bar{M}_2^2\right](\delta K)^2 + \mu_1^2\delta N\delta\mathcal{R} + \\ & \left[2\dot{H}M_{\rm pl}^2\mathfrak{f} + \ddot{\mathfrak{f}}M_{\rm pl}^2 - HM_{\rm pl}^2\dot{\mathfrak{f}} + 3c + 2M_2^4\right](\delta N)^2 + 4m_2^2h^{\mu\nu}\partial_\mu\delta N\partial_\nu\delta\Bigg\} \end{aligned} \tag{3.38}$$

And now we compare the equations and identify the operators (*map*)

$$\begin{aligned} & \mathfrak{f}(t) = \frac{2}{M_{\rm pl}^2}L_{\mathcal{R}}, \quad c(t) = -\frac{1}{2}\left(L_N + \dot{\mathcal{F}}\right) + \left(H\dot{L}_{\mathcal{R}} - \ddot{L}_{\mathcal{R}} - 2L_{\mathcal{R}}\dot{H}\right), \\ & \Lambda(t) = -\bar{L} + \dot{\mathcal{F}} + 3H\mathcal{F} + 2\left(3H^2L_{\mathcal{R}} + \ddot{L}_{\mathcal{R}} + 2H\dot{L}_{\mathcal{R}} + 2\dot{H}L_{\mathcal{R}}\right) + c, \\ & \bar{M}_2^2(t) = -\mathcal{A} - 2L_{\mathcal{R}}, \quad M_2^4(t) = \frac{1}{2}\left(L_N + \frac{L_{NN}}{2}\right) - \frac{c}{2}, \\ & \bar{m}_1^3(t) = -\mathcal{B} - 2\dot{L}_{\mathcal{R}}, \quad \bar{M}_3^2(t) = -2L_{\mathcal{S}} + 2L_{\mathcal{R}}, \\ & m_2^2(t) = \frac{L_{\alpha_1}}{4}, \quad \mu_1^2(t) = L_{N\mathcal{R}}. \end{aligned} \tag{3.39}$$

We have just sketched the main steps and results of the procedure, and we refer the reader for more details and the full computations. A practical example is a clearer way to show the actual computations: let's consider then a $f(R)$ theory with the Lagrangian

$$S_f = \int d^4x\sqrt{-g}\frac{M_{pl}^2}{2}[R + f(R)] \tag{3.40}$$

where $f(R)$ is a general function of the four dimensional Ricci scalar. Following the prescription, we expand around the background value of the Ricci scalar $\bar{R}$:

$$S_f = \int d^4x\sqrt{-g}\frac{M_{pl}^2}{2}\left\{[1 + \frac{df}{dR}(\bar{R})]R + f(\bar{R}) - \bar{R}\frac{df}{dR}(\bar{R})\right\} \tag{3.41}$$

Now we use the Gauss-Codazzi relation to write the action in the ADM formalism:

$$\begin{aligned} S_f = \int d^4x\sqrt{-g}\frac{M_{pl}^2}{2}\Bigg\{ & [1 + \frac{df}{dR}(\bar{R})][\mathcal{R} + \mathcal{S} - K^2] \\ & + \frac{2}{N}\dot{f}_R K + f(\bar{R}) - \bar{R}\frac{df}{dR}(\bar{R})\Bigg\} \end{aligned} \tag{3.42}$$

from which it is possible to identify

$$\mathfrak{f}(t) = 1 + \frac{df}{dR}(\bar{R}) \qquad\qquad \Lambda(t) = \frac{M_{pl}^2}{2}f(\bar{R}) - \bar{R}\frac{df}{dR}(\bar{R}). \tag{3.43}$$

3.2.6 EFTCAMB

The link between theory and observations is exploited thanks to Einstein-Boltzmann codes constructed on top of the EFT framework. The one used in this thesis is the so called EFTCAMB (Raveri et al. 2014,B. Hu et al. 2017), a modification of the primary code CAMB[4]. CAMB (Code for Anisotropies in the Microwave Background) is a cosmology code for calculating CMB, lensing, galaxy count, dark-age 21cm power spectra, matter power spectra and transfer functions. There are also general utility functions for cosmological calculations such as the background expansion, distances, etc. The main code is Python with numerical calculations implemented efficiently in Python-wrapped modern Fortran. EFTCAMB is a patch of CAMB, which implements the Effective Field Theory approach to cosmic acceleration. The code can be used to investigate the effect of different EFT operators on linear perturbations as well as to study perturbations in any specific DE/MG model that can be cast into the EFT framework. In addition, it integrates a module that checks for instabilities in the models. To interface EFTCAMB with cosmological data sets, it is equipped with a modified version of CosmoMC (Lewis and Bridle 2002), namely EFTCosmoMC, creating a bridge between the EFT parametrization of the dynamics of perturbations and observations. In the case of our thesis, we exploited EFTCAMB to take into account specific models of gravity, and we used CAMB to compute the cross-correlations of CMB with LSS. There is one strong advantage in the computation with CAMB and EFTCAMB: they compute the cross-correlations *exactly* without any assumptions or simplifications that analytical results require. The structure of EFTCAMB code is illustrated in the flowchart of Figure 3.1 and exploits a flag system to control the behaviour of the code. In our case, we exploited the full mapping of different models to the EFT action, but the code has other functions too. We briefly explain the functionalities, which are recalled thorugh setting an EFTflag.

- EFTflag = 0: it corresponds to deactivating the EFT modification and the standard CAMB code is used
- EFTflag = 1: enables the *pure* EFT models. The *pure* approach relies on the parametrization of the EFT action through the choice of the EFT functions and the background expansion history, with the corresponding flags. After setting these flags the user has to define the values of the EFT model parameters for the chosen model.
- EFTflag = 2: in this case the built-in parametrization is not used and some other model-independent parametrization has to be implemented.
- EFTflag = 3: it is the *designer mapping* EFT procedure. In this case the matching of the EFT functions is provided and the background evolution is set.
- EFTflag = 4: it corresponds to the *full mapping*. In this case the background expansion history is not set by a choice of w_{DE} and the background equations have to be fully specified. The code will solve the background equations and

[4]https://camb.readthedocs.io/

map it into the EFT framework. Natively, only the low energy Horava gravity is included as a module, and therefore, in this work all the specific models we considered had to be implemented.

Figure 3.1: Flowchart describing the functionality of EFCAMB and its features, from B. Hu et al. 2017

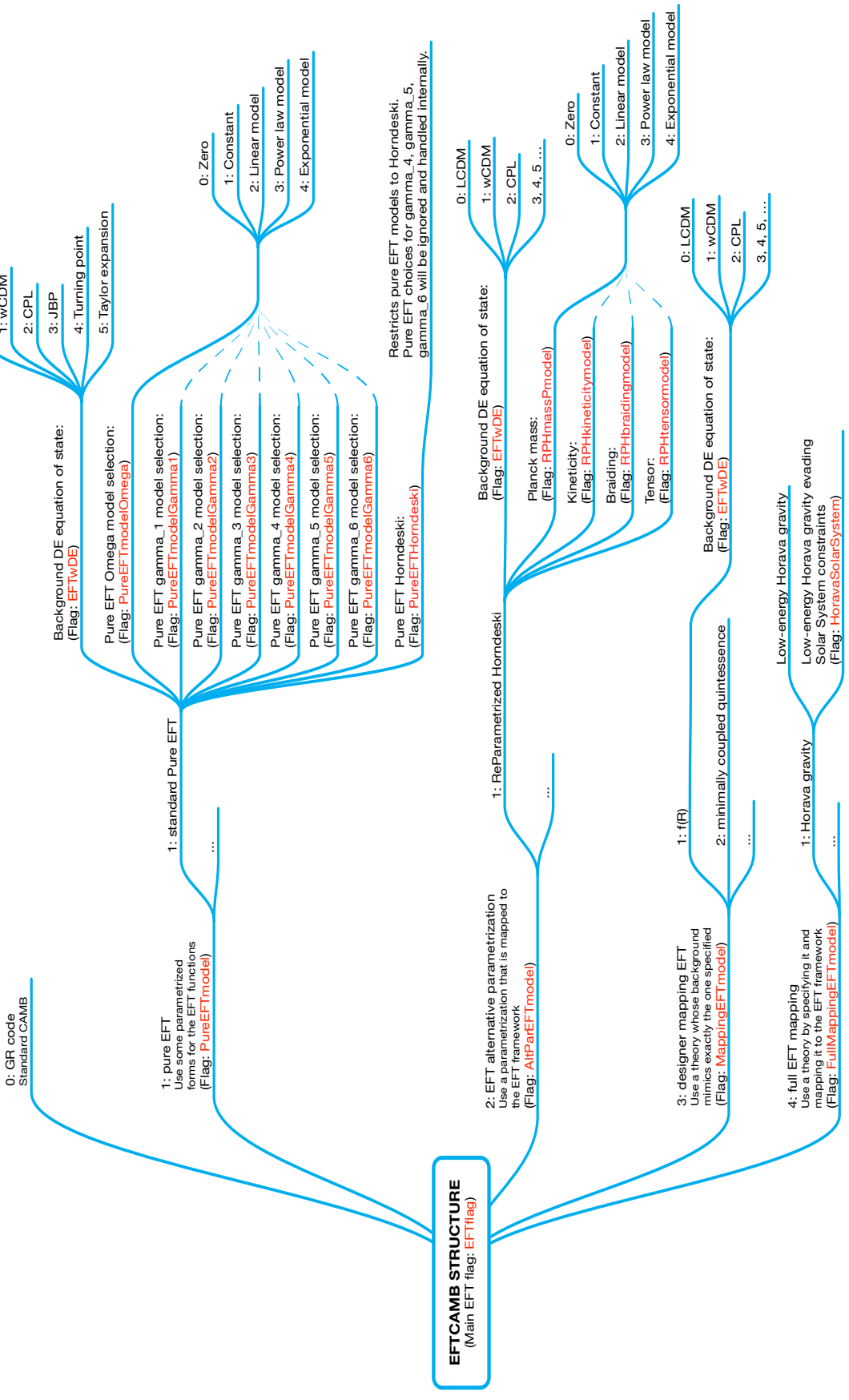

3.3 Horndeski Theories and Generalized Galileons

Since we consider tensor-scalar theories, it is useful to introduce the most general scalar-tensor theory. Historically, it was introduced ahead of time by Horndeski (1974), and only decades later was rediscovered. Coincidentally, the same result have been found by making the galileon theory of gravity covariant. Galileon modification of gravity was first introduced in Nicolis et al. (2009). The action of this model is constitued by 5 terms:

$$\begin{aligned}
\mathcal{L}_1 &= \phi \\
\mathcal{L}_2 &= \frac{1}{2}(\partial\phi)^2 \\
\mathcal{L}_3 &= \frac{1}{2}\Box\phi(\partial\phi)^2 \\
\mathcal{L}_4 &= \frac{1}{4}(\partial\phi)^2\left((\Box\phi)^2 - (\partial_\mu\partial_\nu\phi)^2\right) \\
\mathcal{L}_5 &= \frac{1}{3}(\partial\phi)^2\left((\Box\phi)^3 + 2\left(\partial_\mu\partial_\nu\phi\right)^3 - 3\Box\phi\left(\partial_\mu\partial_\nu\phi\right)^2\right)
\end{aligned} \tag{3.44}$$

that are invariant under the Galilean shift transformation

$$\phi(x) \to \phi(x) + c + b_\mu x^\mu \tag{3.45}$$

and lead to equations of motion that remain at second-order in field derivatives. Covariantizing the galileon Lagrangians, turns out to be rather subtle; the natural thing to do is to promote the background Minkowski metric to be a dynamical field and to promote partial derivatives to covariant derivatives. For the terms $\mathcal{L}_1 - \mathcal{L}_3$, this works fine. However, it turns out that the equations of motion following from the covariantized versions of the last two terms involve third derivatives of both the metric and the field, indicating that the coupled theory of galileons minimally coupled to gravity propagates a ghost (C. Deffayet, Esposito-Farese, et al. 2009). This problem can be removed, by introducing non-minimal couplings of the scalar field with gravity as (C. Deffayet, Esposito-Farese, et al. 2009):

$$\begin{aligned}
\mathcal{L}_1 &= \phi \\
\mathcal{L}_2 &= \frac{1}{2}(\nabla\phi)^2, \\
\mathcal{L}_3 &= \frac{1}{2}\Box\phi(\nabla\phi)^2, \\
\mathcal{L}_4 &= \frac{1}{4}(\nabla\phi)^2\left[(\Box\phi)^2 - (\nabla_\mu\nabla_\nu\phi)^2 - \frac{1}{4}(\nabla\phi)^2 R\right], \\
\mathcal{L}_5 &= \frac{1}{3}(\nabla\phi)^2\left[(\Box\phi)^3 + 2\left(\nabla_\mu\nabla_\nu\phi\right)^3 - 3\Box\phi\left(\nabla_\mu\nabla_\nu\phi\right)^2 - 6G_{\nu\rho}\nabla_\mu\phi\nabla^\mu\nabla^\nu\phi\nabla^\rho\phi\right]
\end{aligned} \tag{3.46}$$

The global galilean symmetry is now broken. The most general Lagrangian which couples a scalar field to gravity non-minimally, and which has second order equations of motion is for the so-called generalized galileons, in C. Deffayet, Deser, et al. (2009), inspired exactly by this interest in covariantizing the galileon theory:

$$\begin{aligned}\mathcal{L}_{\text{gen.gal.}} &= G_2(\phi,X) - G_3(\phi,X)\Box\phi + G_4(\phi,X)R + G_{4,X}(\phi,X)\left[(\Box\phi)^2 - (\nabla_\mu\nabla_\nu\phi)^2\right] \\ &+ G_5(\phi,X)G_{\mu\nu}\nabla^\mu\nabla^\nu\phi \\ &- \frac{1}{6}G_{5,X}(\phi,X)\left[(\Box\phi)^3 - 3(\Box\phi)\left(\nabla_\mu\nabla_\nu\right)^2 + 2\nabla^\mu\nabla_\alpha\phi\nabla^\alpha\nabla_\beta\phi\nabla^\beta\nabla_\mu\phi\right],\end{aligned} \tag{3.47}$$

where the G terms are free functions of the scalar field and $X = \nabla^\mu\phi\nabla_\mu\phi$. In 1974, Horndeski (Horndeski 1974) wrote down the most general scalar-tensor Lagrangian which has second order equations of motion but it has been overlooked for quite some time. It was pointed out in Kobayashi, Yamaguchi, et al. (2010) that the generalized galileons and Horndeski's theory are equivalent (see Kobayashi, Yamaguchi, et al. 2011 for a dictionary translating between the two languages). From the general action of Horndeski theory serveral data constraints should be applied, for instance in light of Planck (Barreira, Li, et al. 2014). In addition,after the gravitational-wave event GW170817 (Kase and Tsujikawa 2019,Sakstein and Jain 2017), the speed of gravitational waves is constrained to be very close to that of light. The Lagrangian of Horndeski theories allowing this constraint is restricted to be of the form

$$\mathcal{L}_{\text{gen.gal.}} = G_2(\phi,X) - G_3(\phi,X)\Box\phi + G_4(\phi,X)R \tag{3.48}$$

This is the general form that K-mouglage, Generalized Cubic Covariant Galileon and Galileon Ghost Condensate have and that we will briefly investigate in the following section.

3.4 The α-parametrization

An alternative parameterization of the EFT action, dubbed the α-basis, was developed in Bellini and Sawicki (2014) in order to describe specific physical properties of the Horndeski theory. In that case any departure from GR is described by four time dependent phenomenological functions, namely $\alpha_M(t), \alpha_B(t), \alpha_K(t), \alpha_T(t)$. This basis was later generalized to include GLPV models by adding an additional function, α_H (Jérôme Gleyzes, Langlois, and Vernizzi 2014,Jérôme Gleyzes, Langlois, Piazza, et al. 2015a), and finally it was further developed to include higher spatial derivatives operators accounting for Lorentz violation, $\alpha_{K_2}(t), \alpha_B^{GLPV}$ (Frusciante, Papadomanolakis, et al. 2016). The α-basis has the benefit of relating the evolution of these α-functions to clear physical effects, hence it is a more phenomenological approach. The quadratic action in the basis encompassing Horndeski, GLPV and low-energy Horava gravity can be written in Anowitt-Deser-Misner ADM formalism (see Section 3.2.5) and Fourier space as follows Frusciante, Papadomanolakis, et al. (2016):

$$\begin{aligned}S = \frac{1}{(2\pi)^3}\int d^3k dt a^3 \frac{M^2}{2}\Big\{&(1+\alpha_H)\,\delta N\delta_1\tilde{\mathcal{R}} + 2H\alpha_B\delta N\delta\tilde{K} \\ &+ \delta\tilde{K}^\mu_\nu\delta\tilde{K}^\nu_\mu - \left(\alpha_B^{GLPV}+1\right)(\delta\tilde{K})^2 + \left(\alpha_K + \alpha_{K_2}\frac{k^2}{a^2}\right)H^2(\delta N)^2 \\ &+ (1+\alpha_T)\,\delta_2(\tilde{\mathcal{R}}\delta(\sqrt{h}))\Big\}\end{aligned} \tag{3.49}$$

where in this case the tildas do not represent Einstein or Jordan frame but simply the Fourer transforms. The δ_2 refers to taking the expansion at second order, and h is the determinant of the spatial metric h_{ij}. The identification with the EFT functions reads:

$$\begin{aligned} &\alpha_B(t) = -\frac{M_{\rm pl}^2\dot{\mathfrak{f}} + \bar{m}_1^3}{HM^2}, \quad \alpha_T(t) = \frac{\bar{M}_3^2}{M^2} \equiv c_t^2 - 1, \quad \alpha_K(t) = \frac{2c + 4M_2^4}{H^2M^2}, \\ &\alpha_{K_2}(t) = \frac{8m_2^2}{M^2H^2}, \quad \alpha_H(t) = \frac{2\mu_1^2 + M_3^2}{M^2}, \quad \alpha_B^{GLPV}(t) = \frac{M_3^2 + M_2^2}{M^2}, \end{aligned} \tag{3.50}$$

where $M^2(t) = M_{pl}^2\dot{\mathfrak{f}} - \bar{M}_3^2$ is the *effective Planck mass* and c_t is the speed of propagation of gravitational waves. Another α-function can be implemented to take into account the running of the effective Planck mass.

$$\alpha_M = \frac{1}{H}\frac{d\ln M^2}{d\ln t} \tag{3.51}$$

We can now discuss the physical interpretation of the functions:

- α_B is the *braiding function*. It describes the mixing between the metric and the new scalar field. Thus, it is different from zero in all theores with non-minimal coupling. The braiding function lies in the kinetic part and the propagation speed of the scalar mode. The additional extended α_B^{GLPV} is to extend the braiding effect to scalar-tensor theories beyond GLPV.

- α_K is called *kineticity* is called kineticity and is purely a kinetic function and α_{K_2} is the extension to Lorentz violating theories. They both enter into the definition of the kinetic term. They affect the speed of propagation of the DE field hence the condition for the absence of a scalar ghost. In particular, large positive values of these functions suppress the sound speed of scalar perturbations. α_K is the only coupling present in quintessence or perfect-fluid DE models (Tsujikawa 2015).

- α_T is the *tensor speed excess* and describes the deviation of the speed of propagation of gravitational waves from the speed of light.

- α_H describes the departure from Horndeski theories. It also contributes to the speed of propagation of the scalar and it couples gravity to the velocity of matter.

3.5 The Adopted models

In this section we provide a brief summary of the models considered with their general features. These models are state-of-the-art MG models that are well constrained by the data and observations. The first model is the so called K-mouflage (Babichev et al. 2009), due to the name of its screening mechanism. Other two models are subclasses of Hordenski theory, specifically the Generalized Cubic Covariant Galileon (Frusciante, Peirone, et al. 2020) and the Galileon Ghost Condensate (Arkani-Hamed et al. 2004, Peirone et al. 2019). The Galileon Ghost Condensate is reveiwed in this

work, but the computation of the cross-correlation of CMB and Large Scale Structure is postponed to the near future, Finally, the Transitional Planck Mass model (Benevento, Raveri, et al. 2019) is an EFT model, built starting from the general EFT, characterized by a running Planck Mass with a step-like transition.

3.5.1 Shift-Symmetric Horndeski Action

The Generalized Cubic Covariant Galileon (GCCG) and the Galileon Ghost Condensate (GGC) share the same peculiarity when considering the relative Horndeski lagrangian since they are minimally coupled with the Ricci scalar term. The common cubic-order shift-symmetric Lagrangian is:

$$S = \int d^4x\sqrt{-g}\left(\frac{M_{pl}^2}{2}R + G_2(X) + G_3(X)\Box\phi\right) + S_m(\psi_m, g_{\mu\nu}) \tag{3.52}$$

The interaction term $G_3(X)\Box\phi$ contains a scalar-tensor kinetic coupling, due to the Christoffel symbols present in the covariant D'Alembertian operator. A consequence of these couplings is a novel kind of mixing which is named *kinetic braiding* (Cedric Deffayet et al. 2010). We can investigate this Lagrangian without making assumptions on the shape of the free functions. The Friedmann equations and Klein-Gordon for the scalar field assume the form:

$$\begin{aligned} 3M_{\rm pl}^2H^2 &= \rho_{\rm DE} + \rho_{\rm m} + \rho_{\rm r} \\ 2M_{\rm pl}^2\dot{H} &= -\rho_{\rm DE} - P_{\rm DE} - \rho_{\rm m} - \frac{4}{3}\rho_{\rm r} \\ &\quad \left(G_{2,X} - 2\dot{\phi}^2G_{2,XX} - 6H\dot{\phi}G_{3,X} + 6H\dot{\phi}^3G_{3,XX}\right)\ddot{\phi} \\ &\quad + 3\left(HG_{2,X} - \dot{H}\dot{\phi}G_{3,X} - 3H^2\dot{\phi}G_{3,X}\right)\dot{\phi} = 0 \end{aligned} \tag{3.53}$$

where we use the coma (,) to denote the derivative in order to lighten the notation. In the above equations we have introduced:

$$\begin{aligned} \rho_{DE} &= -G_2 - 2\dot{\phi}^2G_{2,X} + 6H\dot{\phi}^3G_{3,X} \\ P_{DE} &= G_2 - 2\ddot{\phi}\dot{\phi}^2G_{3,X} \end{aligned} \tag{3.54}$$

We can see that the equations of motion contain a second derivative of the scalar field. In order to find the form of the functions Σ and μ we apply the quasi static approximation so we can relate the gravitational potentials to the matter density contrast δ_m with 3.28. Therefore, an expression for δ_m is required and can be found by looking at perturbations in the matter sector. Perturbing the line element in the Newtonian gauge, equations of motions for the linear perturbation of the non relativistic matter density $\delta\rho_m$ and velocity potential v in Fourier space can be found. We present the recasted version in terms of density contrast:

$$\ddot{\delta}_m + 2H\dot{\delta}_m + \frac{k^2}{a^2}\Psi = 3\ddot{\Phi} + 6H\dot{\Phi} \tag{3.55}$$

The quasi-static approximation let us compute:

$$\mu = \Sigma = 1 + \frac{4\dot{\phi}^4 G_{3,X}^2}{q_s c_s^2} \tag{3.56}$$

where

$$\begin{aligned} q_s &= 4M_{pl}^2 \left(-G_{2,X} + 2\dot{\phi}^2 G_{2,XX} + 6H\dot{\phi} G_{3,X} - 6H\dot{\phi}^3 G_{3,XX}\right) + 12\dot{\phi}^4 G_{3,X}^2 \\ c_s^2 &= \frac{-4M_{pl}^2 (G_{2,X-2\ddot{\phi}} G_{3,X} - 4H\dot{\phi} G_{3,X} + 2\ddot{\phi}\dot{\phi}^2 G_{3,XX}) - 4\dot{\phi}^4 G_{3,X}^2}{q_s} \end{aligned} \tag{3.57}$$

c_s^2 correpsonds to the scalar sound speed in the sub-horizon limit. Both quantities are necessarily positive for stability requirements. Specifically $q_s \geq 0$ for the absence of ghosts and $c_s^2 > 0$ for the absence of Laplacian instability. Under these conditions we can see that Σ and μ are larger than 1, making the gravitational interaction inside the sound horizon stronger compared to the ΛCDM counterpart.

3.5.1.1 Generalized Cubic Covariant Galileon

The generalized covariant Galileon model (De Felice and Tsujikawa 2010) extends the covariant Galileon (De Felice and Tsujikawa 2012a) by considering in the Lagrangians power laws functions of X ($G_i \approx X^{p_i}$, where p_i are free constant parameters). The chosen form of the G_i functions allows for the existence of tracker solutions (De Felice and Tsujikawa 2012a, De Felice, Frusciante, et al. 2017, Frusciante, Kase, et al. 2019). This model has a viable parameter space, free from ghosts and Laplacian instabilities (De Felice and Tsujikawa 2012a). Cosmological constraints at the background level show that the DE equation of state w_{DE} can take values very close to 1, allowing for the tracker to mimic ΛCDM (De Felice and Tsujikawa 2012b). Furthermore, the additional freedom given by the parameters p_i might overcome the large enhancement of perturbations of the covariant Galileon model which is proven to be disfavored by cosmological measurements (Renk, Zumalacárregui, et al. 2017, Leloup et al. 2019). Let's consider the GCCG as investigated in Kable et al. (2021). In the paper they went further in the investigation of the generalized covariant galileon, by considering the latest observational constraints that reduce the free-functions to be only G_2, G_3. Hence, the name cubic and the reduction to the case of (3.52) The choice is:

$$G_2(X) = -c_2 \alpha_2^{4(1-p_2)} (-X)^{p_2} \qquad G_3(X) = -c_3 \alpha_3^{1-4p_3} (-X)^{p_3} \tag{3.58}$$

Where c_i, α_i, p_i are dimensionless constants in particular:

$$\alpha = \sqrt{H_0 M_{pl}} \qquad \alpha_3 = \left(\frac{M_{pl}^{1-2p_3}}{H_0^{2p_3}}\right)^{\frac{1}{1-p_3}} \tag{3.59}$$

As a sidenote, the form of the functions is different from the original introduction, but it is equivalent: it is a matter of definition of X. The cubic covariant Galileon

(C. Deffayet, Esposito-Farese, et al. 2009) is recovered in the limit $p_2 = p_3 = 1$. It is possible to fix $c_2 = \frac{1}{2}$ without loss of generality (Renk, Zumalacárregui, et al. 2017,Barreira, Li, et al. 2014). In this thesis, it is more useful to recast the free functions, following the treatment of Kable et al. (2021) and follow their analysis;

$$G_2(X) = -c_2 M_2^{4(1-p)} \left(-\frac{X}{2}\right)^2 \qquad G_3(X) = -c_3 M_3^{1-4p_3} \left(-\frac{X}{2}\right)^{p_3} \tag{3.60}$$

where c_2, c_3, p, p_3 are dimensionless constants, and $M_2.M_3$ are constants having a dimension of a mass. We can simplify the expression by introducing a parameter q defined by:

$$q = p_3 - p + \frac{1}{2}. \tag{3.61}$$

This will prove useful in the investigation of a tracker solution[5] that GCCG allows. The tracker solution obeys the relation $H\dot{\phi}^{2q} = const.$ and in the following we will assume p and q to be positive so that the stability conditions are set. To study the cosmological dynamics, we introduce:

$$\begin{aligned} x &= \frac{\dot{\phi}}{HM_{pl}}, \\ r_1 &= \left(\frac{x_{dS}}{x}\right)^{2q} \left(\frac{H_{dS}}{H}\right)^{1+2q}, \\ r_2 &= \left[\left(\frac{x}{x_{dS}}\right)^2 \frac{1}{r_1^3}\right]^{\frac{p+2q}{1+2q}} \end{aligned} \tag{3.62}$$

Since the interest is on late-time self accelerating de Sitter solution, we introduced x_{dS} and H_{dS} as the values at which $\dot{\phi}$ and H are constants with $r_1 = r_2 = 1$. Armed with these variables, we can recast M_2, M_3, c_2, c_3 as functions of them and obtain the equivalent DE equation of state w_{DE}:

$$w_{\rm DE} = -\frac{\left(\Omega_{\rm r} - 3 + 12r_1 - 6r_1^2\right)p + 3(2q-1)r_1 + 3r_1^2}{3\left[\left(2 - 2r_1 + r_1^{1+\alpha} r_2\right)p + 2q - 1 + r_1\right]\left[2p + (1-2p)r_1\right]} \tag{3.63}$$

where

$$\alpha = \frac{p + 2q}{1 + 2q} \tag{3.64}$$

We can ispect different phases according to the values of r_1 and r_2. The differential equations for r_1, r_2 (De Felice and Tsujikawa 2012a) show that fixed points are at $r_{1,2} = 0$ and $r_{1,2} = 1$, making the behaviour close to those values interesting. The

[5]It is possible to introduce tracker fields that have an equation-of-motion with attractor-like solutions in which a very wide range of initial conditions rapidly converge to a common, cosmic evolutionary track. The term "tracker" is meant to refer to solutions joining a common evolutionary track, as opposed to tracking closely the background energy density. A tracker solution is one which undergoes long periods of attractor-like behavior in which solutions to the equation-of-motion are drawn towards a common solution. For more details we refer to Steinhardt et al. (1998)

- The tracker corresponds to the fixed point with $r = 1$ and $r_2 \ll 1$
- The de Sitter solution is given by $r_1 = r_2 = 1$.
- For the initial conditions $r_1, r_2 \ll 1$ the evolution is set for r_1 up to 1 during the radiation and matter epochs. Then, the r_2 has to evolve up to 1 and reach the De Sitter fixed point.

Let us introduce some useful quantities associated with perturbations

$$\begin{aligned}
s =& \frac{p}{q} \\
\tilde{q}_s \equiv& \frac{q_s}{4\dot{\phi}^4 G_{3,X}^2} = 3 + \frac{3}{p r_1^{1+\alpha} r_2} \left[2p + 2q - 1 + (1-2p) r_1\right] \\
c_s^2 =& \left(6\left\{\left(2 - 2r_1 + r_1^{1+\alpha} r_2\right) p + 2q - 1 + r_1\right\}^2\right)^{-1} \cdot \left[(2p + 2q - 1)\Omega_{\rm r}\right. \\
& - 5 + r_1\left(8 - 6r_1 + 3r_1^{1+\alpha} r_2\right) + 2p\left\{5 - 8r_1 + 6r_1^2 + (5 - 2q - 7r_1) r_1^{1+\alpha} r_2\right\} \\
& \left. + 2q\left(5 - 3r_1^{2+\alpha} r_2\right) - 2p^2 r_1^{1+\alpha} r_2\left(2 - 2r_1 + r_1^{1+\alpha} r_2\right)\right] \\
\mu =& \Sigma = 1 + \frac{1}{\tilde{q}_s c_s^2}
\end{aligned} \tag{3.65}$$

Now, if we investigates the regimes:

- $r_1 \ll 1$ and $r_2 \ll 2$: we obtain

$$w_{DE} \simeq \frac{3 - \Omega_r}{12(p+q) - 6} \tag{3.66}$$

and the stability conditions for $q_s >$ and c_s^2 are satisfied for

$$2p + 2q - 1 > 0 \tag{3.67}$$

. Specifically, expanding μ for small values of r_1, r_2 we obtain:

$$\mu = \Sigma \simeq 1 + \frac{2p}{5 + \Omega_r} r_1^{1+\alpha} r_2 \tag{3.68}$$

- $r_1 = 1$ and $r_2 \ll 1$: we obtain

$$w_{DE} = -1 - \frac{1}{6}(3 + \Omega_r) s \tag{3.69}$$

and for the stability conditions:

$$\begin{aligned}
\tilde{q}_s &= 3 + \frac{6q}{p r_2} > 0 \\
c_s^2 &= \frac{6p + 10q - 3 + (2p + 2q - 1)\Omega_r}{24 q^2} > 0
\end{aligned} \tag{3.70}$$

and expanding μ in respect to values of r_2:

$$\mu = \Sigma \simeq 1 + \frac{4pq}{6p + 10q - 3 + (2p + 2q - 1)\Omega_r} r_2 \tag{3.71}$$

- $r_1 = 1$ and $r_2 = 1$ de Sitter solution. In this case $w_{DE} = -1$ and the stability conditions read:

$$\begin{aligned} \tilde{q}_s &= \frac{3(p+2q)}{p} > 0 \\ c_s^2 &= \frac{1-p}{3(p+2q) > 0} \end{aligned} \tag{3.72}$$

and the coupling functionals

$$\mu = \Sigma = \frac{1}{1-p} \tag{3.73}$$

which is larger that 1, for $0 < p < 1$.

3.5.1.2 Galileon Ghost Condensate

Ghost condensation as modification of gravity was first introduced by Arkani-Hamed et al. (2004). The so-called *ghost condensate* is a kind of fluid that can fill the universe with the same equation of state of a cosmological constant, $p = -\rho$, but it is not a cosmologocial constant. Thus, it gives rise to a de Sitter phase of the universe and it is a physical fluid with physical scalar excitation. The background arises from a theory where a real scalar field (ϕ) is changing with constant velocity and with a scalar field excitation π around the background:

$$\langle\phi\rangle = M^2 t \qquad\qquad \phi = M^2 t + \pi \tag{3.74}$$

with an assumed shift symmetry of the field ϕ. The name Ghost Condensation comes from the "wrong" sign of the ϕ-kinetic term. This wrong-sing implies that the background $\langle\phi\rangle = 0$ has a false vacuum and thus a vacuum decay. In the theory, the idea is that there are higher order terms such as $(\partial\phi)^4$ in the lagrangian that "stabilize" the ghost (thus with vacuum $\langle\phi\rangle \neq 0$) in the same way the ϕ^4 term stabilizes the tachyon in the analogous tachyon condensation. The Ghost Condensation theory can be recovered from the shift-symmetric Horndeski Lagrangian (3.52) with the free functions (hence we refer as the Galileon ghost condensate):

$$G_2(X) = a_1 X + a_2 X^2 \qquad\qquad G_3(X) = 3a_3 X \tag{3.75}$$

where $a_{1,2,3}$ are constants. The existence of term $a_2 X^2$ leads to the modified evolution of w_{DE} and different cosmic growth history compared to those of the cubic Galileon which corresponds to $a_2 = 0$ (C. Deffayet, Esposito-Farese, et al. 2009). The ghost condensate model can be recovered by taking the limit $a_3 \to 0$. Leaving the term $a_3 \neq 0$ involves rather than a ghost condensation a *kinetic condensation* for which we refer to Cedric Deffayet et al. (2010). We introduce dimensionelss variables for the analysis

$$x_1 = -\frac{a_1\dot{\phi}^2}{3M_{pl}^2 H^2} \qquad x_2 = \frac{a_2\dot{\phi}^4}{M_{pl}^2 H^2} \qquad x_3 = \frac{6a_3\dot{\phi}^3}{M_{pl}^2 H^2} \tag{3.76}$$

which to correspond to density parameters arising from the couplings. Armed with these variables, we can express the background equations

$$\begin{aligned}
\Omega_{DE} &= x_1 + x_2 + x_3 \\
\frac{\dot{H}}{H^2} &= -\frac{12x_1^2 + 2\left(16x_2 + 12x_3 + 3\Omega_{\rm m} + 4\Omega_{\rm r}\right)x_1 + 16x_2^2}{4x_1 + 8x_2 + 4x_3 + x_3^2} \\
&\quad + \frac{+4\left(6x_3 + 3\Omega_{\rm m} + 4\Omega_{\rm r}\right)x_2 + \left(9x_3 + 6\Omega_{\rm m} + 8\Omega_{\rm r}\right)x_3}{4x_1 + 8x_2 + 4x_3 + x_3^2} \\
\frac{\dot{\phi}}{H\phi} &= \frac{-12x_1 - 8x_2 + \left(6x_1 + 4x_2 + 3\Omega_{\rm m} + 4\Omega_{\rm r} - 6\right)x_3 + 3x_3^2}{4x_1 + 8x_2 + 4x_3 + x_3^2}
\end{aligned} \tag{3.77}$$

from which we can get the dark energy equation of state

$$w_{DE} = \frac{3x_1 + x_2 - \frac{\dot{\phi}}{H\phi}x_3}{3\Omega_{DE}} \tag{3.78}$$

The detailed dynamics investigation can be found in Kase and Tsujikawa (2018) which we summarize here since they are fundamental when costraining the stability conditions.

- The de Sitter fixed point at which trajectories converge is set by

$$1 - x_1 = -x_2 - x_3 \qquad\qquad x_3 = -\frac{1}{3}(18x_1 + 8x_2 + 12) \tag{3.79}$$

- The radiation and matter dominated epochs are characterized by $\Omega \ll 1$ allowing us to consider the regime in which G_3 dominates over G_2 with the condition of $|x_1|, |x_2| \ll |x_3| \ll 1$. We have $w_{DE} \approx \frac{1}{6}$ in the radiation era and $w_{DE} \approx \frac{1}{4}$ in the matter era.
- In the limit $x_2 \to 0$ there's a tracker solution for which $x_3 = -2x_1$. In this case $w_{DE} = -2$ in the matter era and $w_{DE} = -\frac{7}{3}$

The stability conditions are given from (3.57):

$$\begin{aligned}
q_s &= \frac{3H^2M_{\rm pl}^4}{\dot{\phi}^2}\left(4x_1 + 8x_2 + 4x_3 + x_3^2\right) > 0 \\
c_s^2 &= \frac{12x_1 + 8x_2 + 4\left(\epsilon_\phi + 2\right)x_3 - x_3^2}{3\left(4x_1 + 8x_2 + 4x_3 + x_3^2\right)} > 0
\end{aligned} \tag{3.80}$$

which are satisfied for different values of x_i according to the regime we set ourselves in. Intersecting the possible x_i values and accounting for all the regimes, we have conditions on x_i.

- In $|x_1|, |x_2| \ll |x_3| \ll 1$, the conditions are satisfied for $x_3 > 0$
- In $x_2 \to 0$, $x_3 = -2x_1$ (the tracker solution) we require $x_1 < 0$
- In de Sitter solution the quatities are

$$q_s = \frac{4H^2M_{\rm pl}^4}{3\dot{\phi}^2}\left(x_2^2 + 3x_2 + 18\right), \quad c_8^2 = \frac{x_2\left(3 - x_2\right)}{3\left(x_2^2 + 3x_2 + 18\right)} \tag{3.81}$$

  with the condition of $0 < x_2 < 3$

These leave the conditions

$$x_1 < 0, \qquad x_2 > 0, \qquad x_3 > 0. \tag{3.82}$$

In this regard we can see the values the gravitational coupling function can adopt. In general, from (3.56):

$$\mu = \Sigma = 1 + \frac{x_3^2}{12x_1 + 8x_2 + 4(\frac{\dot{\phi}}{H\phi} + 2)x_3 - x_3^2}. \tag{3.83}$$

We can see that since $x_3 > 0$ the coupling are larger than one and therefore both Ψ and $\Psi + \Phi$ are enhanced compare to those in GR.

3.5.2 K-mouflage

K-mouflage is a general structure for a large class of scalar-tensor theories (Babichev et al. 2009, Brax and Valageas 2014a, Brax and Valageas 2014b, Benevento, Raveri, et al. 2019), in which the scalar field "camouflages" in strong enough gravitational fields, via a derivative self-interaction (the K in K-mouflage stands for "kinetic"). This is its peculiar screening mechanism which we mentioned in Section 3.1.2: the K-mouflage screening mechanism is present in models where the Lagrangian involves an arbitrary function $K(\chi)$ of the kinetic terms. The case of the small-scale, specifically the small-scale static configurations (Brax and Valageas 2014c), shows that the fifth force is screened by the nonlinear K-mouflage mechanism if $K'(\chi)$ grows sufficiently fast for large negative χ. Let us see the general features of the K-mouflage. The model is defined by the action

$$S = \int d^4x\sqrt{-\tilde{g}}\left(\frac{M_{pl}^2}{2}\tilde{R} + \mathcal{M}^4 K(\tilde{\chi})\right) + S_m(\psi_m, g_{\mu\nu}) \tag{3.84}$$

where $\tilde{g}_{\mu\nu}$ is the Einstein-frame metric and $g_{\mu\nu}$ the Jordan-frame metric, given by the relation between the two

$$g_{\mu\nu} = A^2(\phi)\tilde{g}_{\mu\nu} \tag{3.85}$$

The peculiarity of the K-mouflage model is that the Lagrangian of the scalar field ϕ involves a non-canonical kinetic term, defined by a dimensionless function $K(\tilde{\chi})$ with

$$\tilde{\chi} = -\frac{\tilde{g}^{\mu\nu}\partial_\mu\phi\partial_\nu\phi}{2\mathcal{M}^4} \tag{3.86}$$

where $\mathcal{M}^4$ is of the order of the dark energy scale today, set by the cosmological constant, to recover the late time accelerated expansion of the Universe. In the Jordan frame, the Friedmann equation takes the form

$$H^2 = \frac{1}{3M_{pl}^2(1-\epsilon_2)^2}(\bar{\rho} + \bar{\rho}_{rad} + \bar{\rho}_\phi) \tag{3.87}$$

with

$$M_{pl} = \bar{A}^{-2}\bar{M}_{pl} \qquad\qquad \epsilon_2 = \frac{d\ln\bar{A}}{d\ln a} \tag{3.88}$$

where the background quantities are denoted with a bar. In the above expressions we introduced the scalar field energy density with $\bar{\tilde{\chi}} = \frac{\bar{A}^2}{2\mathcal{M}^4}\left(\frac{d\bar{\phi}}{dt}\right)^2$:

$$\bar{\rho}_\phi = \bar{A}^{-4}\mathcal{M}^4(-\bar{K} + 2\bar{\tilde{\chi}}\bar{K}') \tag{3.89}$$

where t is the Jordan-frame cosmic time. The Klein-Gordon equation satisfied by the scalar field writes as:

$$\frac{\mathrm{d}}{\mathrm{d}t}\left(\bar{A}^{-2}a^3\frac{d\bar{\phi}}{dt}\bar{K}'\right) = -a^3\bar{\rho}\frac{d\ln\bar{A}}{d\bar{\phi}} \tag{3.90}$$

Where in this case the derivative with respect to t is a total derivative. Considering linear scalar perturbations around a FLRW background in the Newtonian gauge, the two coupling functions (3.28) assume the form

$$\mu = (1+\epsilon_1)\bar{A}^2 \qquad\qquad \Sigma = \bar{A}^2 \tag{3.91}$$

with

$$\epsilon_1 = \frac{2\bar{M}_{pl}}{\bar{K}'}\frac{d\ln\bar{A}}{d\bar{\phi}}. \tag{3.92}$$

From these equations we can see how the kinetic term can supress the modification of gravity in (3.28). As said, the function μ represents the effective gravitational constant $\mu = G_{N,eff}/G_N$ (Pogosian and Silvestri 2016) and at the linear level in perturbations, screening occurs when $\epsilon \ll 1$, which corresponds to backgrounds where $K' \gg 1$.
For the stability conditions it is useful to recast the action in the form of Hornseski class. The action is similar to (3.52) without the $G\Box\phi$ term and with the Ricci scalar. In the Jordan frame:

$$S = \int \mathrm{d}^4x\sqrt{-g}\left[G_4(\phi)R + G_2(\phi, X)\right] + S_\mathrm{m}\left(\psi_\mathrm{m}, g_{\mu\nu}\right) \tag{3.93}$$

which corresponds to a nonminimally coupled-kessence. We can recast the action in the Einstein frame exploiting the relations

$$R = \tilde{R} + 6\tilde{\Box}\omega - 6\tilde{g}^{\mu\nu}\partial_\mu\omega\partial_\nu\omega, \qquad \omega = -\ln A \qquad G_4(\phi) = \frac{M_{pl}^2}{2A^2(\phi)} \tag{3.94}$$

with the normalizations of $A(\phi_0)$ to be 1 and to recover $G_4(\phi_0) = \frac{M_{pl}^2}{2}$. Then the action becomes:

$$\mathcal{S} = \int \mathrm{d}^4x\sqrt{-\tilde{g}}\left(\frac{M_\mathrm{pl}^2}{2}\tilde{R} + \frac{6M_\mathrm{pl}^2\mathcal{M}^4A_{,\phi}^2}{A^2}\tilde{\chi} + A^4G_2\right) + \mathcal{S}_\mathrm{m}\left(\psi_\mathrm{m}, g_{\mu\nu}\right) \tag{3.95}$$

and if we compare it with (3.84) we find the correspondence for G_2:

$$G_2(\phi, X) = \frac{\mathcal{M}^4}{A^4(\phi)}K(\tilde{\chi}) - \frac{6\mathcal{M}^4M_\mathrm{pl}^2A_{,\phi}^2(\phi)}{A^6(\phi)}\tilde{\chi} \tag{3.96}$$

Since we have found the shape of the K-mouflage action in the Horndeski form of (3.52), we can use its results for stability (3.57):

$$\begin{aligned} q_s &= \frac{2M_{\rm pl}^2}{A^4}\left(K_{,\tilde{\chi}} + 2\tilde{\chi}K_{,\tilde{\chi}}\right) > 0, \\ c_s^2 &= \frac{K_{,\tilde{\chi}}}{K_{,\tilde{\chi}} + 2\tilde{\chi}K_{,\tilde{\chi}\tilde{\chi}}} > 0, \end{aligned} \tag{3.97}$$

In order to consider the EFT version of the theory (Brax and Valageas 2016), and study the dark energy dynamics, the functionals $K(\tilde{\chi})$ and $A(\phi)$ need to be specified (Benevento, Raveri, et al. 2019). The parametrization adopted is the one used in (Brax and Valageas 2016), where five parameters are introduced: $\epsilon_{2,0}, \gamma_A, m, \alpha_U.\gamma_U$. The theoretically allowed parameter space were investigated in (Brax and Valageas 2014a, Brax and Valageas 2014b). The parametrisation comes from defining the coupling function and the kinetic term as functions of the scale factor in terms of a set of parameters. The background coupling functions are defined in terms of three parameters: $\epsilon_{2,0}, \gamma_A, m$ as:

$$\bar{A}(a) = 1 + \alpha_A - \alpha_A\left[\frac{a\left(\gamma_A+1\right)}{a+\gamma_A}\right]^{\nu_A} \tag{3.98}$$

with

$$\alpha_A = -\frac{\epsilon_{2,0}(\gamma_A+1)}{\gamma_A\nu_A}, \quad \nu_A = \frac{3(m-1)}{2m-1} \tag{3.99}$$

For K-mouflage models the kinetic function can be computed integrating the expression:

$$\begin{aligned} \frac{\mathrm{d}\bar{K}}{\mathrm{d}\tilde{\chi}} &= \frac{U(a)}{a^3\sqrt{\tilde{\tilde{\chi}}}}, \\ U(a) &= U_0\left(\left(\sqrt{a_{\rm eq}}+1\right) + \frac{\alpha_U}{\ln\left(\gamma_U+1\right)}\right)\frac{a^2\ln\left(\gamma_U+a\right)}{\left(\sqrt{a_{\rm eq}}+\sqrt{a}\right)\ln\left(\gamma_U+a\right)+\alpha_U a^2}, \\ \sqrt{\tilde{\tilde{\chi}}} &= -\frac{\bar{\rho}_{m0}}{\mathcal{M}^4}\frac{c_2\bar{A}^4}{2U\left(-3\epsilon_2+\frac{d\ln U}{d\ln a}\right)}, \end{aligned} \tag{3.100}$$

where we introduced two additional parameters α_U and γ_U. The allowed range of parameters is restricted to fit the natural domain of the two functions $U(a)$ and $\bar{A}(a)$ and additional costraints that ensure the stability of the solutions have to be satisfied. Specifically, all K-mouflage models must satisfy the conditions (Brax and Valageas 2016) as well as Solar System and cosmological constraints (Barreira, Brax, et al. 2015). For a more clear interpretation of the parametrizaion, let us describe the physical meaning of the parameters and the bound they have to satisfy:

- $\epsilon_{2,0}$; this parameter sets the value of the ϵ_2 function today. The ΛCDM limit is recovered when $\epsilon_{2,0} \to 0$, independently of the values of the other four parameters. For K-mouflage models, adopting the same convention as (Benevento, Raveri, et al. 2019, Brax and Valageas 2016) we choose this parameter to be negative. Solar System tests (Barreira, Brax, et al. 2015) impose $|\epsilon_{2,0}| \lesssim 0.01$.

- $m > 1$; describes the large χ behaviour of the kinetic function. It is possible to show (Brax and Valageas 2016) that, given the parametrization described by (3.98), (3.99), in the limit of large χ the kinetic term follows the asymptotic power-law behaviour: $K(\chi) \sim \chi^m$. We study the particular case called *cubic model* which is obtained by fixing $m = 3$ (Benevento, Kable, et al. 2022 Benevento, Raveri, et al. 2019)

- $\gamma_A > 0$; describes the transition to the dark energy dominated epoch in the $A(a)$ coupling function. Natural values for this parameter are of order unity (Brax and Valageas 2016). High values for this parameter push the model toward the ΛCDM limit, however values of $\gamma_A \gtrsim 20$ are likely to be excluded by the stability conditions (Benevento, Raveri, et al. 2019).

- $\gamma_U \geq 1$ and $\alpha_U > 0$; these two parameters set the transition to the dark energy dominated epoch in the $K(a)$ kinetic function (Benevento, Raveri, et al. 2019). Early time probes (like CMB temperature anisotropies), as well as late time probes (CMB lensing) are practically insensitive to the parameter γ_U which can be safely fixed to 1, i.e. the minimum value that that avoids negative values of the $U(a)$ function. The parameter α_U has some influence on late-time probes on large scales (Benevento, Raveri, et al. 2019)

3.5.3 Transitional Planck Mass

The last model we consider has been been presented just recently by Benevento, Kable, et al. (2022). It prescribes a modification of gravity that arises at early time, during which the Planck Mass goes through a smooth step-like transition between two values. Such a Planck Mass is known as Running Planck Mass and models implementing a transition of it are known in the context of modified gravity. For instance, the K-mouflage model prescribes an evolving Planck Mass, ad the $f(R)$-gravity too. Modification of gravity arising at early time, before recombination, is known in literature and it is shown that it could alleviate tensions in the fundamental parameters (Mario Ballardini et al. 2020, Ballesteros et al. 2020, Benevento, Raveri, et al. 2019, Braglia et al. 2021, Lima et al. 2016, Lin, Raveri, et al. 2019,Zumalacárregui 2020). In the Transitional Planck Mass (TPM) model, the approach is to directly use the EFT. The step-like transition is directly implemented in the EFT-functions, specifically in the scalar Ricci term. The action is built starting from a subset of the EFT action (3.16) up to second order expansion. It consists of all the operators consistent with time-dependent spatial diffeomorphism invariance

up to quadratic order in the perturbations:

$$\begin{aligned} S = \int d^4x\sqrt{-g}\Big\{ & \frac{m_0^2}{2}[1+\Omega(t)]R + \Lambda(t) - c(t)\delta g^{00} \\ & + \frac{M_2^4(t)}{2}\left(\delta g^{00}\right)^2 - \frac{M_1^3(t)}{2}\delta g^{00}\delta K_\mu^\mu - \frac{M_2^2(t)}{2}\left(\delta K_\mu^\mu\right)^2 \\ & - \frac{\bar{M}_3^2(t)}{2}\delta K_\nu^\mu \delta K_\mu^\nu + \frac{\hat{M}^2(t)}{2}\delta g^{00}\delta R^{(3)} \\ & + m_2^2(t)\left(g^{\mu\nu}+n^\mu n^\nu\right)\partial_\mu\left(g^{00}\right)\partial_\nu\left(g^{00}\right)\Big\} \\ & + S_M\left[g_{\mu\nu}, \psi_m^{(i)}\right] \end{aligned} \tag{3.101}$$

where the notation is the same as the EFT action. The factors $\langle \Omega, \Lambda, c\rangle$ and $\langle M_2^4, \bar{M}_1^3, \bar{M}_2^2, \bar{M}_3^2, m_2^2, \hat{M}^2\rangle$ are the EFT functions. In particular $\langle \Omega, \Lambda, c\rangle$ are the EFT functions contributing to both the background and perturbation equations, while the rest contribute only to perturbations. The Ω function is the rescaling of the reduced Planck mass m_0, on the cosmological background. We can define an effective Planck mass M_* which is given on large scale by $M_*^2 = m_0^2(1+\Omega)$. The TPM model is then defined by the choice of the EFT functions that are compatible with Horndeski models and by imposing that the speed of gravitational waves is constant and equal to the speed of light. This leaves with:

$$S = \int d^4x\sqrt{-g}\left\{\frac{m_0^2}{2}[1+\Omega(t)]R + \Lambda(t) - c(t)\delta g^{00} + \frac{M_2^4(t)}{2}\left(\delta g^{00}\right)^2 - \frac{M_1^3(t)}{2}\delta g^{00}\right\} \tag{3.102}$$

with the EFT functions left $\langle \Omega, \Lambda, c, M_2^4, \bar{M}_1^3, \rangle$. If we also consider the scale factor of the metric $a(t)$, or rather the Hubble expansion rate H, we have in theory 6 degrees of freedom.The background Friedman equations can fix 2 and the rest needs to be fixed.

- Ω: Given the model, the Ω function shape is fixed by the assumption of the step-like transition

$$\Omega(x) = \frac{\Omega_0}{2}\left(1 - erf\left(\frac{\mu - x}{\sqrt{2\pi}\sigma}\right)\right) \tag{3.103}$$

Where

$$x = \ln(a) \qquad \mu = \ln(a_T) \qquad a_T = 10^{x_T} \tag{3.104}$$

determine the transition; σ is the width of the transition (to which we refer with the subscript T) and Ω_0 sets its amplitude, assuming an initial value $\Omega(x_i) = 0$. This choice implies that the value today of the effective Planck Mass is not the local value obtained from the Solar System, therefore requiring some kind of screening mechanism.

- c: it is required to be a constant at all times.

$$\frac{c}{3H_0^2 m_0^2} = c_0 \tag{3.105}$$

  In this way c does not contribute to the energy balance of the Universe.

- $M_2^4, \bar{M}_1^3$ are to be fixed to guarantee that the effect on linear cosmological perurbations is suppressed by a factor H^{-2}:

$$\frac{M_2^4}{3H_0^2 m_0^2} = c_0 \qquad\qquad \frac{\bar{M}_1^3}{3H_0^2 m_0^2} = \frac{2c_0}{H} \tag{3.106}$$

Armed with these prescriptions we can write the Friedmann euqations:

$$\begin{aligned} H^2 &= \frac{1}{3m_0^2}\left(\rho_{m,rad} + \rho_{\rm TPM}\right) \\ H' &= -\frac{3H^2 m_0^2 + P_{\rm TPM} + P_{m,rad}}{2Hm_0^2} \end{aligned} \tag{3.107}$$

where

$$\begin{aligned} \rho_{\rm TPM} &= 2c - \Lambda - 3m_0^2 H^2\left(\Omega' + \Omega\right) \\ P_{\rm TPM} &= \Lambda + H^2 m_0^2\left[\Omega'' + \Omega'\left(\frac{H'}{H} + 2\right) + \Omega\left(2\frac{H'}{H} + 3\right)\right]. \end{aligned} \tag{3.108}$$

The prime denotes derivatives with respect to the variable x. The fluid equation of state is set as:

$$w_{DE} = \frac{P_{\rm TPM}}{\rho_{\rm TPM}} = \frac{\Lambda + H^2 m_0^2\left[\Omega'' + \Omega'\left(\frac{H'}{H} + 2\right) + \Omega\left(2\frac{H'}{H} + 3\right)\right]}{\rho_{\rm TPM} = 2c - \Lambda - 3m_0^2 H^2\left(\Omega' + \Omega\right)} \tag{3.109}$$

which can be simplified in the regime after the transition, i.e. when $x > \ln(a_T) + \sigma$. We can make the assumption $\Omega \to \Omega_0$ so that:

$$w_{\rm TPM} = \frac{\Lambda - \Omega_0 P_{m,rad}}{2c - \Lambda - \Omega_0 \rho_{m,rad}}. \tag{3.110}$$

If we want to consider the gravitational couplings μ and Σ, we have to adopt the QS approximation (Benevento, Kable, et al. 2022). For the TPM model:

$$\begin{aligned} \mu(k,a) &= \frac{1}{1+\Omega}\frac{1 + M_C^2\frac{a^2}{k^2}}{f_3/\left(2f_1(1+\Omega)m_0^2\right) + M_C^2\frac{a^2}{k^2}}, \\ \Sigma(k,a) &= \frac{1}{2(1+\Omega)}\frac{1 + f_5/f_1 + 2M_C^2\frac{a^2}{k^2}}{f_3/\left(2f_1(1+\Omega)m_0^2\right) + M_C^2\frac{a^2}{k^2}}, \end{aligned} \tag{3.111}$$

with

$$
\begin{aligned}
M_C^2 &= \frac{3}{f_1}\left[m_0^2\left(2H\dot{H}+\frac{\ddot{H}}{2}\right)\dot{\Omega}+c\left(2\dot{H}-\left(\frac{\dot{H}}{H}\right)^2+\frac{\ddot{H}}{H}\right)\right]\\
f_1 &= m_0^2\frac{\dot{\Omega}^2}{1+\Omega}+c\frac{\dot{H}}{H^2}\\
f_3 &= \frac{3}{2}\left(m_0^2\dot{\Omega}\right)^2+m_0^2\dot{\Omega}\frac{2c}{H}+m_0^2(1+\Omega)\frac{2c\dot{H}}{H^2}-2\left(\frac{c}{H}\right)^2\\
f_5 &= m_0^2\frac{\dot{\Omega}^2}{2(1+\Omega)}+c\frac{\dot{H}}{H^2}
\end{aligned}
\tag{3.112}
$$

where the overdot represents derivatives with respect to time and M_C is the so-called Compton mass of the scalar field. M_C sets a crucial transition scale: the one below which the scalar field mediates a fifth force (Joyce et al. 2015). A fifth force is characteristic of MG theories with extra DoFs and the transition scale depends on the dynamical mechanism which screens the strength of the scalar fifth force in local environments (Joyce et al. 2015). Astrophysical scales are typical examples of screened environments. In other words, the transition scale relates to the Compton wavelength of the scalar field, λ_C, as $M_C \propto \lambda_C^{-1}$. Theories of the chameleon type (Khoury and Weltman 2004b, Khoury and Weltman 2004a) display a small Compton wavelength $\lambda_C \lesssim 1$ Mpc, whereas models exhibiting self acceleration, and in a more general sense, models where the extra DoF sources cosmic acceleration, bare a very large Compton wavelength $\lambda_C \propto H^{-1}$. In the case of the TPM, on large scales compared to the Compton mass $k/a \ll M_C$, the effect of modified gravity on matter perturbations is small, and $\mu \sim \mu_0 = (1+\Omega)^{-1}, \Sigma \sim \Sigma_0 = (1+\Omega)^{-1}$, recovering the background value. In the opposite regime, on sub-Compton scales, $k/a \gg M_C$, matter perturbations feel the effect of an increased μ. Indeed taking the limit $k \to \infty$ in (3.111) we find$\mu_\infty = 2f_1/f_3, \Sigma_\infty = (1+f_5/f_1)\mu_\infty$.
For the stability condition it is useful to express the TPM model as a subclass of Horndeski models, specified by the usual action:

$$
\mathcal{S} = \int \mathrm{d}^4x\sqrt{-g}\left[\frac{m_0^2}{2}G_4(\phi)R + G_2(\phi,X) + G_3(X)\Box\phi\right] + \mathcal{S}_m(\psi_m, g_{\mu\nu}) \tag{3.113}
$$

It is possible to obtain the shape of the G_i functions following the mapping rules specified in this chapter. Specifically for the case $c_0 = 0$, the model corresponds to the standard $f(R)$ model, with the identifications:

$$
\begin{aligned}
G_2(\phi,X) &= -f(R) + R\tfrac{df}{dR},\\
G_3(X) &= 0,\\
G_4(\phi) &= \phi,\\
\phi = 1+\tfrac{df}{dR}, R &= 6\left(2H^2+\dot{H}\right).
\end{aligned}
\tag{3.114}
$$

Rather than expressing the general G_i function and determine the stability conditions, the general TPM model can be recasted using the α prescription. For the

TPM model we can identify the following correspondences:

$$\begin{aligned} \alpha_M &= \frac{\Omega'}{1+\Omega} \\ \alpha_B &= \frac{\Omega'}{2(1+\Omega)} + \frac{c_0}{H^2(1+\Omega)}, \\ \alpha_K &= -\frac{2c_0}{H^2(1+\Omega)} \end{aligned} \tag{3.115}$$

In the assumption of an early-time transition ($a_T \ll 1, \sigma \sim 1$) there are two regimes:

- **early times**: close to the transition we have $\Omega' \gg \frac{c_0}{H^2}$ and the behaviour is the one of a $f(R)$ model, with

$$\alpha_M = 2\alpha_B \qquad\qquad \alpha_K = 0 \tag{3.116}$$

- **late times**: the regime resembles the kinetic gravity braiding model (Cedric Deffayet et al. 2010). It is given by

$$\alpha_M = 0 \qquad\qquad \alpha_K \propto \alpha_B \propto \frac{c_0}{H^2} \tag{3.117}$$

Requiring a ghost free theory and no gradient instabilities gives the conditions on the α-functions as:

- The no-ghost can be expressed as

$$\alpha_K + \frac{3}{2}\alpha_B^2 > 0 \tag{3.118}$$

  and it is satisfied for $c_0 < 0$, which gives, $\alpha_K > 0$.

- The no-gradient instability condition is given by a positive speed of propagation of scalar perturbations squared $c_s^2 > 0$. We can express this quantity with the α prescription:

$$c_s^2 = -\frac{(2+2\alpha_B)\left[\dot{H} + H^2(\alpha_B - \alpha_M)\right] - 2H\dot{\alpha}_B}{H^2\left(\alpha_K + \frac{3}{2}\alpha_B^2\right)} - \frac{(\rho_{m,\text{ rad}} + P_{m,rad})}{(1+\Omega)H^2\left(\alpha_K + \frac{3}{2}\alpha_B^2\right)} \tag{3.119}$$

The stability conditions are satisfied for the enitre cosmic evolution by the choice $\Omega_0 < 0$ and $c_0 < 0$. The ΛCDM model is recovered in the limits $\Omega_0 \to 0$, $c_0 \to 0$.

CHAPTER 4

Cross-correlation analysis

We have seen in Chapter 2 where the ISW signal comes from and what it represents. In addition, we have seen how information on structures in the Universe is encoded in the Matter Power Spectrum. In Chapter 3 we have seen how alternative theories of gravity (with respect to General Relativity) can be described and their peculiarities. Now, in this chapter, we present how to exploit the ISW signal to test different models. Specifically, the *late ISW* effect is due to the decay of the gravitational potentials because of the accelerated expansion of the Universe at late times (W. Hu, Sugiyama, and Silk 1997). Different models would lead to a different redshift evolution of the gravitational potential, thus different imprints on the CMB anisotropies (Kofman and Starobinskij 1985). Measuring the *late ISW* is difficult per se since the signal is faint compared to the other anisotropies. In addition, on the largest scales, cosmic variance strongly affects the contribution. Crittenden and Turok (Crittenden and Turok 1996) first proposed cross-correlation as a tool to probe the ISW effect: the idea behind their method of investigation is to correlate the ISW effect with sources of gravitational potentials. Specifically, we can use tracers of the Large-Scale-Structure, e.g. galaxy counts. At the linear level in the perturbations[1], the gravitational potential is linked to the matter distribution by Poisson's equation and the ISW can test the rate of evolution of the growth factor with redshift (Crittenden and Turok 1996). If the late ISW signal is non-zero, we expect a non-zero correlation too, allowing us to isolate the ISW contribution. Unlike the case for the CMB, we do not have a direct way of measuring the matter's power spectrum. However, some observables indirectly probe the matter distribution (see e.g., *Modern Cosmology* (2021)). Perhaps the most important one is galaxy clustering (Mo et al. 2010), which uses galaxies as *tracers* of the large-scale matter distribution. The most direct measurement of galaxy density field is supplied by galaxy redshift surveys, i.e. angular positions and the redshifts of galaxies are recorded (Kaiser 1987). This allows us to measure the 3D position of each galaxy and its three-dimensional statistics. There are, however, several problems

[1] to be precise, it is valid at any order, but here we consider the linear level

with the interpretation of the galaxy power spectrum as measured from redshift surveys. First, there is the problem of bias (Desjacques et al. 2018), second the fact that most galaxies are not stationary but rather are characterized with peculiar velocities, and last, there are modifications of galaxy statistics like redshift-space distortions (Hamilton 1998, Raccanelli, Bertacca, Pietrobon, et al. 2013). However, at first order, these effects do not change the shape of the large-scale clustering of galaxies. In this chapter we will see the analytical shape of the cross-correlation (Stölzner et al. 2018, Afshordi 2004), accounting for MG models too (Kable et al. 2021). Since the cross-correlation involves galaxy number counts, we will describe the prescription chosen for its statistics, i.e. the Euclid mission[2] and its statistical prescription. Eventually, we will show the results obtained for each of the models described in the previous chapter.

4.1 ISW-LSS cross-correlation

The idea behind cross-correlation is to correlate two different quantities (Rhodes et al. 2014). In our case, in the sky map, we correlate the ISW effect (thus the CMB temperature anisotropies) and tracers of gravitational potentials (Crittenden and Turok 1996). Naively, one can consider cross-correlation as mixing the coefficients of the spherical harmonics of different C_l. So, as for (2.56),

$$C_l \delta_{ll'} \delta_{mm'} = \langle a_{lm} a^*_{l'm'} \rangle \tag{4.1}$$

we consider a^{ISW}_{lm} and $(a^{galaxies}_{l'm'})^*$ while up until now we considered the a_{lm} of the same observable. Let us first develop the theoretical expectation value of the cross-correlation of two random fields, projected on the sky (Rhodes et al. 2014, Afshordi et al. 2004).

4.1.1 Cross-correlation of two random fields

Let us consider the fields $A(x)$ and $B(x)$ with their Fourier transforms:

$$A_{\mathbf{k}} = \int \mathrm{d}^3\mathbf{x} e^{-i\mathbf{k}\cdot\mathbf{x}} A(\mathbf{x}), \text{ and } B_{\mathbf{k}} = \int \mathbf{d}^3\mathbf{x} e^{-i\mathbf{k}\cdot\mathbf{x}} B(\mathbf{x}). \tag{4.2}$$

The cross-correlation power spectrum $P_{AB}(k)$ is defined by:

$$\langle A_{\mathbf{k}_1} B_{\mathbf{k}_2} \rangle = (2\pi)^3 \delta^3 (\mathbf{k}_1 - \mathbf{k}_2) P_{AB}(k_1) \tag{4.3}$$

and the projections of A and B on the sky are defined using F_A and F_B projection kernels

$$\tilde{A}(\hat{\mathbf{n}}) = \int dr F_A(r) A(r\hat{\mathbf{n}}), \text{ and } \tilde{B}(\hat{\mathbf{n}}) = \int dr F_B(r) B(r\hat{\mathbf{n}}). \tag{4.4}$$

[2] https://www.euclid-ec.org/

Now expanding $\tilde{A}$ and $\tilde{B}$ in terms of spherical harmonics, the angular cross-power spectrum C_l^{AB} is defined as:

$$\begin{aligned} C_l^{AB} &\equiv \left\langle \tilde{A}_{lm} \tilde{B}^*_{lm} \right\rangle \\ &= \int dr_1 dr_2 F_A\left(r_1\right) F_B\left(r_2\right) \times \\ &\int \frac{\mathrm{d}^3\mathrm{k}}{(2\pi)^3} P_{AB}(k) (4\pi)^2 j_l\left(kr_1\right) j_l\left(kr_2\right) Y_{lm}(\hat{\mathbf{k}}) Y^*_{lm}(\hat{\mathbf{k}}) \\ &= \int dr_1 dr_2 F_A\left(r_1\right) F_B\left(r_2\right) \int \frac{2k^2 dk}{\pi} j_l\left(kr_1\right) j_l\left(kr_2\right) P_{AB}(k). \end{aligned} \tag{4.5}$$

where we have used the orthogonality of the spherical harmonics. The small angle approximation (large l) for the spherical Bessel function is

$$j_l(x) = \sqrt{\frac{\pi}{2l+1}} \left[\delta_{\mathrm{Dirac}} \left(l + \frac{1}{2} - x \right) + \mathrm{O}\left(l^{-2}\right) \right], \tag{4.6}$$

which gives

$$C_l^{AB} = \int \frac{dr}{r^2} F_A(r) F_B(r) P_{AB} \left(\frac{l+1/2}{r} \right) \cdot \left[1 + \mathrm{O}\left(l^{-2}\right) \right] \tag{4.7}$$

in the Limber approximation (Limber 1954). We can apply the same procedure to the case of the ISW effect and galaxy distributions, the two quantities we want to cross-correlate (Afshordi 2004).

4.1.2 ISW-Galaxy cross-correlation in MG

As we have seen, the aim is to compute the C_ls. We will do it with the Newtonian Gauge without assuming any particular gravity model. This will yield an expression which depends on the gravitational coupling functions Σ and μ (3.28) and hence making it sensible to different descriptions of DE or MG (Kable et al. 2021): Essentially, the computation that needs to be done is:

$$C_l^{Tg} \delta_{ll'} \delta_{mm'} = \langle a_{lm}^{ISW} (a^g_{l'm'})^* \rangle \tag{4.8}$$

while computing the single a_{lm}. To do so we have to consider once again the perturbations. The steps to follow (Afshordi 2004, Giannantonio et al. 2008) are the same as the one described in Chapter 1 for the angular power spectrum. Instead of using the generic Θ perturbation, we write the ISW contribution δT to the CMB temperature divided by the average temperature $\bar{T}$. Let's then start with the ISW effect and recast the anisotropy in terms of the redshift:

$$\frac{\delta T_{ISW}}{\bar{T}}(\hat{n}) = -\int_0^{z_*} dz e^{-\tau(z)} \frac{\partial \Phi_{eff}}{\partial z}(z, \hat{n}\chi(z)), \tag{4.9}$$

where $\hat{n}$ is the unit vector along the line of sight, z_* is the redshift value at recombination, $\Phi_{eff} = \Psi + \Phi$, and $\chi(z)$ is the comoving distance to redshift z. As usual, we expand in terms of spherical harmonics:

$$\frac{\delta T_{ISW}(\hat{n})}{\bar{T}} = -\int_0^{z_*} dz \frac{\delta T_{ISW}}{\bar{T}}(z, \hat{n}\chi(z)) = \sum_{l=1}^{\infty} \sum_{m=-l}^{l} a_{lm} Y_{lm}(\hat{n}) \tag{4.10}$$

and in Fourier space:

$$\frac{\delta T_{ISW}}{\bar{T}}(z, \hat{n}\chi(z)) = \int \frac{d^3k}{(2\pi)^3} e^{i\boldsymbol{k}\chi\hat{n}} \frac{\delta T_{ISW}}{\bar{T}}(z, k). \tag{4.11}$$

Using the property

$$\int d\Omega e^{i\boldsymbol{k}\cdot\boldsymbol{r}} Y^*_{lm}(\hat{r}) = 4\pi i^l j_l(kr) Y^*_{lm}(\hat{k}), \tag{4.12}$$

we can express (4.11) in terms of spherical Bessel functions $j_l(kr)$ with the notation $\hat{r} = \boldsymbol{r}/r$ and $\hat{k} = \boldsymbol{k}/k$. In this way we have

$$a_{lm}^{\mathrm{ISW}} = -\frac{i^l}{2\pi^2} \int_0^{z_*} \mathrm{d}z_1 \int \mathrm{d}^3k_1 e^{-\tau(z_1)} \frac{\partial \Phi_{\mathrm{eff}}}{\partial z}(z_1, k_1)\, jl\left(k_1\chi\left(z_1\right)\right) Y^*_{lm}\left(\hat{k}_1\right). \tag{4.13}$$

We can repeat the same reasoning for the angular distribution of galaxies, with the average number $\bar{N}_g$:

$$\frac{\delta N_g(\hat{n})}{\bar{N}_g} = \int_0^{z_*} dz \delta_g(z, x^i) W(z) \tag{4.14}$$

where δ_g is the galaxy density contrast which we can relate with the usual matter density contrast with:

$$\delta_g(z, x^i) = b\delta_m(z, \chi(\hat{n})), \tag{4.15}$$

being b the bias factor (Desjacques et al. 2018). $W(z)$ is a selection function that is given by the survey of choice. In our case, we considered the shape of a Euclid-like distribution (Laureijs et al. 2011) and the term will be discussed later in detail. For now, the shape itself of $W(z)$ does not matter (we will explain this term later). Rehearsing the same calculations, we expand in terms of spherical harmonics

$$\frac{\delta N_g(\hat{n})}{\bar{N}} = -\int_0^{z_*} dz \frac{\delta N_g}{\bar{N}}(z, \hat{n}\chi(z)) = \sum_{l=1}^{\infty} \sum_{m=-l}^{l} a_{lm} Y_{lm}(\hat{n}) \tag{4.16}$$

and in the Fourier series:

$$\frac{\delta N_g}{\bar{N}}(z, \hat{n}\chi(z)) = \int \frac{d^3k}{(2\pi)^3} e^{i\boldsymbol{k}\chi\hat{n}} \frac{\delta N_g}{\bar{N}}(z, k). \tag{4.17}$$

and eventually obtaining:

$$a_{lm}^{\mathrm{g}} = \frac{i^l}{2\pi^2} \int_0^{z_*} \mathrm{d}z_2 \int \mathrm{d}^3k_2 bW(z_2)\delta_m(z_2, k_2) j_l\left(k_2\chi\left(z_2\right)\right) Y^*_{lm}\left(\hat{k}_2\right). \tag{4.18}$$

The cross-correlation is then expressed in terms of Legendre polynomials $\mathcal{P}_l$ with the angle θ between the two unit vectors:

$$\left\langle \frac{\delta T_{\mathrm{ISW}}\left(\hat{n}_1\right)}{\bar{T}} \frac{\delta N_{\mathrm{g}}\left(\hat{n}_2\right)}{N_{\mathrm{g}}} \right\rangle = \sum_{l=2}^{\infty} \frac{2l+1}{4\pi} C_l^{\mathrm{Tg}} \mathcal{P}_l(\cos\theta) \tag{4.19}$$

The amplitude of this cross-correlation is given by:

$$C_l^{Tg} = \langle a_{lm}^{ISW} (a_{lm}^{g})^* \rangle. \tag{4.20}$$

Up until now, we did not consider the specific case of late time ISW and its implications, nor the fact that we should consider MG models. First of all, we can consider the importance of the DE component in the late universe by explicitly considering the growth factor D, rewriting the matter density contrast (Kable et al. 2021):

$$\delta_m(z, \boldsymbol{k}) = D(z) \frac{\delta_m(0, \boldsymbol{k})}{D_0}. \tag{4.21}$$

We can also introduce the quantity ψ_{ISW} characterizing Φ_{eff}:

$$\frac{\partial \Phi_{eff}}{\partial z} = \psi_{ISW}(z, k) \frac{\delta_m(0, \boldsymbol{k})}{D_0} \tag{4.22}$$

Now we substitute these quantities in (4.13) and (4.18) to compute (4.20):

$$\begin{aligned}
\left\langle a_{lm}^{ISW} \left(a_{l'm'}^{g}\right)^* \right\rangle = & \\
=& \frac{16\pi^2}{(2\pi)^6} \int \mathrm{d}^3k \int \mathrm{d}^3k' \left\langle \delta_m(0, \boldsymbol{k}) \delta_m(0, \boldsymbol{k'})^* \right\rangle I_l^{ISW} I_{l'}^{g} Y_{lm}^*(\hat{k}) Y_{l'm'}(\hat{k'}) \\
=& \frac{16\pi^2}{(2\pi)^3} \int \mathrm{d}^3k \int \mathrm{d}^3k' P_g(k) \delta^3\left(\vec{k} - \vec{k'}\right) I_l^{ISW} I_{l'}^{g} Y_{lm}^*(\hat{k}) Y_{l'm'}(\hat{k'}) \\
=& \frac{2}{\pi} \int \mathrm{d}k k^2 P_g(k) I_l^{ISW} I_{l'}^{g} \delta_{ll'} \delta_{mm'},
\end{aligned} \tag{4.23}$$

where we exploited (2.34) for $P_g(k)$ Thus, we get:

$$C_l^{Tg} = \frac{2}{\pi} \int \mathrm{d}k k^2 P_g(k) I_l^{ISW}(k) I_l^{g}(k) \tag{4.24}$$

where we defined the quantities I^{ISW} and I^g to simplify the notation:

$$\begin{aligned}
I_l^{\mathrm{ISW}}(k) &= \int_0^{z*} \mathrm{d}z_1 e^{-\tau(z_1)} \frac{\psi_{\mathrm{ISW}}(z, k)}{D_0} j_l\left(k\chi\left(z_1\right)\right), \\
I_l^{\mathrm{g}}(k) &= \int_0^{z*} \mathrm{d}z_2 bW\left(z_2\right) \frac{D(z)}{D_0} j_l\left(k\chi\left(z_2\right)\right).
\end{aligned} \tag{4.25}$$

Now it is useful to insert the gravitational couplings (3.28) that MG models introduce. While for ΛCDM the functions $\mu = \Sigma = \eta = 1$, for MG models they differ from one.

To put them into the C_l equation, let's consider the case in which matter fields are minimally coupled to gravity. The background equation for ρ_m nonrelativistic matter density:

$$\rho_m = \rho_{m,0}(1+z)^3 = \frac{3H_0^2}{8\pi G_N} \Omega_{m,0} (1+z)^3 \tag{4.26}$$

where the 0 subscripts refer to quantities evaluated at the present day. Using (3.28), (4.21), (4.26), we obtain an expression of $\Phi_{eff} = \Phi + \Psi$ in terms of the new gravitational couplings:

$$\Phi_{eff} = -\frac{3H_0^2\Omega_{m,0}}{k^2}(1+z)D(z)\Sigma(z,k)\frac{\delta_m(0,\boldsymbol{k})}{D_0}. \tag{4.27}$$

which we can refer to ψ_{ISW} by taking the derivative of the previous equation:

$$\psi_{ISW} = \frac{3H_0^2\Omega_{m,0}}{k^2}D\Sigma(1+(1+z)\frac{\mathrm{d}}{\mathrm{d}z}\ln(D(z)\Sigma(z,k))) \tag{4.28}$$

Defining $\mathcal{F}(z,k) = 1+(1+z)\frac{\mathrm{d}}{\mathrm{d}z}\ln(D(z)\Sigma(z,k))$, we get

$$C_l^{\mathrm{Tg}} = \frac{6H_0^2\Omega_{\mathrm{m},0}}{\pi D_0^2}\int \mathrm{d}k P_g(k) \int_0^{z_*} \mathrm{d}z_1 e^{-\tau(z_1)}D(z)\Sigma(z,k)\mathcal{F}(z,k)j_l\left(k\chi(z_1)\right)\int_0^{z_*}\mathrm{d}z_2 bW(z)D(z)j_l\left(k\chi(z_2)\right). \tag{4.29}$$

For large values of k, we can use the Limber approximation:

$$\int \mathrm{d}k k^2 f(k) j_l\left(k\chi(z_1)\right) j_l\left(k\chi(z_2)\right) \simeq \frac{\pi}{2}\frac{\delta\left(\chi(z_1)-\chi(z_2)\right)}{\chi(z_1)^2} f\left(\frac{l+1/2}{\chi(z_1)}\right). \tag{4.30}$$

It must be stressed that the Limber approximation is used for an analytical approach in order to simplify the result form. However, the ISW effect is present for low values of k. This problem is not present in the actual computation through the codes EFCAMB and CAMB since they do not approximate any formula. We obtain the final expression:

$$C_l^{Tg} \approx \frac{6H_0^2\Omega_{m,0}}{D_0^2(2l+1)^2}\int_0^{z_*} dz e^{-\tau}H(z)bW(z)D^2(z)\Sigma(z,k)\mathcal{F}(z,k)P_g\left(\frac{2l+1}{2\chi}\right) \tag{4.31}$$

This is an analytical result (Nakamura et al. 2019, Kable et al. 2021) to show how the gravitational couplings enter the cross-correlation value. We can ponder on the sign of the C_l we can obtain. In ΛCDM we have $\Sigma = \mu = 1$, hence the cross-correlation is always positive. However, in MG theories, some dark energy models can realize negative ISW-galaxy cross-correlation. We can see the condition necessary to obtain $C_l^{Tg} < 0$: from (4.31) we can see that it is necessary that

$$\mathcal{F} < 0 \tag{4.32}$$

which we can express in terms of e-folding number $\mathcal{N} = \ln a = -\ln(1+z)$:

$$\mathcal{F} = 1 - \frac{D'(\mathcal{N})}{D(\mathcal{N})} - \frac{\Sigma'(\mathcal{N})}{\Sigma(\mathcal{N})} < 0. \tag{4.33}$$

In the standard model of cosmology, the linear growth rate can be efficiently parametrized as $D'/D = \Omega_m^{\gamma(a)}$ (Peebles 1980) where $\Omega_m = \Omega_b + \Omega_c$ and the parameter $\gamma(a)$ is

the so-called growth index (Linder 2005). MG models can predict a slight deviation from ΛCDM parameterization yet detectable. Thus, we can write D'/D in Eq. (4.33) in terms of the matter density parameter Ω_m and the growth index $\gamma(a)$, as $D'/D = (\Omega_m)^{\gamma(a)}$, it follows that:

$$\mathcal{F} = 1 - (\Omega_m)^{\gamma(a)} - \frac{\Sigma'(\mathcal{N})}{\Sigma(\mathcal{N})} < 0. \tag{4.34}$$

In the ΛCDM model, the growth index is well approximated by $\gamma(a) \approx 0.55$ at low redshifts (Wang and Steinhardt 1998). Since $\Sigma = 1$ in this case, we have $\mathcal{F} = 1 - (\Omega_m)^{\gamma(a)} > 0$ and hence the ISW-galaxy cross-correlation is positive in the ΛCDM model. In modified gravity theories the growth index is generally different from 0.55. In $f(R)$ gravity, for example, it is in the range $0.40 \lesssim \gamma(a) \lesssim 0.55$ (Tsujikawa et al. 2009). The observational data of RSDs and the clustering of luminous red galaxies placed the bound $\gamma(a) = 0.56 \pm 0.05$ for constant $\gamma(a)$ (Pouri et al. 2014), so the quantity $1 - (\Omega_m)^{\gamma(a)}$ is positive for the redshift z relevant to the galaxy surveys ($z \lesssim 2$). We can relate the growth rate D with the matter density parameter Ω_m with growth index $\gamma(a)$:

$$\mathcal{F} = 1 - (\Omega_m)^{\gamma(a)} - \frac{\Sigma'(\mathcal{N})}{\Sigma(\mathcal{N})} < 0. \tag{4.35}$$

For $0 < \Omega_m < 1$ and $0 < \gamma(a) < 1$ we have $D'/D < 1$, thus the realization of negative ISW-galaxy cross-correlation is given by $\Sigma'(\mathcal{N}) > 0$.

4.1.3 Error Analysis

Associated with the cross-correlation we can find a variance in the C_ls. C_l themselves are the variance of the harmonic coefficient a_{lm}. We cannot make predictions about any particular a_{lm}, just about the distribution from which they are drawn, an (almost) Gaussian distribution whose origin is in the quantum fluctuations during inflation. The mean value of a_{lm} is zero, while the variance is the actual C_l. There is a fundamental uncertainty in the knowledge about the C_l. This uncertainty is called *cosmic variance* (Somerville et al. 2004) and it is the uncertainty on the estimate of C_l after using $2l + 1$ samples to infer it.

$$\left(\frac{\Delta C_l}{C_l}\right) = \sqrt{\frac{2}{2l+1}}. \tag{4.36}$$

A way to test the effectiveness of the survey chosen and the results obtained is to compute the Signal-to-Noise Ratio (SNR) for the cross-correlation we computed. It is the ratio of the values of the C_ls and the associated variance ΔC_l. The computation is known in the literature (Afshordi et al. 2004, Giannantonio et al. 2008, Afshordi 2004). To estimate the theoretical error, we restrict to the small angle limit and the cross-correlation function can be approximated by:

$$C_l^{AB} \simeq \frac{4\pi}{\Delta\Omega}\langle \tilde{A}_{lm}\tilde{B}^*_{lm}\rangle \tag{4.37}$$

where $\Delta\Omega$ is the common solid angle of the patch of the sky covered by observations of both $\tilde{A}$ and $\tilde{B}$. Assuming gaussianity, the standard deviation in C_l^{AB} for a single harmonic mode is given by:

$$\begin{aligned}(\Delta C^{AB})_l^2 &= \left\langle (C^{AB})_l^2 \right\rangle - \left\langle C_l^{AB} \right\rangle^2 \\ &= \Delta\Omega^{-2} \left[\left\langle \tilde{A}_{lm}\tilde{B}^*_{lm} \right\rangle \left\langle \tilde{A}_{lm}\tilde{B}^*_{lm} \right\rangle + \left\langle \tilde{A}_{lm}\tilde{A}^*_{lm} \right\rangle \left\langle \tilde{B}_{lm}\tilde{B}^*_{lm} \right\rangle \right] \\ &= (C^{AB})_l^2 + C_l^{AA} C_l^{BB}.\end{aligned} \tag{4.38}$$

The equality from the first to the second line is actually a force of notation since what is done is to call $\langle C^{AB} \rangle^2$ the quantity $\langle C^{AB} \rangle \langle C^{A'B'} \rangle$. The product is calculated directly from (4.5) and we used the orthogonality of the spherical harmonics (2.52). Eventually, thanks to the Wick Theorem (Wick 1950, Leclercq et al. 2014), we have the remaining terms. Returning to the case of the SNR for the ISW-galaxy cross-correlation, we get:

$$\left(\frac{S}{N} \right)^2 = \sum_l (2l+1) \frac{\left[C_l^{Tg} \right]^2}{C_l^{gg} C_l^{TT} + \left[C_l^{Tg} \right]^2}. \tag{4.39}$$

4.2 Euclid Survey

The modeling of the galaxy distribution is based on the *Euclid* preparations for the upcoming mission (Laureijs et al. 2011). Euclid is a space mission planned by the European Space Agency[3] and the Euclid Consortium[4] and it aims to provide a better understanding of the late Universe, particularly on why the Universe is accelerating at the present epoch. It will be set at its nominal L2 Sun-Earth Lagrangian position, and will start 6 years observing mission to complete two surveys:

- A "Euclid Wide Survey" covering 15000 deg^2 of the darkest sky. That is, the sky free of contamination by light from our Galaxy and our Solar System. The wide survey is the core of the dark energy mission out of which weak lensing, baryon acoustic oscillation, and redshift space distortion signals will be measured.

- Three "Euclid Deep Fields" about 2 magnitudes deeper than the wide survey and covering around 40 deg^2 in total will be also observed, primarily for calibrations of the wide survey data but also extending the scientific scope of the mission to faint high redshift galaxies, quasars, and AGNs.

4.2.1 Spacecraft

The spacecraft itself is about 4.1 meters tall and 3.1 in diameter, for a total of 2100Kg. It is a medium-class mission and it is part of the Cosmic Vision campaign of ESA's Science Programme with an ESA budget cap of around €500 million. Euclid was chosen in October 2011 together with Solar Orbiter, out of several competing missions. The spacecraft is made up of two major assemblies:

- Payload module: houses the telescope, the focal plane components of the instruments, and some of the data processing electronics;

- Service module: contains the satellite systems: power distribution, attitude control, propulsion, telecommand, telemetry, and data handling.

Specifically, the mounted telescope (a Korsch-type) is connected to electronic instrumentation that detects the spam from the visible wavelengths to the near-infrared. The visible (VIS) instrument will be used to measure the shapes of galaxies and derive the gravitational lensing effects induced by large-scale structures of the universe on distant background galaxies. It will probe how dark matter is distributed and how its distribution changed over the last 10 billion years. The wavelength range is 550-900nm. The Near Infrared Spectrometer and Photometer (NISP) instrument will be combined with VIS data to derive photometric redshifts and rough estimates of the distances of galaxies seen by VIS. The near-infrared spectra will be used to derive accurate redshifts and distances of galaxies and their 3-dimensional position in the Universe. The NISP spectroscopic data will primarily be used to describe the distribution and clustering of galaxies and how they changed over the last 10 billion

[3]https://www.cosmos.esa.int/web/euclid/euclid-survey
[4]https://www.euclid-ec.org/

years under the effects of the dark matter and dark energy content of the Universe and gravity. The wavelength range is 1100-2000nm.

4.2.2 Science implementation

The Euclid mission (Laureijs et al. 2011) distinguishes the so-called *primary science* and the *legacy science*. The former is given by the direct imprints of the Dark Energy, while the latter is consequential astrophysical and cosmological science that comes from the observations. Regarding the *primary Science*, the imprints of dark energy and gravity will be detected from their signatures on the expansion rate of the Universe and the growth of cosmic structures using gravitational lensing effects on galaxies (Weak Lensing) and the properties of galaxy clustering (Baryonic Acoustic Oscillations and Redshift Space Distortion). Baryon acoustic oscillations provide a direct distance-redshift probe to explore the expansion rate of the Universe. Weak lensing provides an almost direct probe of dark matter but combines angular distances that probe the expansion rate and the mass density contrast that probes the growth rate of structure and gravity. In contrast, redshift space distortion probes the growth rate of cosmic structures and gravity. Combined these three probes are solid and complementary probes of the effects of dark energy. These observations will be complemented by independent observations also derived from Euclid data on clusters of galaxies in combination with CMB data. They will be used to cross-check the results obtained from Weak Lensing, Baryonic Acoustic Oscillations, and Redshift Space Distortion and to better understand and control systematic errors (Scaramella et al. 2022). Although primarily designed as a tool for cosmologists to quantify the various components of the Universe in detail, Euclid's unprecedented survey will provide other astronomers with a treasure trove of information that can be used in many fields of astrophysics. The Euclid Consortium set several Science Working Groups that focus on the following "Legacy" or "Additional" science projects (E. Collaboration et al. 2022, Euclid Collaboration et al. 2020): clusters of galaxies; CMB Euclid galaxy survey cross-correlations; strong lensing statistics; galaxy-galaxy lensing; cool brown dwarfs; large streams and merger history of galaxies; study of resolved stellar populations in the Galaxy and the universe nearby; galaxy evolution (galaxies, AGNs, highly magnified high redshift galaxies, study of the primeval universe); high-z Lyman Break Galaxies Supernovae and transients; exo-planets.

4.2.3 Galaxy Counting Distribution in the C_l

One of the most important parts of the *Euclid* mission is setting up the implemented cosmological science. In particular, the Euclid Consortium "prepared" cosmological forecasts for *Euclid* (E. Collaboration et al. 2022). Reliable cosmological forecasts are required for the verification of *Euclid*'s performance before launch for an updated technical description of the mission design (Laureijs et al. 2011). The cosmological probes considered in the mission are weak lensing (WL); photometric galaxy clustering (GCph); spectroscopic galaxy clustering (GCs); their combination; and the addition of the data vector of cross-correlation (XC) between GCph and WL. The statistical constraining power of a galaxy survey depends mainly on the abundance of its target galaxy sample and how the survey strategy determines the survey's se-

lection function. Modeled simply, this means that the statistical errors on the power spectrum can be estimated by knowing the observed number density of its galaxy targets and the survey volume. This can be converted to the number density in each redshift bin. This is actually what we used in the thesis since the computation of the cross-correlation through CAMB just requires the $n(z)$, the observed number density of galaxies. Let us first see how the observables are described according to the Euclid survey (Euclid Collaboration et al. 2020). The theoretical modeling of the WL, GCp, and cross-correlation power spectra in each of those redshift bins consists of computing integrals of the following form, assuming the flat-sky and Limber approximations:

$$C_\ell^{XY} = c \int \frac{\mathrm{d}z}{H(z) r^2(z)} \mathcal{W}^X(z) \mathcal{W}^Y(z) P_{\delta\delta}\left(\frac{\ell + 1/2}{r(z)}, z\right) + \mathcal{N}_\ell^{Xy}. \tag{4.40}$$

In the above expression, the letters X and Y can stand either for WL_i or GCp_i (the subscript i referring to the ith redshift bin considered), and $\mathcal{W}^X$ represents the so-called 'kernel' associated with observable X. $\mathcal{N}_\ell^{Xy}$ is the *shot noise*. The shot noise, according to how the computation is made in this work, does not enter in the C_l but has to be taken into account when computing the SNR. The kernel corresponding to the GCp is

$$\mathcal{W}^{\mathrm{GCp}_i}(z) = b_i(z) \frac{n_i(z)}{\bar{n}_i} \frac{H(z)}{c}. \tag{4.41}$$

where $\bar{n}_i$ is the galaxy surface density per bin, and b_i is the bias factor for each bin calculated as $b_i = \sqrt{1 + z_{c,i}}$. The kernel itself is based on one key ingredient: the number density distribution $n_i(z)$ of the observed galaxies in the ith bin. For a photometric redshift estimate, this can be written as:

$$n_i(z) = \frac{\int_{z_i^-}^{z_i^+} \mathrm{d}z_\mathrm{p} n(z) p_\mathrm{ph}\left(z_\mathrm{p} \mid z\right)}{\int_{z_\mathrm{min}}^{z_\mathrm{max}} \mathrm{d}z \int_{z_i^-}^{z_i^+} \mathrm{d}z_\mathrm{p} n(z) p_\mathrm{ph}\left(z_\mathrm{p}, \mid z\right)} \tag{4.42}$$

where (z_i^-, z_i^+) are the edges of the ith redshift bin. The underlying true distribution $n(z)$ appearing in this expression is chosed to be in agreement with the *Euclid* Red Book (Laureijs et al. 2011):

$$n(z) \propto \left(\frac{z}{z_0}\right)^2 \exp\left[-\left(\frac{z}{z_0}\right)^{3/2}\right] \tag{4.43}$$

Figure 4.1: the galaxy number density distribution $n(z)$

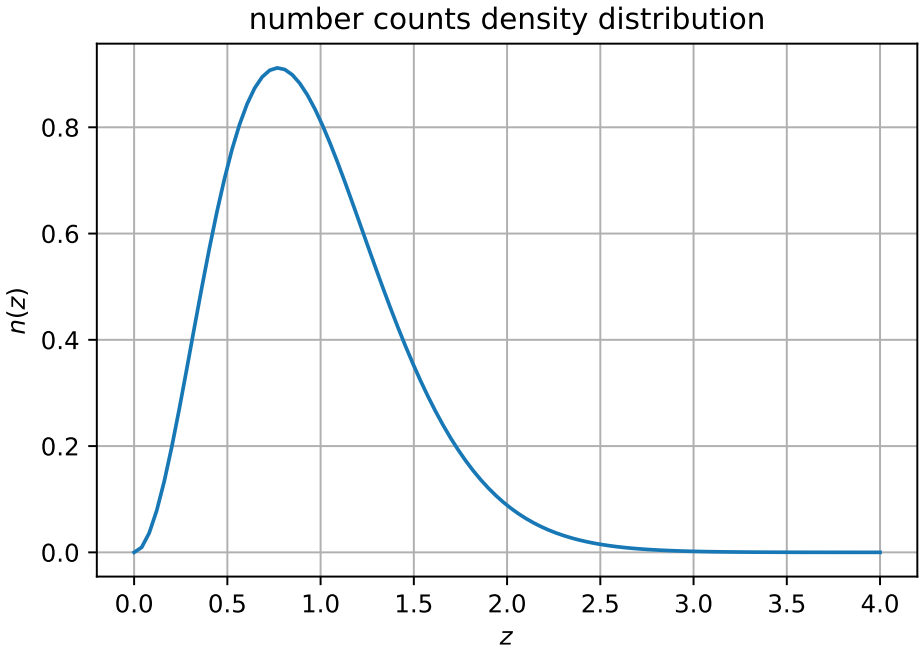

where $z_0 = \frac{z_m}{\sqrt{2}}$ with $z_m = 0.9$ the median redshift according to the Red Book. According to the same book, the surface density of galaxies is $\bar{n}_g = 30 arcmin^{-2}$. With this choice, the set edges of the 10-equi populated bins are:

$$z_i = 0.0010, 0.42, 0.56, 0.68, 0.79, 0.90, 1.02, 1.15, 1.32, 1.58, 2.50. \tag{4.44}$$

The distribution $n(z)$ is convoluted in (4.42) with the probability distribution function $p_{ph}(z_p|z)$ describing the probability that a galaxy with redshift z has a measured redshift z_p (Kitching et al. 2009). A parametrization of it is:

$$\begin{aligned} p_{\rm ph}\left(z_{\rm p} \mid z\right) = & \frac{1-f_{\rm out}}{\sqrt{2\pi}\sigma_{\rm b}(1+z)} \exp\left\{-\frac{1}{2}\left[\frac{z-c_{\rm b}z_{\rm p}-z_{\rm b}}{\sigma_{\rm b}(1+z)}\right]^2\right\} \\ & + \frac{f_{\rm out}}{\sqrt{2\pi}\sigma_{\rm o}(1+z)} \exp\left\{-\frac{1}{2}\left[\frac{z-c_0 z_{\rm p}-z_0}{\sigma_0(1+z)}\right]^2\right\} \end{aligned} \tag{4.45}$$

where $c_b, z_b, \sigma_b, c_o, z_o, \sigma_o, f_{out}$ are constant parameters. While we have described the *Euclid* prescription for the C_l, the computation used in our thesis invokes a simple spline interpolation for the galaxy counting kernel. CAMB, the tool used, builds the window function (the kernel) starting from the underlying true galaxy distribution $n(z)$ with the provided redshift bin vector (4.44) and the respective bias vector. The latter can be obtained through $b_i = \sqrt{1+z_{c,i}}$ where $z_{c,i}$ is the central redshift of the ith bin. To put it simply, instead of using (4.41), we use a spline interpolation of $n(z)$. This procedure does not lose any information, it is simply an alternative way for numerical computation (Kitching et al. 2009). The C_l computation has been

performed up until $l = 300$. This is to not stretch the computation to useless modes for the scales we are considering.
Let us open a small parenthesis and briefly explain what spline interpolation is (Prenter and Mathematics 2008,Lyche and Schumaker 1973). Let us define what a spline is: a function $S_m(\Delta_n, x)$ which is defined and has continuous $(m-1)$-st derivative on an interval $[a, b]$, and which coincides on each interval $[x_i, x_{i+1}]$ formed by the partition Δ_n: $a = x_0 \leq x_1 \leq ... \leq x_n = b$ with a certain algebraic polynomial of degree at most m. Splines can be represented in the following way:

$$S_m(\Delta_n, x) = P_{m-1}(x) + \sum_{k=0}^{n-1} c_k (x - x_k)_+^m \tag{4.46}$$

where the c_k are real numbers, $P_{m-1}(x)$ is a polynomial of degree at most $m-1$, and $(x-t)_+^m = \max(0, (x-t)^m)$. The points $x_i{}_{i=1}^{n-1}$ are called the knots of the spline. If a spline $S_m(\Delta_n, x)$ has a continuous $(m-k)$-th derivative on $[a, b]$ for $k \gtrsim 1$ and at the knots the $(m-k+1)$-st derivative of the spline is discontinuous, then it is said to have defect k. Besides these polynomial splines, one also considers more general splines (L-splines), which are "tied together" from solutions of a homogeneous linear differential equation $Ly = 0$, splines (L_g-splines) with different smoothness properties at various knots, and also splines in several variables. Splines and their generalizations often occur as extremal functions when solving extremum problems, e.g. in obtaining best quadrature formulas and best numerical differentiation formulas. Splines are applied to approximate functions (such as in our case the Spline interpolation), and in constructing approximate solutions of ordinary and partial differential equations. Interpolation by means of splines is the construction of an interpolation spline taking given values $f(x_i)$ at prescribed points x_i with $i = 0, ..., n$. Interpolation splines usually satisfy the conditions at the endpoints. For example, for cubic spline $S_3(\Delta_n, x)$ where Δ_n is a partition $a = x_0 \leq x_1 \leq ... \leq x_n = b$, which on $[a, b]$, consists of piecewise-cubic polynomials and has a continuous second-order derivative, one requires that $S_3(\Delta_n, x_i) = f(x_i)$ and, in addition, one condition at each endpoint (e.g., $S_3'(\Delta_n, a) = y_0'$) and $S_3(\Delta_n, b) = y_n'$ or $S_3''(\Delta_n, a) = y_0''$ and $S_3''(\Delta_n, b) = y_n''$[5]. If the $f(x_i)$ are the values of a $b-a$ periodic function, then one requires the spline to be $b-a$ periodic too. For polynomial splines of degree $2k+1$, the number of extra conditions at each endpoint a or b is increased by k. For interpolation splines of degree $2k$, the knots of the spline (the points of discontinuity of the $2k$-th derivative) are usually chosen halfway between the points x_i, and a further k conditions are assigned at a and b. Spline interpolation has some advantages when compared to polynomial interpolation. There are sequences of partitions $\Delta_n : a = x_0(k) < x_1(k) < ... < x_{n_k}(k) = b$ and interpolation splines for which the interpolation process converges for any continuous function, provided that

$$\|\Delta_{n_k}\| = \max_{0 \leq i \leq n_k - 1} (x_{i+1}(k) - x_i(k)) \to 0 \tag{4.47}$$

Many processes of spline interpolation give the same order of approximation as the best approximation. Moreover, spline interpolation of some classes of differentiable

[5]the derivatives are with respect to x

functions has the property that the error does not exceed the width of the corresponding class. Spline interpolation can be used to solve certain variational problems. E.g., under sufficiently general additional conditions at a and b, interpolation splines satisfy the relation:

$$\begin{aligned} &\int_a^b \left[f^{(m)}(t) - S_{2m-1}(m)\left(\Delta_n, t\right)\right]^2 dt = \\ &= \int_a^b \left[f^{(m)}(t)\right]^2 dt - \int_a^b \left[S_{2m-1}(m)\left(\Delta_n, t\right)\right]^2 dt. \end{aligned} \tag{4.48}$$

This implies the existence and uniqueness of interpolation splines of odd degree, and also the simplest results on convergence:

$$\begin{aligned} &\| f^{(i)}(t) - S_{2m-1}(i)\left(\Delta_n, t\right) \|_{L_2[a,b]} \leq \\ &\leq c_{i,m} \left\|\Delta_n\right\|^{m-i} \left\| f^{(m)}(t) \right\|_{L_2[a,b]} \\ &\| f^{(i)}(t) - S_{2m-1}(i)\left(\Delta_n, t\right) \|_{C[a,b]} \leq \\ &\leq c_{i,m} \left\|\Delta_n\right\|^{m-i-1/2} \left\| f^{(m)}(t) \right\|_{L_2[a,b]} \end{aligned} \tag{4.49}$$

$i = 0...m-1$, where the $c_{i,m}$ depend only on i and m, and

$$\left\|\Delta_{n_k}\right\| = \max_{0 \leq i \leq n_k - 1} \left(x_{i+1}(k) - x_i(k)\right). \tag{4.50}$$

For some classes of differentiable functions, the sequence of interpolation splines converges to the function to be interpolated on any sequence of partitions Δ_{n_k} for which $\left\|\Delta_{n_k}\right\| \to 0$. In addition to polynomial interpolation splines, one can also use splines of a more general form. For many of these, results analogous also hold. For splines with defects greater than 1 one usually carries out interpolation with multiple knots.

4.3 Initial Conditions for the Models

Before presenting the C_l of cross-correlation, it is important to describe the initial conditions set in the models so that the computation can happen. As we have shown, each model has additional cosmological parameters whose values have to be fixed. For K-mouflage, Galileon Ghost Condensate (GGC), Generalized Cubic Covariant Galileon (GCCG) the best fit values are taken from the results of Kable et al. 2021, and for Transitional Planck Mass (TPM), the values given by Benevento, Kable, et al. 2022. In the first case, the model parameters are obtained through a likelihood analysis. To construct an ISW-galaxy cross-correlation likelihood, the tomographic analysis of the ISW signal has been extended to MG models (Kable et al. 2021), using photometric measurements of the redshift of galaxies applied to the ΛCDM model (see e.g. Stölzner et al. 2018). The Galileon Ghost Condensate has been reviewed but the computation of the cross-correlation is left as a (near) future work. Nevertheless, being one important candidate of an alternative theory, we decided to review its most recent features and in this section we describe the costraints set

by the theory on the cross-correlation. For the K-mouflage and GCCG, The best-fit values for the MG models' parameters are obtained from combining different datasets:

- *Planck* 2018 measurements of CMB temperature and polarization anisotropy (P. Collaboration, Aghanim, Akrami, Ashdown, Aumont, Baccigalupi, M. Ballardini, Banday, Barreiro, N. Bartolo, Basak, Benabed, et al. 2020.
- Measurements of the BAO from BOSS DR12 (Alam et al. 2017), SDSS Main Galaxy Sample DR7 (Ross et al. 2015), and 6dFGS (Beutler et al. 2011).
- The 2018 Pantheon Supernova compilation (Scolnic et al. 2018), which includes 1048 SNIa data in the redshift range $0.01 < z < 2.3$.

For the TPM model, instead of a minimization, (Markov-Chain-Montecarlo), MCMC simulations were run. In addition, the Gelman-Rubin convergence statistic $R-1 = 0.02$ was used, for the least constrained parameter to determine when the chains have converged (Gelman and Rubin 1992). It is interesting to notice that minimization and MCMC give the same conclusion in the ΛCDM model (Stölzner et al. 2018). In the TPM case, the observational datasets used to obtain the constraints include Planck CMB likelihood, various BAO measurements, and a complete catalog of type Ia supernovae. Specifically:

- For CMB, it was used the 2018 Plik Lite TTTEEE + Low ell TT + Low E likelihoods as well as the Planck 2018 Lensing likelihood (P. Collaboration, Aghanim, Akrami, Ashdown, Aumont, Baccigalupi, M. Ballardini, Banday, Barreiro, N. Bartolo, Basak, Benabed, et al. 2020)
- For BAO, we use the completed SDSS-III Baryon Oscillation Spectroscopic Survey (BOSS) survey DR 12 (Alam et al. 2017), the SDSS Main Galaxy Sample (Ross et al. 2015), and the 6dFGS survey (Beutler et al. 2011).
- For Type Ia supernovae, we use the 2018 Pantheon compilation (Scolnic et al. 2018).
- A prior on H_0 was included, which is obtained by comparing the independent results of Riess, Yuan, et al. 2022 with Pesce et al. 2020 and Blakeslee et al. 2021

A fair comparison with the ΛCDM model can only be done by comparing each model with the ΛCDM obtained from the same dataset. We then differentiate the ΛCDM A as the one obtained from the first dataset used in (Kable et al. 2021); the ΛCDM B as the one obtained from the second dataset used in (Benevento, Kable, et al. 2022). As we said, the parametrization used for the K-mouflage model is given by Brax and Valageas (2016) and described in the previous chapter (see section 3.5.2). Consequently, the EFTCAMB parametrization will have in input $\epsilon_{2,0}, \gamma_A, m, \alpha_U, \gamma_U$. The parameters fixed are $\gamma_U = 1, \gamma_A = 0.2, m = 3$ as these are unconstrained by the likelihood. In the case of the GCCG, the key quantities to set are the two parameters q and $s = p/q$. At the background level, the deviation from $w_{DE} = -1$ is quantified by the parameter s. In the case of the GGC the x_i parameters play the fundamental

role of deviation from the ΛCDM, giving rise to a different cosmic growth history. Specifically, x_3 leads to deviations of μ and Σ from 1. The initialization parameters are then x_1^0 and x_3^0, which are today's values of x_1 and x_3.

Table 4.1: Best fit parameters used for the computation of the cross-correlations. Taken from Kable et al. (2021)

Model	H_0	$\Omega_{b,0}h^2$	$\Omega_{c,0}h^2$	$10^9 A_s$	n_s	τ	S_8
ΛCDM A	67.69	0.02242	0.1193	2.099	0.9673	0.055	0.8234
GGC	68.24	0.02245	0.1196	2.108	0.9656	0.057	0.8502
GCCG	68.93	0.02240	0.1200	2.106	0.9656	0.056	0.8394
K-mouflage	68.37	0.02241	0.1198	2.106	0.9670	0.056	0.8250

with the additional parameters:

Table 4.2: Best fit additional parameters used for the computation of the cross-correlations. Taken from Kable et al. (2021)

Model	Additional Parameters
GGC	$x_1^0 = -1.20$, $x_3^0 = 0.38$
GCCG	s=0.182, q=1.49
K-mouflage	$\alpha_U = 0.505$, $\epsilon_{2,0} = -6.9 \times 10^{-4}$, $\gamma_U = 1$, $\gamma_A = 0.2$, $m = 3$

In the case of the TPM, the additional parameters are mostly given by the transition of the Planck Mass. The amplitude is set by Ω_0, with σ its width. Another important parameter is x_T which sets the time at which the transition happens $a_T = 10^{x_T}$. In addition, the final parameter is c_0 which enters the background and perturbative equations since it is what has been used to parametrize the EFT functions.

Table 4.3: Best fit parameters used for the computation of the cross-correlations. Taken from Benevento, Kable, et al. (2022)

Model	H_0	$\Omega_{b,0}h^2$	$\Omega_{c,0}h^2$	$10^9 A_s$	n_s	τ	S_8
ΛCDM B	68.44	0.02257	0.11777	3.058	0.9698	0.0621	0.811
TPM	71.38	0.022649	0.1191	3.049	0.9772	0.054	0.825

with the additional parameters:

Table 4.4: Best fit additional parameters used for the computation of the cross-correlations. Taken from Kable et al. (2021)

Parameter	Value
Ω_0	-0.045
x_T	-4.29
σ	0.88
c_0	-0.0176

4.4 Results

The results presentation is split into two distinct sections, given the different datasets from which the best-fit model parameters are considered (one for K-mouflage and GCCG, and one for TPM). In addition to the cross-correlation, for all the models we have computed the modes of the C_ls of CMB angular power spectra. Generally, the K-mouflage, and GCCG are much closer to the ΛCDM A values and it is shown in all the plots presented. The TPM model, on the other hand, shows a slight but noticeable different behavior on the largest scales, where the ISW is relevant. This is reflected not only in angular power spectrum of the CMB temperature but specifically in the amplitude of the cross-correlation. For all the models we investigated different values of the additional parameters and we report the most interesting case referring to the TPM model. While the cross-correlation obtained with the Euclid description is a novelty, the parameters space of K-mouflage and GCCG had already been investigated (Kable et al. 2021). Instead, the results for the TPM are new (Benevento, Kable, et al. 2022). In light of the future work on the GGC, we report here what can be said on the possible values of the cross-correlation according to the stability constraints that are imposed on the theory.

4.4.1 K-mouflage, GCCG results and GGC discussion

In the case of the K-mouflage models, for $A > 0$ and $\frac{dA}{d\phi} > 0$ with the general stability criteria derived for full Horndeski theories (3.97), i.e. the absence of scalar ghosts and Laplacian instabilities, the time derivative of ϕ is constrained to be negative, when compatible with the background equations. This translates in $\epsilon_2 < 0$. Thus the coupling function (3.91) becomes,

$$\Sigma'(\ln a) = \epsilon_2 A^2 \tag{4.51}$$

which is negative given $\epsilon_2 < 0$. The necessary condition for realizing negative ISW-galaxy cross-correlation is not satisfied in K-mouflage theories. This is well reflected by the result obtained and by the data. Regarding the impact of the parameters on the amplitude of the cross-correlation, $\epsilon_{2,0}$ affects it, with a tradeoff. A high value of $\epsilon_{2,0}$ enhances the cosmic expansion at late times, suppressing the growth of matter perturbations. However, the coupling $\mu = (1 + \epsilon_1)A^2$ is enhanced by a positive ϵ_1, which at leading order $\epsilon_1 \sim -\epsilon_2$ during matter era. The trade-off leads to a higher amplitude of the ISW effect in the K-mouflage theories with respect to its ΛCDM limit ($\epsilon_{2,0} \to 0$). The behavior is confirmed by the plot 4.3, and variations of the parameter $\epsilon_{2,0}$ confirm the limit.
Contrary to the K-mouflage model, a negative ISW-galaxy is allowed for GGC and GCCG. The cubic-order derivative interaction term $G_3(X)\Box\phi$ gives rise to a different cosmic growth history which can induce negative ISW-galaxy cross-correlation. (more details are given in the next paragraph) Since $G_3(X)$ contributes to the dark energy density, Σ grows at low redshifts, which then satisfies the negative cross-correlation condition $\Sigma'(\ln a) > 0$. In the case of the GCCG, the sign depends on the two parameters s and q, making it possible to realize either negative or positive cross-correlation (Giacomello et al. 2019, De Felice and Tsujikawa 2012b). Given

the best fit values, we can see from the plot that in the case of GCCG a positive cross-correlation is realized, with an amplitude slightly bigger than the ΛCDM one.

Considering the GGC, we leave the computation of the cross-correlation to a future work but we can make some insightful considerations and use it as an example to explain the possibility of a negative ISW-LSS cross-correlation. This is another critical difference between Galileon cosmologies and ΛCDM and concerns the evolution of the gravitational potentials (Renk, Zumalacárregui, et al. 2017, Kobayashi, Tashiro, et al. 2010). In Barreira, Li, et al. (2014) the authors demonstrated that the modifications to gravity in the Galileon model are such that the lensing potential can deepen with time after matter domination, rather than strictly decaying as it is the case in standard ΛCDM. This means that in ΛCDM the sign of the ISW effect is always positive, whereas it can be negative in the Galileon model. In detail, let us consider for instance a photon travelling through a supercluster whose potential is getting shallower with time. This photon will get blueshifted (increase of temperature) as it goes into the center of the potential well, but redshifted (decrease of temperature) as it comes out of it. Since the potential was deeper at the time the photon was entering it, overall the temperature of the photon will increase. This causes a so-called *hot spot* in the CMB maps. If the potential of the supercluster is getting deeper with time, then one would end up with a *cold spot* instead. The amplitude of the ISW effect is proportional to the time derivative of the lensing potential. In the standard ΛCDM picture, the lensing potential grows at the transition from the radiation to the matter dominated eras, stays approximately constant during the matter era, and starts decaying at the onset of the Dark Energy era. The physical picture in the Galileon models is more complex, since it is scale-dependent (Barreira, Li, et al. 2014). At late times, on smaller length scales, the Galileon field contributes significantly to the lensing potential, making it deeper. On the other hand, on larger length scales, the Galileon terms become less important, which leads to a gradual recovery of the ΛCDM behaviour, i.e., the lensing potential decays at late times. Data analyses from galaxy surveys correlated with the CMB temperature result in a $\sim 3\sigma$ detection of a positive ISW-LSS cross-correlation amplitude (e.g. Giannantonio et al. 2008, P. Collaboration, Aghanim, Akrami, Ashdown, Aumont, Baccigalupi, M. Ballardini, Banday, Barreiro, N. Bartolo, Basak, Benabed, et al. 2020). This implies that MG models that have a strictly growing lensing potential on sub-horizon scales can be ruled out with at least 3σ significance since they predict a negative ISW-LSS cross-correlation amplitude. The analysis of Barreira, Li, et al. 2014 suggested that this could well be the case for their resulting best-fitting models but the discussion there was kept mostly qualitative. In the case of the GGC, we can have a negative ISW-LSS cross-correlation value: consider the effective coupling functions for the GGC (3.83). In the two early-time cosmological epochs discussed in 3.5.1.2, the right hand side of (3.83) reduces to:

$$\mu = \Sigma \simeq \begin{cases} 1 + \frac{x_3}{2+3\Omega_{\mathrm{m}}+4\Omega_{\mathrm{r}}} & \text{for } \{|x_1|, |x_2|\} \ll |x_3| \ll 1 \\ 1 + \frac{x_3}{2(1+3\Omega_{\mathrm{m}}+4\Omega_{\mathrm{r}})} & \text{for } x_3 = -2x_1, \quad x_2 \to 0 \end{cases} \tag{4.52}$$

With the growth of x_3, Σ increases in time. The growth of Σ is particularly significant in the late universe at which x_3 contributes to the Dark Energy density. Hence

it is possible to realize the negative ISW-galaxy cross-correlations in the GGC model. As an example we can see the resulting cross-correlation obtained in Kable et al. (2021). In their plot (Fig.4.2) the ISW-galaxy cross-correlation power spectra for two different redshift bins are presented: (1) $0.1 \leq z < 0.3$ (left) and (2) $0.5 \leq z < 0.7$ (right). The C_l angular power spectra has been computed for three different cases: (i) $x_1^0 = -1.35, x_3^0 = 0.05$, $(ii) x_1^0 = -1.20, x_3^0 = 0.36$, and (iii) $x_1^0 = -0.85, x_3^0 = 1.06$, where x_1^0 and x_3^0 are today's values of x_1 and x_3 respectively. The Sloan Digital Sky Surveys (SDSS) data are shown as black points with error bars. Besides the ΛCDM model, the cross-correlation power spectrum in the Cubic Galileon (G3) model is shown. We can see the possibility for a negative GGC (but also a negative value for the Cubic Galileon, which in our case resulted to be positive). They have found that if the magnitude of $|x_1^0|$ increases relative to x_3^0, the ISW signal approaches the ΛCDM limit. For x_3^0 exceeding the order of $|x_1^0|$, the ISW signal approaches the G3 limit. In this latter case, it is possible to generate a negative ISW-galaxy cross-correlation, which is disfavored when data from all redshift bins are included. In our case, if the ISW signal approaches the G3 limit, we expect this time a positive value for the GGC. The behavior would correspond to their case (x_3^0 exceeding the order of $|x_1^0|$), but the result would be different, given our positive cross-correlation for GCCG. Future work will go into details regarding the cross-correlation of the GGC model.

Figure 4.2: C_l of angular cross-correlation for the models GGC and GCCG compared to ΛCDM model. Plot from Kable et al. (2021)

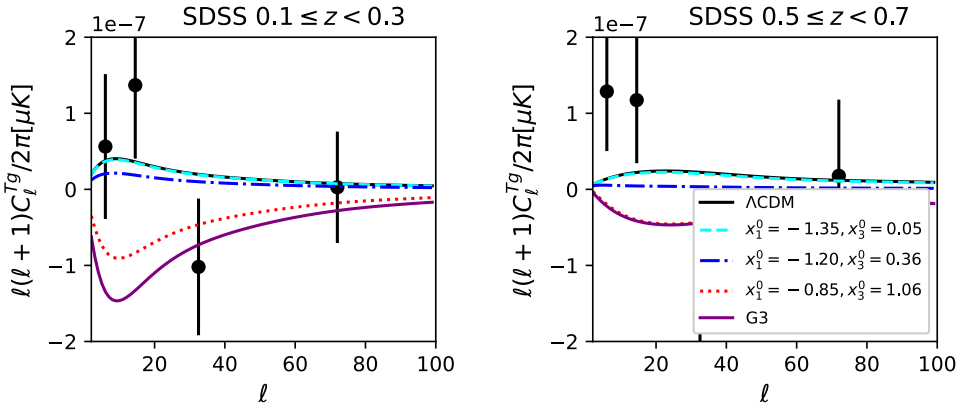

It has been shown (Peirone et al. 2019, Frusciante, Peirone, et al. 2020) that both GCCG and GGC are significantly favored over the ΛCDM for particular combinations of data sets. In detail, The GCCG is able to ease the tension in the estimation of the present-day value of the Hubble parameter between CMB and low-z measurements. However, the tension is again present when including the BAO data. GCCG is favored when considering the Planck data alone because the GCCG is able to better fit the ISW tail (Frusciante, Peirone, et al. 2020). To quantify the preference of the GCCG model with respect to the ΛCDM, the Deviance Information Criterion (DIC) has been considered (Spiegelhalter et al. 2014). The DIC accounts for both the goodness of the fit and the Bayesian complexity of the model. The DIC test

favors the GCCG when considering the Planck dataset. However, when considering the combined datasets (the so called *PBRS*) of Planck (P. Collaboration, Aghanim, Akrami, Ashdown, Aumont, Baccigalupi, M. Ballardini, Banday, Barreiro, N. Bartolo, Basak, Battye, et al. 2020), BAO (Beutler et al. 2011), RSD (Alam et al. 2017), SNIa (Betoule et al. 2014) the ΛCDM is once again favored (Frusciante, Peirone, et al. 2020). In the case of the GGC, the DIC exhibits a preference for the GGC in both Planck and PBRS dataset (Peirone et al. 2019). In addition, the Bayesian evidence factor has been considered (along the lines of Heavens et al. 2017) and it shows a significant preference for GGC.

Figure 4.3: C_l of cross-correlation for the models K-mouflage and GCCG compared to ΛCDM model

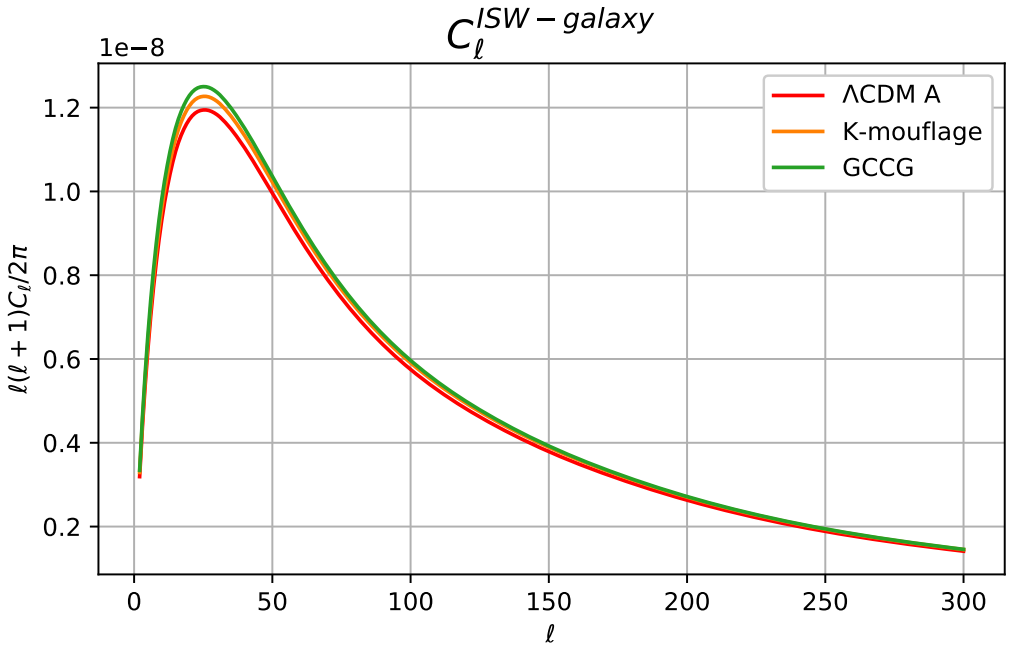

In addition, we have computed the SNR (4.39) expected for a detection of the cross-correlation signal in each model, using a Euclid-like galaxy redshift distribution. The possible sources of noise entering in SNR computation are the *cosmic variance* and the *shot noise*. Regarding the latter, the uncorrelated part of the intrinsic (unlensed) ellipticity field (Schäfer and Merkel 2017) acts as a shot noise term in the observed galaxy matter power spectrum. This is non-zero for auto-correlation (intra-bin) power spectra but is zero for cross-correlation (inter-bin) power spectra because ellipticities of galaxies at different redshifts should be uncorrelated (Euclid Collaboration et al. 2020). Therefore, the shot-noise does not enter into the Noise term for our cross-correlations since the intrinsic ellipticity dispersion is zero for cross-correlations(E. Collaboration et al. 2022). The values are quite similar:

$$SNR_{K-mouflage} \sim 6.43; \qquad SNR_{GCCG} \sim 6.46; \qquad SNR_{GR} \sim 6.34. \tag{4.53}$$

Figure 4.4: C_l modes of CMB angular power spectrum for the ΛCDM A, K-mouflage, and GCCG.

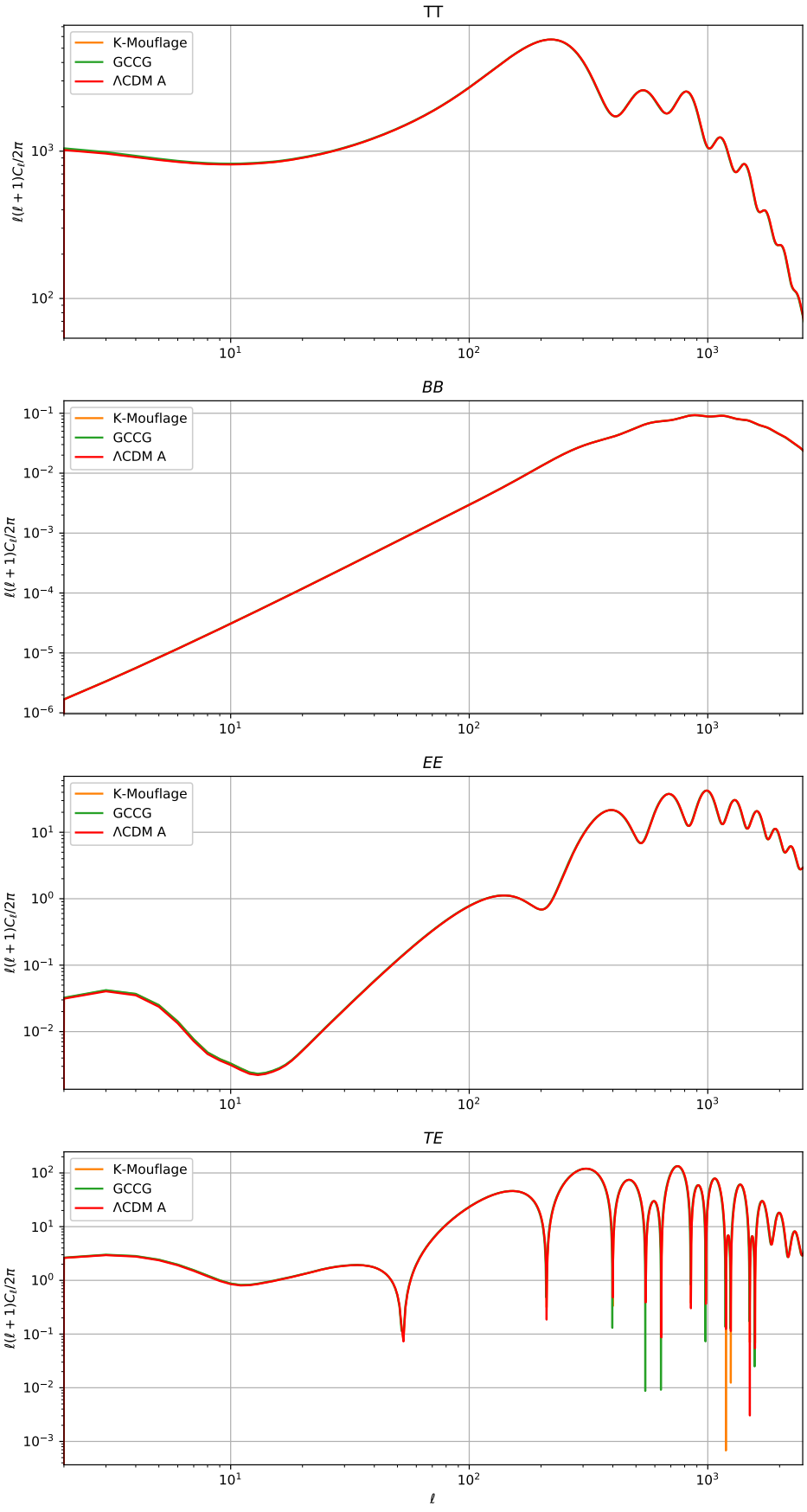

4.4.2 TPM results

In the case of the TPM, the departure on large scales is evident from the CMB angular power spectra. We can see in Fig. 4.9 that for low l the distinction is remarkable. Thus the computation of the residuals has been performed as:

$$\frac{\Delta C_X}{\sigma_X} = \frac{C_X^{TPM} - C_X^{\Lambda CDM}}{\sigma_X} \tag{4.54}$$

where X can stand for TT, EE, TE, BB. It can be seen in Fig.(4.10). The denominator σ is the cosmic variance, used to normalize the residuals shown in Fig 4.10, which prescription is given by (Lin, W. Hu, et al. 2020):

$$\sigma_{\mathrm{X}} = \begin{cases} \sqrt{\frac{2}{2\ell+1}} C_l^{TT}, & \mathrm{X} = \mathrm{TT} \\ \sqrt{\frac{1}{2\ell+1}} \sqrt{C_\ell^{TT} C_\ell^{EE} + \left(C_\ell^{TE}\right)^2}, & \mathrm{X} = \mathrm{TE} \\ \sqrt{\frac{2}{2\ell+1}} C_\ell^{EE}, & \mathrm{X} = \mathrm{EE} \end{cases} \tag{4.55}$$

which is obtained from the C_l of ΛCDM. For the BB modes, the normalization is with respect to simply $C_{BB}^{\Lambda CDM}$.

When considering the cross-correlation (Fig. 4.5), we can see the significantly different amplitude compared to the ΛCDM. This is also reflected in the SNR computation, which shows $SNR_{GR} \sim 6.48$ and $SNR_{TPM} \sim 3.49$. Some considerations on the parameters of the model have to be done in regard to the smallness of the amplitude. Specifically, we have to look at the effective coupling functions (3.111). As we can see, they depend on the form of the transition function (thus Ω_0, σ) and c_0. On the largest scales $\mu \sim (1-\Omega)^{-1}$ and $\Sigma \sim (1+\Omega)^{-1}$. On the smaller scales, the dependence lies also on c_0. This parameter plays a pivotal role when defining 2 regimes, at early epochs and later epochs. At early epochs the main effect on μ and Σ is sourced by the evolution of Ω, having $\dot{\Omega} \gg c/H$. At later epochs the effect of c_0 becomes dominant and μ and Σ on small scales grow again. Given the interest in the late ISW effect, the contribution of c_0 greatly affects the amplitude of the cross-correlation.

Figure 4.5: C_l of cross-correlation for the TPM and ΛCDM B models. We can clearly see the difference in amplitude.

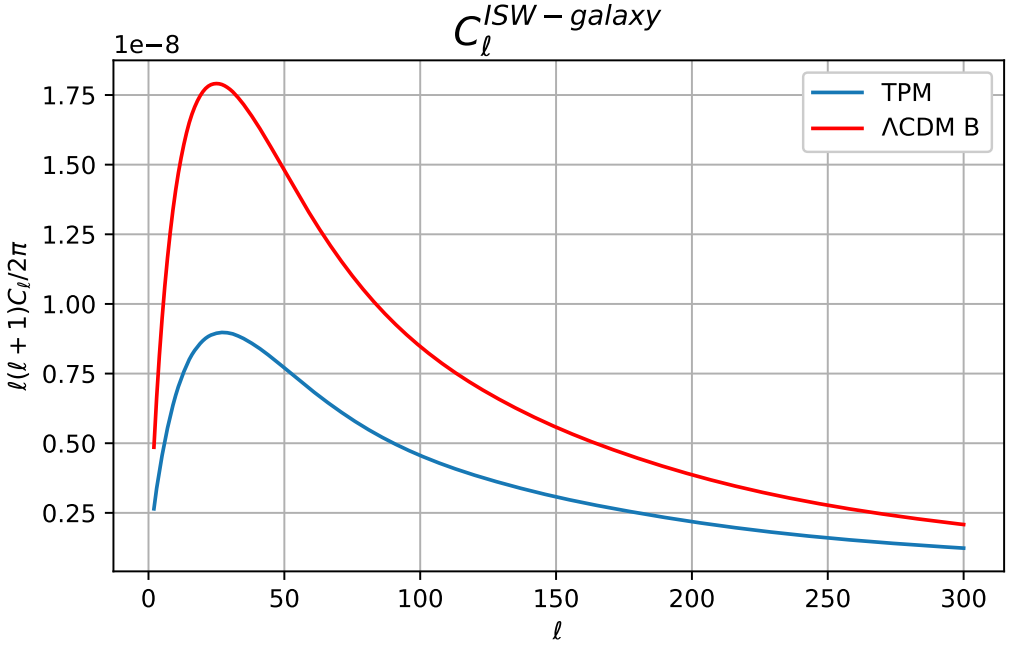

A first approach to understanding what makes the amplitude so small is to vary the relevant cosmological parameters. We varied all the parameters of the model of a value of 1σ of the best-fit value. In this way, we identified the key quantities. In detail, small[6] variations (see Figs. 4.8, 4.7) happen when varying A_s (the amplitude of primordial perturbations) and Ω_0 (the amplitude of the transition of the Mass Planck), while varying the other parameters produce no distinguishable difference, including σ (the width of the transition). The last two parameters modify the expansion history and the growth of perturbations only before recombination. For this reason they do not affect the late ISW-LSS cross-correlation amplitude, as confirmed by our results. While they should be relevant on large scales, at later epochs c_0 is the key parameter, overcoming Ω. In fact, varying c_0[7] greatly affects the amplitude and we report here the same cross-correlation computed with 3 different values of c_0 each one closer to the limit 0. In agreement with Benevento, Kable, et al. (2022), in the limit $c_0 \to 0$ we recover ΛCDM. The parameter c_0 itself alleviates the tension on H_0: the late-time effect of a negative c_0 parameter also contributes to bringing the present H_0 to higher values, through a reduction of the present value of $w_{TPM,0}$ to below -1 for negative values of c_0.

[6] these are small variations in amplitude if compared to the amplitude variations that happen when varying the parameter c_0, which is discussed shortly after

[7] the c_0 parameter regulates the EFT function $c(t)$ that enters into the background equations. See (3.105)

Figure 4.6: C_l of cross-correlation for the TPM model in the case of different values of the parameter c_0.

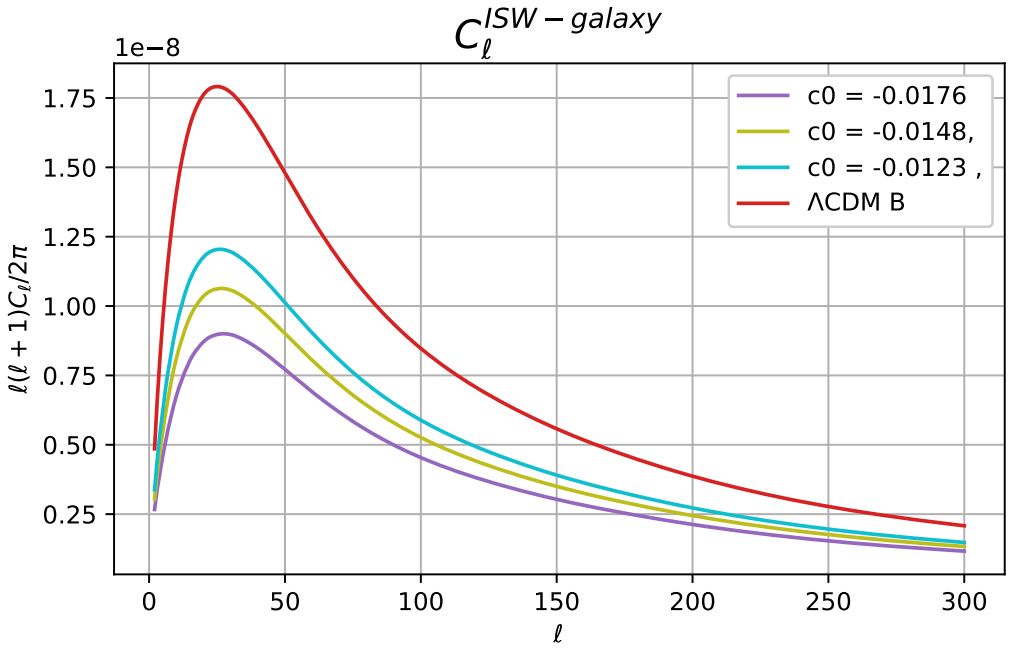

Figure 4.7: C_l of cross-correlation for the TPM model in the case of different values of the parameter Ω_0.

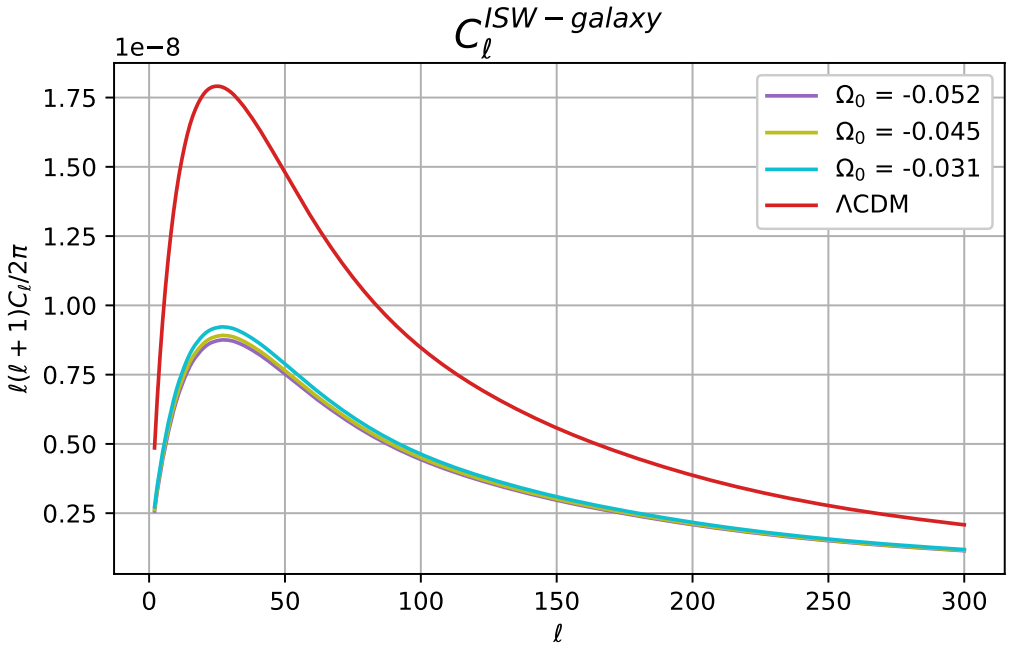

Figure 4.8: C_l of cross-correlation for the TPM model in the case of different values of the parameter A_s.

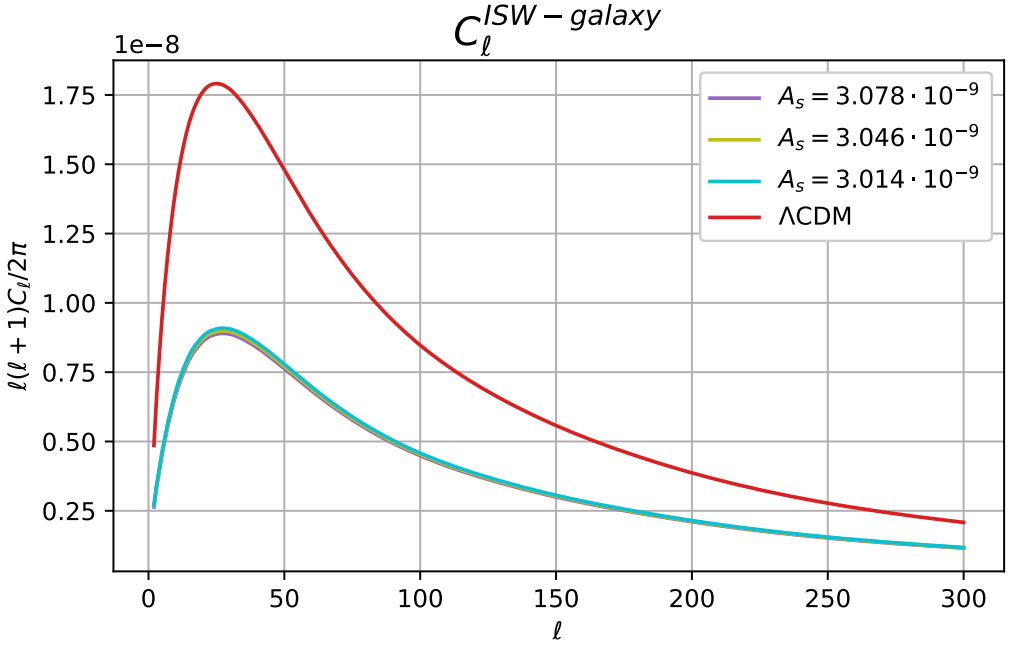

Figure 4.9: C_l modes for the ΛCDM B and TPM.

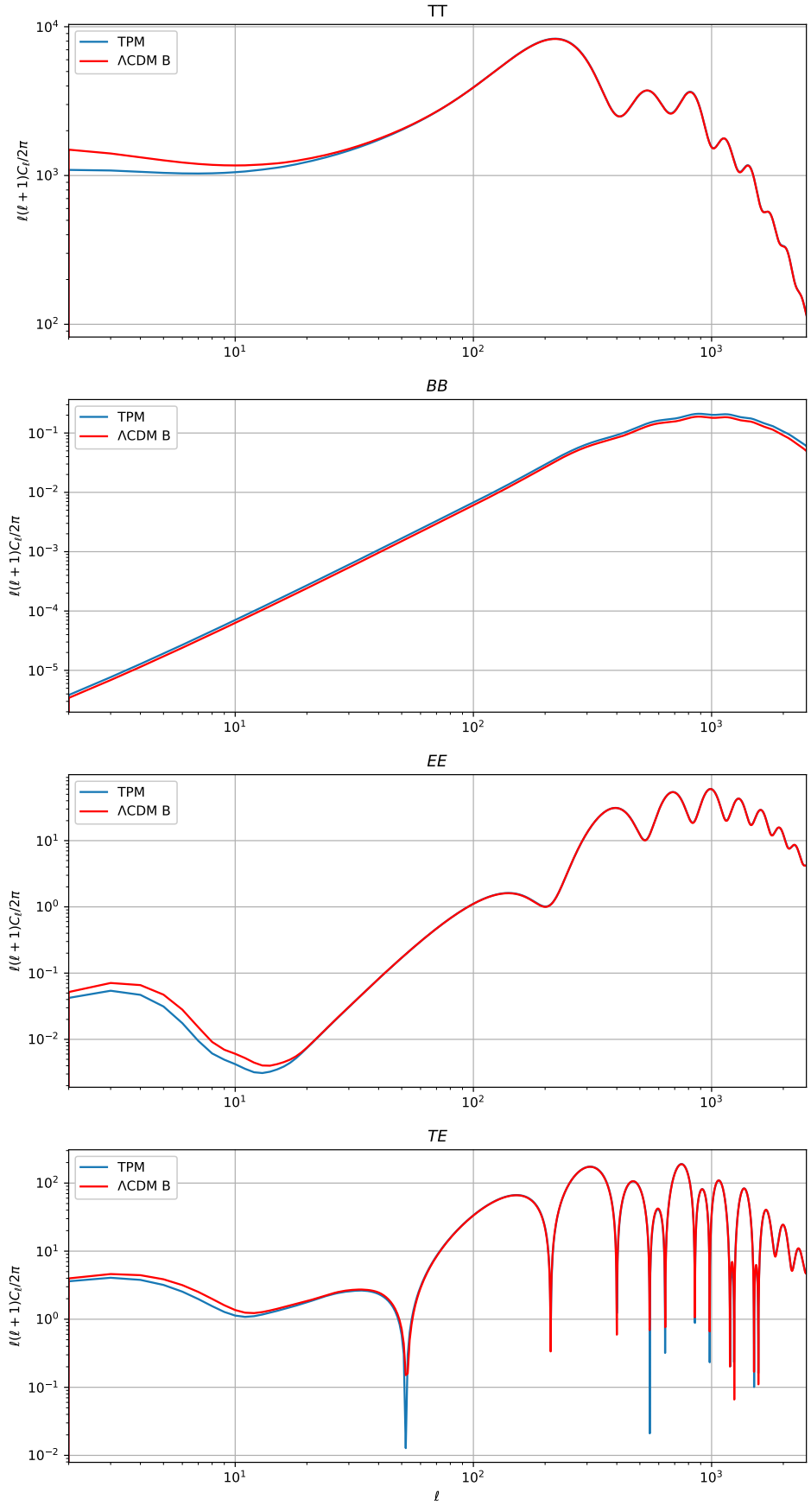

Figure 4.10: Residuals computed for the TPM model.

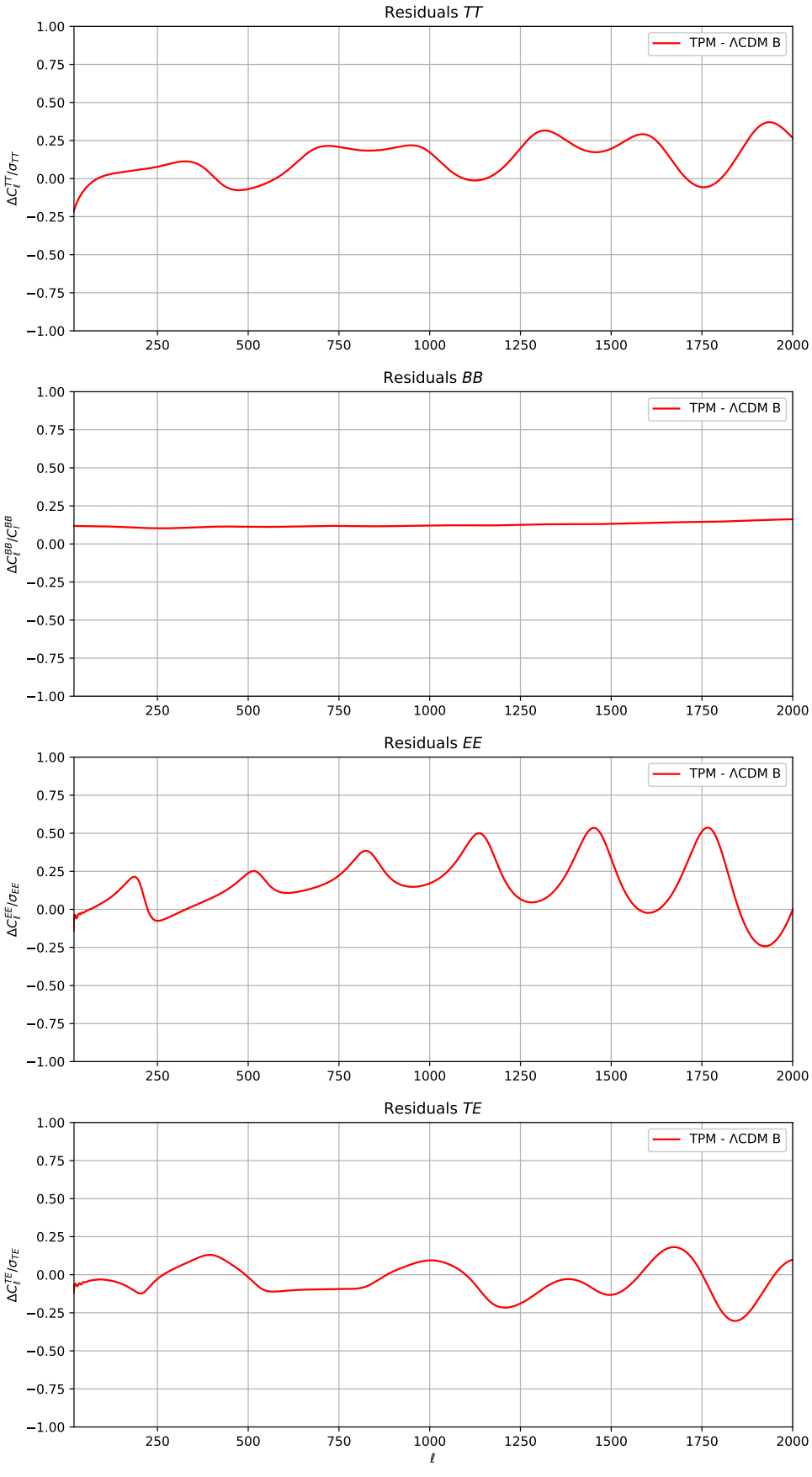

CHAPTER 5

Conclusions

In this work, we wanted to investigate gravity through the so called CMB ISW (Integrated Sachs-Wolfe) effect, exploiting the statistical tool of cross-correlation of the CMB temperature anisotropies and the Large-Scale-Strctures. As we have seen, the current standard cosmological model is the most robust description of the Universe we have today. With plenty of observations supporting it, it can describe in a precise manner both the early Universe and the late Universe (P. Collaboration, Aghanim, Akrami, Ashdown, Aumont, Baccigalupi, M. Ballardini, Banday, Barreiro, N. Bartolo, Basak, Benabed, et al. 2020). However, one thing that still eludes cosmologists is the accelerated expansion of the Universe: as we know, this latest phase is characterized by an accelerated expansion and an inexplicable growth of matter (Abdalla et al. 2022). The reason behind this behavior is attributed to the so-called Dark Energy, a component that constitutes most of the cosmic inventory today. Its fundamental nature however is still completely unknown: in the ΛCDM it is described by a cosmological constant Λ and set to be constant. The nature of it is, however, unknown. Moreover, from the quantum field theory theoretical depiction of the constant, we have a colossal difference with the observed constant: about 60 orders of magnitude (S. Weinberg 1989). Looking at our measurements, there is still room for improvement. Moreover, cosmological tensions arise from the discrepancies in the values of fundamental parameters (Abdalla et al. 2022). Parameters obtained from late Universe measurements are in contrast with the values derived from the early universe observations: this is still an open question in Cosmology with multiple possibilities for an answer. One could be a fundamental flaw in the procedure of late time measurements: distance ladders are usually the offspring of several approximations; another could be that the standard description of gravity and our Universe that we assume today isn't the best one. At the largest scales, ΛCDM constraints are not so tight (see e.g. Joyce et al. 2015), and at such scales, modifications of gravity are a concrete possibility. This is the route we wanted to explore in this thesis, by looking at what nature has given us to test gravity: the late Integrated-Sachs-Wolfe effect (W. Hu, Sugiyama, and Silk 1997). As we have seen in Chapter

2, the Cosmic Microwave Background is a rich environment for cosmological studies since it is an imprint of our early universe. The anisotropies in temperature of the CMB are one of the best tools to study the tumultuous evolution of our Universe. A secondary contribution to these anisotropies is the so-called ISW effect and the main goal of our thesis. The Integrated-Sachs-Wolfe, as the name says, is an integrated effect that takes into account the anisotropies in temperature of a photon during its travel up to us. As this is an effect that arises *after* the decoupling of photons from electrons, it can be a test of our late universe too. In particular, the ISW is sensitive to time-dependent gravitational potentials: the photon traveling thorugh such potential would result redshifted/blueshifted, leaving imprinting on it. Given this behavior, it is natural to try to use it to test the environment of an accelerated expansion of the Universe, since it alters the gravitational potential. In this way, everything is set to probe gravity described in different ways in different models. In Chapter 3 we have introduced these alternative theories: ones that change the description of Dark Energy as dynamical, and ones that introduce a modification in the gravitational sector. Among the plethora of different prescriptions, a useful methodoolgy of investigation is the so called Effective Field Theory approach : the EFT approach (Gubitosi et al. 2013). Using the EFT action of gravity has numerous advantages that we have reviewed. In a few words, the EFT encompasses not only specific models, but also classes of Dark energy/modified models, making it a powerful way to test gravity without specific assumptions. Nevertheless, it allows to recover specific solutions, once mapped into the EFT fomalism. This is an approach that we found not only convenient from a theoretical standpoint but also from a computational point of view. EFTCAMB (B. Hu et al. 2017), the code used in the thesis, is a large patch to CAMB, the main code, that incorporates the EFT description of modified gravity models. The EFT approach, with its mapping procedure, let us compute the same quantities for different models in a more efficient way: the general action is "shared" among the models and the specific result is given by mapping and applying the necessary constraints. The full mapping to a theory can just be set by inserting modules containing the background equations and a parametrization. We then exploited this feature by setting the modules for the state-of-the-art theories we wanted to explore. These models have been introduced in Chapter 3 and briefly described in their parametrization and their stability conditions. Two models are sub-cases of Horndeski theories (Horndeski 1974) that are with the latest constraints. One model is the K-mouflage (Babichev et al. 2009), a large set of theories with its screening mechanism. Finally, we explored for the first time a recent model, the so-called Transitional Planck Mass model (Benevento, Kable, et al. 2022). It has been written directly in the EFT language and prescribes a peculiar transition of the Planck Mass at early times. Testing the ISW effect for each of these models is difficult. The ISW effect is faint, being a secondary effect, and the cosmic variance can be dominant on the largest scales. In Chapter 4 we introduce the solution to this problem and the effective tool we used to test gravity: cross-correlation. Correlating the CMB temperature to the tracers of time-dependent gravitational potentials can effectively highlight the ISW effect. These tracers, to put it simply, are the galaxies of the LSS and of its gravitational potentials. Thus, we cross-correlated the CMB temperature anisotropies with galaxy number counts. The idea, first proposed by

Crittenden and Turok 1996, is that if there is an evolving late time potential, this is a source for the cross-correlation between these two quantities. The modelization of the galaxy number counts has been carefully chosen. In light of the future Euclid mission, choosing the distribution prescribed by the Euclid Consortium has many advantages: first and foremost the fact that the promising data that Euclid will gather would allow a future analysis (E. Collaboration et al. 2022) be based on the latest dataset. We then presented the results in Chapter 4, having found that all but one (the TPM) cross-correlation is similar to the ΛCDM counterpart. Investigating each cross-correlation, we have found promising results. All the amplitudes are of positive value, which is established by previous ISW observations (Stölzner et al. 2018). In addition, the stability criteria that are necessary to impose to each model parametrizaion translate well into the cross-correlation obtained, confirming the behavior of the parameters. Specifically, this is shown in the effective coupling functions which depend on the parametrizaion of each model. Moreover, considering the limit of the parameters in which we recover General Relativity, the ΛCDM cross-correlation is recovered. These considerations are valid for the Transitional Planck Mass model too, even if is characterized by a smaller cross-correlation. By investigating further this model, we have found that the key parameter affecting the amplitude is c_0, a parameter (prescribed by the model) that enetrs into the background equations and which is relevant on large scales. Looking forward from these results, there is plenty to build upon. The immediate next step is to compute the Fisher Information Matrix (see e.g. Verde 2009) for these cross-correlations. The Fisher matrix can provide (under some assumptions) forecasting errors from a given experimental setup and thus is often the work-horse of experimental design. It is defined as:

$$F_{ij} = -\left\langle \frac{\partial^2 \ln \mathscr{L}}{\partial\theta_i \partial\theta_j} \right\rangle \tag{5.1}$$

where $\mathscr{L}$ is the likelihood and θ_i are the parameters of $\mathscr{L}$. Here the average is the ensemble average over observational data (those that would be gathered if the real Universe was given by the model around which the derivative is taken). The power of the Fisher Matrix lies within the Cràmer-Rao relation (see e.g. Verde 2009):

$$\sigma_{\theta_i} \geq \left(F^{-1}\right)_{ii}^{1/2} \tag{5.2}$$

Let's spell it out for clarity: this is the square root of the element ii of the inverse of the Fisher information matrix. This assumes that the likelihood is Gaussian around its maximum. The terrific utility of the Fisher Information matrix is that, if you can compute it, it enables you to estimate the parameters errors for a given survey. If it can be computed quickly, it also enables one to explore different experimental setups and optimize the experiment. This is a procedure that is planned for the very near future and it will put forecasted errors on the parameters of the model. Hopefully, in the long run, future data analysis and comparison will help us constrain these gravity models and direct us to a better understanding of the Universe. The method of investigation used in this thesis can be very well applied to some related topics. So far we investigated the cross-correlation of ISW and LSS, but relativistic corrections (Raccanelli, Bertacca, Jeong, et al. 2016) can be found even in the correlation LSS-LSS. In that direction, it would be interesting to study which contribution is relevant

in different models of gravity. In the same fashion as Renk, Zumalacarregui, et al. (2016), the relativistic contributions can be investigated in an EFT formalism. Specifically, if we consider the galaxy number counts:

$$\Delta(\mathbf{n}, z) = \frac{n_{\rm g}(\mathbf{n}, z) - \langle n_{\rm g} \rangle (z)}{\langle n_{\rm g} \rangle (z)} \tag{5.3}$$

In the Newtonian gauge, the Δ is given by a multitude of contributions (Raccanelli, Bertacca, Maartens, et al. 2016, Raccanelli, Bertacca, Jeong, et al. 2016, Raccanelli, Bertacca, Dore, et al. 2014, Raccanelli, Bertacca, Pietrobon, et al. 2013, Challinor and Lewis 2011):

$$\begin{aligned}
\Delta_{\delta}(\mathbf{n}, z) =& b(z)\delta_{\rm co}(r(z)\mathbf{n}, \tau(z)) \\
\Delta_{\rm rsd}(\mathbf{n}, z) =& \frac{1}{\mathcal{H}(z)}\partial_r(\mathbf{v}\cdot\mathbf{n}), \\
\Delta_{\kappa}(\mathbf{n}, z) =& -\frac{(2-5s(z))}{2}\int_0^{r(z)} dr \frac{r(z)-r}{r(z)r}\Delta_2(\Phi+\Psi), \\
\Delta_{\rm dop}(\mathbf{n}, z) =& \left[\frac{\mathcal{H}'}{\mathcal{H}^2} + \frac{2-5s(z)}{r\mathcal{H}} + 5s(z) - \int_{\rm evo}(z)\right](\mathbf{v}\cdot\mathbf{n}) + \\
&+ \left[3 - \int_{\rm evo}(z)\right]\mathcal{H}\Delta^{-1}(\nabla\cdot\mathbf{v}), \\
\Delta_{\rm lp}(\mathbf{n}, z) =& (5s(z)-2)\Phi + \Psi + \mathcal{H}^{-1}\Phi' \\
&+ \left[\frac{\mathcal{H}'}{\mathcal{H}^2} + \frac{2-5s}{r\mathcal{H}} + 5s(z) - f_{\rm evo}(z)\right]\Psi, \\
\Delta_{\rm td}(\mathbf{n}, z) =& \frac{2-5s}{r(z)}\int_0^{r(z)} dr(\Phi+\Psi), \\
\Delta_{\rm ISW}(\mathbf{n}, z) =& \left[\frac{\mathcal{H}'}{\mathcal{H}^2} + \frac{2-5s}{r\mathcal{H}} + 5s(z) - f_{\rm evo}(z)\right]\int_0^{r(z)} dr\left(\Phi'+\Psi'\right)
\end{aligned} \tag{5.4}$$

which all depend on the gravitational potentials. This would be interesting to study with an EFT approach in Modified Gravity models. There is one final topic that could be explored following the same method of investigation we used so far. This time, the cross-correlation would be between the weak lensing of the CMB and the LSS. It would be a further probe to test gravity. The results obtained so far are promising in the near future more will be built upon, since the methodology used is general and not bound to some specific model or case. Hopefully, all these areas of investigation will be covered, and eventually a data analysis and matching will shed some light on our dark energy-driven Universe.

Bibliography

Abdalla, Elcio et al. (June 2022). "Cosmology Intertwined: A Review of the Particle Physics, Astrophysics, and Cosmology Associated with the Cosmological Tensions and Anomalies". In: *Journal of High Energy Astrophysics* **34**. DOI: 10.1016/j.jheap.2022.04.002. arXiv: 2203.06142 [astro-ph, physics:hep-ph] (cit. on pp. vii, viii, 6, 10, 12, 13, 95).

Abdurro'uf et al. (Apr. 1, 2022). "The Seventeenth Data Release of the Sloan Digital Sky Surveys: Complete Release of MaNGA, MaStar, and APOGEE-2 Data". In: *The Astrophysical Journal Supplement Series* **259**. DOI: 10.3847/1538-4365/ac4414 (cit. on p. 22).

Afshordi, Niayesh (Oct. 29, 2004). "Integrated Sachs-Wolfe Effect in Cross-Correlation: The Observer's Manual". In: *Physical Review D* **70**.8. DOI: 10.1103/PhysRevD.70.083536. arXiv: astro-ph/0401166 (cit. on pp. 68, 69, 73).

Afshordi, Niayesh, Yeong-Shang Loh, and Michael A. Strauss (Apr. 28, 2004). "Cross-Correlation of the Cosmic Microwave Background with the 2MASS Galaxy Survey: Signatures of Dark Energy, Hot Gas, and Point Sources". In: *Physical Review D* **69**.8. DOI: 10.1103/PhysRevD.69.083524. arXiv: astro-ph/0308260 (cit. on pp. 68, 73).

Aiola, Simone et al. (Dec. 30, 2020). "The Atacama Cosmology Telescope: DR4 Maps and Cosmological Parameters". In: *Journal of Cosmology and Astroparticle Physics* **2020**.12. DOI: 10.1088/1475-7516/2020/12/047. arXiv: 2007.07288 [astro-ph] (cit. on p. 10).

Alam, Shadab et al. (Sept. 2017). "The Clustering of Galaxies in the Completed SDSS-III Baryon Oscillation Spectroscopic Survey: Cosmological Analysis of the DR12 Galaxy Sample". In: *Monthly Notices of the Royal Astronomical Society* **470**.3. DOI: 10.1093/mnras/stx721. arXiv: 1607.03155 [astro-ph] (cit. on pp. 7, 81, 86).

Amendola, Luca, Martin Kunz, and Domenico Sapone (Apr. 19, 2007). *Measuring the Dark Side (with Weak Lensing)*. DOI: 10.1088/1475-7516/2008/04/013. arXiv: 0704.2421 [astro-ph] (cit. on pp. 43, 44).

Arkani-Hamed, Nima et al. (May 29, 2004). "Ghost Condensation and a Consistent Infrared Modification of Gravity". In: *Journal of High Energy Physics* **2004**.05.

DOI: 10.1088/1126-6708/2004/05/074. arXiv: hep-th/0312099 (cit. on pp. 52, 57).

Armendariz-Picon, C., V. Mukhanov, and Paul J. Steinhardt (Apr. 24, 2001). "Essentials of K-Essence". In: *Physical Review D* **63**.10. DOI: 10.1103/PhysRevD.63.103510. arXiv: astro-ph/0006373 (cit. on p. 36).

Arnowitt, R., S. Deser, and C. W. Misner (Dec. 1, 1959). "Dynamical Structure and Definition of Energy in General Relativity". In: *Physical Review* **116**.5. DOI: 10.1103/PhysRev.116.1322 (cit. on p. 45).

Babichev, E., C. Deffayet, and R. Ziour (Dec. 31, 2009). "K-MOUFLAGE GRAVITY". In: *International Journal of Modern Physics D* **18**.14. DOI: 10.1142/S0218271809016107 (cit. on pp. 36, 52, 59, 96).

Balkenhol, L. et al. (Oct. 4, 2021). "Constraints on ΛCDM Extensions from the SPT-3G 2018 EE and TE Power Spectra". In: *Physical Review D* **104**.8. DOI: 10.1103/PhysRevD.104.083509. arXiv: 2103.13618 [astro-ph] (cit. on p. 10).

Ballardini, Mario et al. (Oct. 2020). "Scalar-Tensor Theories of Gravity, Neutrino Physics, and the H_0 Tension". In: *Journal of Cosmology and Astroparticle Physics* **2020**.10. DOI: 10.1088/1475-7516/2020/10/044 (cit. on p. 62).

Ballesteros, Guillermo, Alessio Notari, and Fabrizio Rompineve (Nov. 2020). "The H_0 tension: ΔG_N vs. ΔN_{eff}". In: **2020**.11. DOI: 10.1088/1475-7516/2020/11/024 (cit. on p. 62).

Barreira, Alexandre, Philippe Brax, et al. (June 15, 2015). "K-Mouflage Gravity Models That Pass Solar System and Cosmological Constraints". In: *Physical Review D* **91**.12. DOI: 10.1103/PhysRevD.91.123522. arXiv: 1504.01493 [astro-ph, physics:gr-qc] (cit. on p. 61).

Barreira, Alexandre, Baojiu Li, et al. (Aug. 27, 2014). "The Observational Status of Galileon Gravity after Planck". In: *Journal of Cosmology and Astroparticle Physics* **2014**.08. DOI: 10.1088/1475-7516/2014/08/059. arXiv: 1406.0485 [astro-ph] (cit. on pp. 51, 55, 84).

Bellini, Emilio, Nicola Bartolo, and Sabino Matarrese (June 2012). "Spherical Collapse in Covariant Galileon Theory". In: *Journal of Cosmology and Astroparticle Physics* **2012**.06. DOI: 10.1088/1475-7516/2012/06/019 (cit. on p. 37).

Bellini, Emilio, Raul Jimenez, and Licia Verde (May 28, 2015). "Signatures of Horndeski Gravity on the Dark Matter Bispectrum". In: *Journal of Cosmology and Astroparticle Physics* **2015**.05. DOI: 10.1088/1475-7516/2015/05/057. arXiv: 1504.04341 [astro-ph, physics:gr-qc, physics:hep-th] (cit. on p. 37).

Bellini, Emilio and Ignacy Sawicki (July 25, 2014). "Maximal Freedom at Minimum Cost: Linear Large-Scale Structure in General Modifications of Gravity". In: *Journal of Cosmology and Astroparticle Physics* **2014**.07. DOI: 10.1088/1475-7516/2014/07/050. arXiv: 1404.3713 [astro-ph, physics:gr-qc] (cit. on p. 51).

Benevento, Giampaolo, Joshua A. Kable, et al. (Feb. 18, 2022). *An Exploration of an Early Gravity Transition in Light of Cosmological Tensions*. arXiv: 2202.09356 [astro-ph, physics:gr-qc] (cit. on pp. viii, 62, 64, 80–83, 89, 96).

Benevento, Giampaolo, Marco Raveri, et al. (May 16, 2019). "K-Mouflage Imprints on Cosmological Observables and Data Constraints". In: *Journal of Cosmology*

and Astroparticle Physics **2019**.05. DOI: 10.1088/1475-7516/2019/05/027. arXiv: 1809.09958 [astro-ph] (cit. on pp. 53, 59, 61, 62).

Bennett, C. L. et al. (Sept. 20, 2013). "Nine-Year Wilkinson Microwave Anisotropy Probe (WMAP) Observations: Final Maps and Results". In: *The Astrophysical Journal Supplement Series* **208**.2. DOI: 10.1088/0067-0049/208/2/20. arXiv: 1212.5225 [astro-ph] (cit. on p. 8).

Bertschinger, Edmund and Phillip Zukin (June 13, 2008). *Distinguishing Modified Gravity from Dark Energy*. DOI: 10.1103/PhysRevD.78.024015. arXiv: 0801.2431 [astro-ph] (cit. on p. 43).

Betoule, M. et al. (Aug. 2014). "Improved Cosmological Constraints from a Joint Analysis of the SDSS-II and SNLS Supernova Samples". In: *Astronomy & Astrophysics* **568**. DOI: 10.1051/0004-6361/201423413. arXiv: 1401.4064 [astro-ph] (cit. on p. 86).

Beutler, Florian et al. (Oct. 1, 2011). "The 6dF Galaxy Survey: Baryon Acoustic Oscillations and the Local Hubble Constant". In: *Monthly Notices of the Royal Astronomical Society* **416**.4. DOI: 10.1111/j.1365-2966.2011.19250.x. arXiv: 1106.3366 [astro-ph] (cit. on pp. 81, 86).

Blakeslee, John P. et al. (Apr. 2021). "The Hubble Constant from Infrared Surface Brightness Fluctuation Distances". In: *The Astrophysical Journal* **911**.1. DOI: 10.3847/1538-4357/abe86a (cit. on p. 81).

Bleem, L. E. et al. (Jan. 2015). "Galaxy Clusters Discovered via the Sunyaev-Zel'dovich Effect in the 2500-Square-Degree SPT-SZ Survey". In: *The Astrophysical Journal Supplement Series* **216**.2. DOI: 10.1088/0067-0049/216/2/27 (cit. on p. 6).

Bloomfield, Jolyon K. et al. (Aug. 7, 2013). "Dark Energy or Modified Gravity? An Effective Field Theory Approach". In: *Journal of Cosmology and Astroparticle Physics* **2013**.08. DOI: 10.1088/1475-7516/2013/08/010. arXiv: 1211.7054 [astro-ph, physics:gr-qc, physics:hep-th] (cit. on pp. 33, 40).

Braglia, Matteo et al. (Feb. 19, 2021). "Early modified gravity in light of the H_0 tension and LSS data". In: *Physical Review D* **103**.4. DOI: 10.1103/PhysRevD.103.043528 (cit. on p. 62).

Brax, Philippe, Clare Burrage, and Anne-Christine Davis (Jan. 16, 2013). "Screening Fifth Forces in K-Essence and DBI Models". In: *Journal of Cosmology and Astroparticle Physics* **2013**.01. DOI: 10.1088/1475-7516/2013/01/020. arXiv: 1209.1293 [astro-ph, physics:gr-qc, physics:hep-ph, physics:hep-th] (cit. on p. 36).

Brax, Philippe, Santiago Casas, et al. (Dec. 26, 2021). "Testing Screened Modified Gravity". In: *Universe* **8**.1. DOI: 10.3390/universe8010011. arXiv: 2201.10817 [astro-ph, physics:gr-qc, physics:hep-ph] (cit. on p. 35).

Brax, Philippe and Patrick Valageas (July 7, 2014a). "K -Mouflage Cosmology: The Background Evolution". In: *Physical Review D* **90**.2. DOI: 10.1103/PhysRevD.90.023507 (cit. on pp. 59, 61).

– (July 7, 2014b). "K-Mouflage Cosmology: Formation of Large-Scale Structures". In: *Physical Review D* **90**.2. DOI: 10.1103/PhysRevD.90.023508 (cit. on pp. 59, 61).

Brax, Philippe and Patrick Valageas (Nov. 30, 2014c). *Small-Scale Nonlinear Dynamics of K-mouflage Theories*. DOI: 10.1103/PhysRevD.90.123521. arXiv: 1408.0969 [astro-ph] (cit. on p. 59).

– (Jan. 13, 2016). "The Effective Field Theory of K-mouflage". In: *Journal of Cosmology and Astroparticle Physics* **2016**.01. DOI: 10.1088/1475-7516/2016/01/020. arXiv: 1509.00611 [astro-ph, physics:gr-qc, physics:hep-ph] (cit. on pp. 61, 62, 81).

Carroll, Sean M. (Aug. 31, 1998). *Quintessence and the Rest of the World*. DOI: 10.1103/PhysRevLett.81.3067. arXiv: astro-ph/9806099 (cit. on p. 35).

Carroll, Sean M., Mark Hoffman, and Mark Trodden (July 10, 2003). "Can the Dark Energy Equation-of-State Parameter w Be Less than -1?" In: *Physical Review D* **68**.2. DOI: 10.1103/PhysRevD.68.023509. arXiv: astro-ph/0301273 (cit. on p. 42).

Challinor, Anthony and Antony Lewis (Aug. 10, 2011). "The Linear Power Spectrum of Observed Source Number Counts". In: *Physical Review D* **84**.4. DOI: 10.1103/PhysRevD.84.043516. arXiv: 1105.5292 [astro-ph] (cit. on p. 98).

Cheung, Clifford et al. (Mar. 6, 2008). "The Effective Field Theory of Inflation". In: *Journal of High Energy Physics* **2008**.03. DOI: 10.1088/1126-6708/2008/03/014. arXiv: 0709.0293 [astro-ph, physics:hep-ph, physics:hep-th] (cit. on p. 37).

Clifton, Timothy et al. (Mar. 2012). "Modified Gravity and Cosmology". In: *Physics Reports* **513**.1-3. DOI: 10.1016/j.physrep.2012.01.001. arXiv: 1106.2476 [astro-ph, physics:gr-qc, physics:hep-th] (cit. on pp. viii, 34).

Cline, James M., Sangyong Jeon, and Guy D. Moore (Aug. 31, 2004). "The Phantom Menaced: Constraints on Low-Energy Effective Ghosts". In: *Physical Review D* **70**.4. DOI: 10.1103/PhysRevD.70.043543. arXiv: hep-ph/0311312 (cit. on p. 42).

Collaboration, Euclid et al. (Jan. 2022). "Euclid Preparation: XV. Forecasting Cosmological Constraints for the Euclid and CMB Joint Analysis". In: *Astronomy & Astrophysics* **657**. DOI: 10.1051/0004-6361/202141556. arXiv: 2106.08346 [astro-ph] (cit. on pp. 76, 86, 97).

Collaboration, Planck, P. A. R. Ade, et al. (Nov. 2014). "Planck 2013 Results. XVI. Cosmological Parameters". In: *Astronomy & Astrophysics* **571**. DOI: 10.1051/0004-6361/201321591. arXiv: 1303.5076 [astro-ph] (cit. on p. 8).

Collaboration, Planck, N. Aghanim, Y. Akrami, M. Ashdown, J. Aumont, C. Baccigalupi, M. Ballardini, A. J. Banday, R. B. Barreiro, N. Bartolo, S. Basak, R. Battye, et al. (Sept. 2020). "Planck 2018 Results. VI. Cosmological Parameters". In: *Astronomy & Astrophysics* **641**. DOI: 10.1051/0004-6361/201833910. arXiv: 1807.06209 [astro-ph] (cit. on pp. 9, 31, 86).

Collaboration, Planck, N. Aghanim, Y. Akrami, M. Ashdown, J. Aumont, C. Baccigalupi, M. Ballardini, A. J. Banday, R. B. Barreiro, N. Bartolo, S. Basak, K. Benabed, et al. (Sept. 2020). "Planck 2018 Results. V. CMB Power Spectra and Likelihoods". In: *Astronomy & Astrophysics* **641**. DOI: 10.1051/0004-6361/201936386. arXiv: 1907.12875 [astro-ph] (cit. on pp. 8, 9, 81, 84, 95).

Copeland, Edmund J., M. Sami, and Shinji Tsujikawa (Nov. 2006). "Dynamics of Dark Energy". In: *International Journal of Modern Physics D* **15**.11. DOI: 10.1142/S021827180600942X. arXiv: hep-th/0603057 (cit. on p. 34).

Crittenden, Robert G. and Neil Turok (Jan. 22, 1996). "Looking for a Cosmological Constant with the Rees-Sciama Effect". In: *Physical Review Letters* **76**.4. DOI: 10.1103/PhysRevLett.76.575 (cit. on pp. viii, 67, 68, 97).

De Felice, Antonio, Noemi Frusciante, and Georgios Papadomanolakis (Mar. 13, 2017). "On the Stability Conditions for Theories of Modified Gravity in Presence of Matter Fields". In: *Journal of Cosmology and Astroparticle Physics* **2017**.03. DOI: 10.1088/1475-7516/2017/03/027. arXiv: 1609.03599 [astro-ph, physics:gr-qc] (cit. on pp. 42, 43, 54).

De Felice, Antonio and Shinji Tsujikawa (Sept. 7, 2010). "Cosmology of a Covariant Galileon Field". In: *Physical Review Letters* **105**.11. DOI: 10.1103/PhysRevLett.105.111301. arXiv: 1007.2700 [astro-ph, physics:gr-qc, physics:hep-ph, physics:hep-th] (cit. on p. 54).

– (Feb. 6, 2012a). "Conditions for the Cosmological Viability of the Most General Scalar-Tensor Theories and Their Applications to Extended Galileon Dark Energy Models". In: *Journal of Cosmology and Astroparticle Physics* **2012**.02. DOI: 10.1088/1475-7516/2012/02/007. arXiv: 1110.3878 [astro-ph, physics:gr-qc, physics:hep-ph, physics:hep-th] (cit. on pp. 54, 55).

– (Mar. 14, 2012b). "Cosmological Constraints on Extended Galileon Models". In: *Journal of Cosmology and Astroparticle Physics* **2012**.03. DOI: 10.1088/1475-7516/2012/03/025. arXiv: 1112.1774 [astro-ph, physics:gr-qc, physics:hep-th] (cit. on pp. 54, 83).

Deffayet, C., S. Deser, and G. Esposito-Farese (Sept. 10, 2009). "Generalized Galileons: All Scalar Models Whose Curved Background Extensions Maintain Second-Order Field Equations and Stress Tensors". In: *Physical Review D* **80**.6. DOI: 10.1103/PhysRevD.80.064015. arXiv: 0906.1967 [gr-qc, physics:hep-th] (cit. on p. 50).

Deffayet, C., G. Esposito-Farese, and A. Vikman (Apr. 3, 2009). "Covariant Galileon". In: *Physical Review D* **79**.8. DOI: 10.1103/PhysRevD.79.084003. arXiv: 0901.1314 [astro-ph, physics:gr-qc, physics:hep-th] (cit. on pp. 50, 55, 57).

Deffayet, Cedric et al. (Oct. 22, 2010). "Imperfect Dark Energy from Kinetic Gravity Braiding". In: *Journal of Cosmology and Astroparticle Physics* **2010**.10. DOI: 10.1088/1475-7516/2010/10/026. arXiv: 1008.0048 [astro-ph, physics:gr-qc, physics:hep-ph, physics:hep-th] (cit. on pp. 53, 57, 66).

Desjacques, Vincent, Donghui Jeong, and Fabian Schmidt (Feb. 2018). "Large-Scale Galaxy Bias". In: *Physics Reports* **733**. DOI: 10.1016/j.physrep.2017.12.002. arXiv: 1611.09787 [astro-ph, physics:gr-qc, physics:hep-ph] (cit. on pp. 68, 70).

Efstathiou, G. P. et al. (Jan. 15, 1999). "First Results from the 2dF Galaxy Redshift Survey". In: *Philosophical Transactions of the Royal Society of London. Series A: Mathematical, Physical and Engineering Sciences* **357**.1750. DOI: 10.1098/rsta.1999.0317 (cit. on p. 22).

Efstathiou, George and Steven Gratton (Aug. 17, 2021). "A Detailed Description of the CamSpec Likelihood Pipeline and a Reanalysis of the Planck High Frequency Maps". In: *The Open Journal of Astrophysics* **4**.1. DOI: 10.21105/astro.1910.00483. arXiv: 1910.00483 [astro-ph, physics:hep-th] (cit. on p. 9).

Einstein, Albert (1917). "Cosmological Considerations in the General Theory of Relativity". In: *Sitzungsber. Preuss. Akad. Wiss. Berlin (Math. Phys.)* **1917** (cit. on pp. 1, 3, 33).

Ellis, George F. R. and Henk van Elst (Sept. 2, 2008). *Cosmological Models (Cargese Lectures 1998)*. DOI: 10.48550/arXiv.gr-qc/9812046. arXiv: gr-qc/9812046 (cit. on p. 1).

Euclid Collaboration et al. (Oct. 2020). "*Euclid* Preparation: VII. Forecast Validation for *Euclid* Cosmological Probes". In: *Astronomy & Astrophysics* **642**. DOI: 10.1051/0004-6361/202038071 (cit. on pp. viii, 76, 77, 86).

Fermi-LAT Collaboration et al. (Feb. 11, 2014). "Dark Matter Constraints from Observations of 25 Milky Way Satellite Galaxies with the Fermi Large Area Telescope". In: *Physical Review D* **89**.4. DOI: 10.1103/PhysRevD.89.042001 (cit. on p. 6).

Friedman, A. (Dec. 1, 1999). "On the Curvature of Space". In: *General Relativity and Gravitation* **31**.12. DOI: 10.1023/A:1026751225741 (cit. on p. 4).

Frusciante, Noemi, Ryotaro Kase, et al. (Mar. 2019). "Tracker and Scaling Solutions in DHOST Theories". In: *Physics Letters B* **790**. DOI: 10.1016/j.physletb.2019.01.009. arXiv: 1812.05204 [astro-ph, physics:gr-qc, physics:hep-ph, physics:hep-th] (cit. on p. 54).

Frusciante, Noemi, Georgios Papadomanolakis, and Alessandra Silvestri (July 14, 2016). "An Extended Action for the Effective Field Theory of Dark Energy: A Stability Analysis and a Complete Guide to the Mapping at the Basis of EFTCAMB". In: *Journal of Cosmology and Astroparticle Physics* **2016**.07. DOI: 10.1088/1475-7516/2016/07/018. arXiv: 1601.04064 [astro-ph, physics:gr-qc] (cit. on p. 51).

Frusciante, Noemi, Simone Peirone, et al. (Mar. 3, 2020). "Phenomenology of the Generalized Cubic Covariant Galileon Model and Cosmological Bounds". In: *Physical Review D* **101**.6. DOI: 10.1103/PhysRevD.101.064001. arXiv: 1912.07586 [astro-ph, physics:gr-qc] (cit. on pp. viii, 40, 52, 85, 86).

Frusciante, Noemi and Louis Perenon (May 2020). "Effective Field Theory of Dark Energy: A Review". In: *Physics Reports* **857**. DOI: 10.1016/j.physrep.2020.02.004. arXiv: 1907.03150 [astro-ph, physics:gr-qc] (cit. on p. 37).

Gelman, Andrew and Donald B. Rubin (Nov. 1992). "Inference from Iterative Simulation Using Multiple Sequences". In: *Statistical Science* **7**.4. DOI: 10.1214/ss/1177011136 (cit. on p. 81).

Giacomello, Francesco, Antonio De Felice, and Stefano Ansoldi (Mar. 22, 2019). "Bounds from ISW-galaxy Cross-Correlations on Generalized Covariant Galileon Models". In: *Journal of Cosmology and Astroparticle Physics* **2019**.03. DOI: 10.1088/1475-7516/2019/03/038. arXiv: 1811.10885 [astro-ph, physics:gr-qc, physics:hep-ph, physics:hep-th] (cit. on p. 83).

Giannantonio, Tommaso et al. (June 13, 2008). "Combined Analysis of the Integrated Sachs-Wolfe Effect and Cosmological Implications". In: *Physical Review D* **77**.12. DOI: 10.1103/PhysRevD.77.123520. arXiv: 0801.4380 [astro-ph] (cit. on pp. 69, 73, 84).

Gleyzes, Jerome et al. (Aug. 19, 2013). "Essential Building Blocks of Dark Energy". In: *Journal of Cosmology and Astroparticle Physics* **2013**.08. DOI: 10.

1088/1475-7516/2013/08/025. arXiv: 1304.4840 [astro-ph, physics:gr-qc, physics:hep-th] (cit. on p. 40).

Gleyzes, Jérôme, David Langlois, Federico Piazza, et al. (Feb. 16, 2015a). "Exploring Gravitational Theories beyond Horndeski". In: *Journal of Cosmology and Astroparticle Physics* **2015**.02. DOI: 10.1088/1475-7516/2015/02/018. arXiv: 1408.1952 [astro-ph, physics:gr-qc, physics:hep-th] (cit. on p. 51).

– (May 27, 2015b). "Healthy Theories beyond Horndeski". In: *Physical Review Letters* **114**.21. DOI: 10.1103/PhysRevLett.114.211101. arXiv: 1404.6495 [astro-ph, physics:hep-th] (cit. on p. 37).

Gleyzes, Jérôme, David Langlois, and Filippo Vernizzi (Nov. 2014). "A Unifying Description of Dark Energy". In: *International Journal of Modern Physics D* **23**.13. DOI: 10.1142/S021827181443010X. arXiv: 1411.3712 [astro-ph, physics:gr-qc, physics:hep-th] (cit. on pp. 37, 51).

Gourgoulhon, Eric (Mar. 6, 2007). *3+1 Formalism and Bases of Numerical Relativity*. DOI: 10.48550/arXiv.gr-qc/0703035. arXiv: gr-qc/0703035 (cit. on p. 45).

Gubitosi, Giulia, Federico Piazza, and Filippo Vernizzi (Feb. 19, 2013). "The Effective Field Theory of Dark Energy". In: *Journal of Cosmology and Astroparticle Physics* **2013**.02. DOI: 10.1088/1475-7516/2013/02/032. arXiv: 1210.0201 [astro-ph, physics:gr-qc, physics:hep-th] (cit. on pp. viii, 37, 40, 96).

Gumrukcuoglu, A. Emir, Shinji Mukohyama, and Thomas P. Sotiriou (Sept. 1, 2016). "Jeans' Ghost". In: *Physical Review D* **94**.6. DOI: 10.1103/PhysRevD.94.064001. arXiv: 1606.00618 [gr-qc, physics:hep-th] (cit. on pp. 42, 43).

Guth, Alan H. (Jan. 15, 1981). "Inflationary Universe: A Possible Solution to the Horizon and Flatness Problems". In: *Physical Review D* **23**.2. DOI: 10.1103/PhysRevD.23.347 (cit. on pp. vii, 2, 20).

Hamilton, A. J. S. (1998). "Linear Redshift Distortions: A Review". In: vol. 231. DOI: 10.1007/978-94-011-4960-0_17. arXiv: astro-ph/9708102 (cit. on p. 68).

Hassan, S. F. and Rachel A. Rosen (Feb. 2012). "Bimetric Gravity from Ghost-free Massive Gravity". In: *Journal of High Energy Physics* **2012**.2. DOI: 10.1007/JHEP02(2012)126. arXiv: 1109.3515 [hep-th] (cit. on p. 37).

Heavens, Alan et al. (Apr. 11, 2017). *Marginal Likelihoods from Monte Carlo Markov Chains*. DOI: 10.48550/arXiv.1704.03472. arXiv: 1704.03472 [astro-ph, stat] (cit. on p. 86).

Hilbert, David (2007). "The Foundations of Physics (First Communication)". In: *The Genesis of General Relativity*. Ed. by Michel Janssen et al. Boston Studies in the Philosophy of Science. Dordrecht: Springer Netherlands. ISBN: 978-1-4020-4000-9. DOI: 10.1007/978-1-4020-4000-9_44 (cit. on p. 3).

Hinterbichler, Kurt and Justin Khoury (June 10, 2010). "Symmetron Fields: Screening Long-Range Forces Through Local Symmetry Restoration". In: *Physical Review Letters* **104**.23. DOI: 10.1103/PhysRevLett.104.231301. arXiv: 1001.4525 [astro-ph, physics:hep-th] (cit. on p. 36).

Horava, Petr (Mar. 4, 2009). "Membranes at Quantum Criticality". In: *Journal of High Energy Physics* **2009**.03. DOI: 10.1088/1126-6708/2009/03/020. arXiv:

0812.4287 [cond-mat, physics:gr-qc, physics:hep-ph, physics:hep-th] (cit. on p. 37).

Horndeski, Gregory Walter (Sept. 1974). "Second-Order Scalar-Tensor Field Equations in a Four-Dimensional Space". In: *International Journal of Theoretical Physics* **10**.6. DOI: 10.1007/BF01807638 (cit. on pp. 37, 50, 51, 96).

Hu, Bin et al. (May 23, 2014). "Effective Field Theory of Cosmic Acceleration: An Implementation in CAMB". In: *Physical Review D* **89**.10. DOI: 10.1103/PhysRevD.89.103530. arXiv: 1312.5742 [astro-ph, physics:gr-qc, physics:hep-th].

– (Sept. 27, 2017). *EFTCAMB/EFTCosmoMC: Numerical Notes v3.0*. arXiv: 1405.3590 [astro-ph, physics:gr-qc, physics:hep-th, physics:physics] (cit. on pp. 40, 47, 49, 96).

Hu, Wayne and Naoshi Sugiyama (May 1, 1995). "Anisotropies in the Cosmic Microwave Background: An Analytic Approach". In: *The Astrophysical Journal* **444**. DOI: 10.1086/175624 (cit. on p. 15).

Hu, Wayne, Naoshi Sugiyama, and Joseph Silk (Mar. 1997). "The Physics of Microwave Background Anisotropies". In: *Nature* **386**.6620 (6620). DOI: 10.1038/386037a0 (cit. on pp. 67, 95).

Hubble, Edwin (1937). *The Observational Approach to Cosmology*. Oxford: The Clarendon Press. 68 pp. (cit. on p. 2).

Jain, Bhuvnesh et al. (Sept. 24, 2013). *Novel Probes of Gravity and Dark Energy*. arXiv: 1309.5389 [astro-ph] (cit. on p. 35).

Joyce, Austin et al. (Mar. 2015). "Beyond the Cosmological Standard Model". In: *Physics Reports* **568**. DOI: 10.1016/j.physrep.2014.12.002. arXiv: 1407.0059 [astro-ph, physics:gr-qc, physics:hep-ph, physics:hep-th] (cit. on pp. 33, 35, 36, 43, 65, 95).

Kable, Joshua A. et al. (Nov. 19, 2021). *Probing Modified Gravity with Integrated Sachs-Wolfe CMB and Galaxy Cross-correlations*. arXiv: 2111.10432 [astro-ph] (cit. on pp. viii, 54, 55, 68, 69, 71, 72, 80–83, 85).

Kaiser, Nick (July 1, 1987). "Clustering in Real Space and in Redshift Space". In: *Monthly Notices of the Royal Astronomical Society* **227**.1. DOI: 10.1093/mnras/227.1.1 (cit. on p. 67).

Kase, Ryotaro and Shinji Tsujikawa (Nov. 2014). "Effective Field Theory Approach to Modified Gravity Including Horndeski Theory and Ho\v{r}ava-Lifshitz Gravity". In: *International Journal of Modern Physics D* **23**.13. DOI: 10.1142/S0218271814430081. arXiv: 1409.1984 [astro-ph, physics:gr-qc, physics:hep-ph, physics:hep-th] (cit. on p. 45).

– (May 1, 2018). "Dark Energy Scenario Consistent with GW170817 in Theories beyond Horndeski Gravity". In: *Physical Review D* **97**.10. DOI: 10.1103/PhysRevD.97.103501. arXiv: 1802.02728 [astro-ph, physics:gr-qc, physics:hep-ph, physics:hep-th] (cit. on p. 58).

– (Apr. 2019). "Dark Energy in Horndeski Theories after GW170817: A Review". In: *International Journal of Modern Physics D* **28**.05. DOI: 10.1142/S0218271819420057. arXiv: 1809.08735 [astro-ph, physics:gr-qc, physics:hep-ph, physics:hep-th] (cit. on p. 51).

Khoury, Justin and Amanda Weltman (Feb. 27, 2004a). "Chameleon Cosmology". In: *Physical Review D* **69**.4. DOI: 10.1103/PhysRevD.69.044026. arXiv: astro-ph/0309411 (cit. on pp. 36, 65).

– (Oct. 22, 2004b). "Chameleon Fields: Awaiting Surprises for Tests of Gravity in Space". In: *Physical Review Letters* **93**.17. DOI: 10.1103/PhysRevLett.93.171104. arXiv: astro-ph/0309300 (cit. on pp. 36, 65).

Kimura, Rampei, Tsutomu Kobayashi, and Kazuhiro Yamamoto (June 4, 2012). "Observational Constraints on Kinetic Gravity Braiding from the Integrated Sachs-Wolfe Effect". In: *Physical Review D* **85**.12. DOI: 10.1103/PhysRevD.85.123503. arXiv: 1110.3598 [astro-ph, physics:gr-qc, physics:hep-th].

Kitching, T. D. et al. (Nov. 11, 2009). "Cosmological Systematics beyond Nuisance Parameters: Form-Filling Functions". In: *Monthly Notices of the Royal Astronomical Society* **399**.4. DOI: 10.1111/j.1365-2966.2009.15408.x (cit. on p. 78).

Kobayashi, Tsutomu, Hiroyuki Tashiro, and Daichi Suzuki (Mar. 18, 2010). *Evolution of Linear Cosmological Perturbations and Its Observational Implications in Galileon-type Modified Gravity.* DOI: 10.1103/PhysRevD.81.063513. arXiv: 0912.4641 [astro-ph, physics:gr-qc, physics:hep-ph] (cit. on p. 84).

Kobayashi, Tsutomu, Masahide Yamaguchi, and Jun'ichi Yokoyama (Dec. 3, 2010). "G-Inflation: Inflation Driven by the Galileon Field". In: *Physical Review Letters* **105**.23. DOI: 10.1103/PhysRevLett.105.231302. arXiv: 1008.0603 [astro-ph, physics:gr-qc, physics:hep-th] (cit. on p. 51).

– (Sept. 1, 2011). "Generalized G-inflation: Inflation with the Most General Second-Order Field Equations". In: *Progress of Theoretical Physics* **126**.3. DOI: 10.1143/PTP.126.511. arXiv: 1105.5723 [astro-ph, physics:gr-qc, physics:hep-ph, physics:hep-th] (cit. on p. 51).

Kofman, L.A. and A.A. Starobinskij (1985). "Cosmological Constant and Large-Scale Anisotropy of the Relict Radiation". In: *Pis'ma v Astronomicheskij Zhurnal.* Kosmologicheskaya Postoyannaya i Krupnomasshtabnaya Anizotropiya Reliktovogo Izlucheniya **11**.9 (cit. on p. 67).

Langlois, David and Karim Noui (Feb. 2016). "Degenerate Higher Derivative Theories beyond Horndeski: Evading the Ostrogradski Instability". In: *Journal of Cosmology and Astroparticle Physics* **2016**.02. DOI: 10.1088/1475-7516/2016/02/034 (cit. on p. 37).

Laureijs, R. et al. (Oct. 14, 2011). *Euclid Definition Study Report.* DOI: 10.48550/arXiv.1110.3193. arXiv: 1110.3193 [astro-ph] (cit. on pp. 70, 75–77).

Leclercq, Florent, Alice Pisani, and Benjamin D. Wandelt (2014). "Cosmology: From Theory to Data, from Data to Theory". In: *Proceedings of the International School of Physics “Enrico Fermi”* **186** (New Horizons for Observational Cosmology). DOI: 10.3254/978-1-61499-476-3-189. arXiv: 1403.1260 [astro-ph] (cit. on p. 74).

Leloup, Clément et al. (May 8, 2019). "Observational Status of the Galileon Model General Solution from Cosmological Data and Gravitational Waves". In: *Journal of Cosmology and Astroparticle Physics* **2019**.05. DOI: 10.1088/1475-7516/2019/05/011. arXiv: 1902.07065 [astro-ph, physics:gr-qc, physics:hep-ph, physics:hep-th] (cit. on p. 54).

Lewis, Antony and Sarah Bridle (Nov. 25, 2002). "Cosmological Parameters from CMB and Other Data: A Monte-Carlo Approach". In: *Physical Review D* **66**.10. DOI: 10.1103/PhysRevD.66.103511. arXiv: astro-ph/0205436 (cit. on p. 47).

Lima, Nelson A., Vanessa Smer-Barreto, and Lucas Lombriser (Oct. 4, 2016). "Constraints on Decaying Early Modified Gravity from Cosmological Observations". In: *Physical Review D* **94**.8. DOI: 10.1103/PhysRevD.94.083507 (cit. on p. 62).

Limber, D. Nelson (May 1, 1954). "The Analysis of Counts of the Extragalactic Nebulae in Terms of a Fluctuating Density Field. II." In: *The Astrophysical Journal* **119**. DOI: 10.1086/145870 (cit. on p. 69).

Lin, Meng-Xiang, Wayne Hu, and Marco Raveri (Dec. 9, 2020). "Testing H0 in Acoustic Dark Energy Models with Planck and ACT Polarization". In: *Physical Review D* **102**.12. DOI: 10.1103/PhysRevD.102.123523. arXiv: 2009.08974 [astro-ph, physics:gr-qc] (cit. on p. 88).

Lin, Meng-Xiang, Marco Raveri, and Wayne Hu (Feb. 12, 2019). "Phenomenology of Modified Gravity at Recombination". In: *Physical Review D* **99**.4. DOI: 10.1103/PhysRevD.99.043514 (cit. on p. 62).

Linder, Eric V. (Aug. 26, 2005). "Cosmic Growth History and Expansion History". In: *Physical Review D* **72**.4. DOI: 10.1103/PhysRevD.72.043529. arXiv: astro-ph/0507263 (cit. on p. 73).

Lovelock, David (Mar. 1971). "The Einstein Tensor and Its Generalizations". In: *Journal of Mathematical Physics* **12**.3. DOI: 10.1063/1.1665613 (cit. on p. 37).

– (June 1972). "The Four-Dimensionality of Space and the Einstein Tensor". In: *Journal of Mathematical Physics* **13**.6. DOI: 10.1063/1.1666069 (cit. on p. 37).

Lyche, Tom and Larry L. Schumaker (1973). "On the Convergence of Cubic Interpolating Splines". In: *Spline Functions and Approximation Theory: Proceedings of the Symposium Held at the University of Alberta, Edmonton May 29 to June 1, 1972*. Ed. by A. Meir and A. Sharma. ISNM International Series of Numerical Mathematics / Internationale Schriftenreihe Zur Numerischen Mathematik / Série Internationale d'Analyse Numérique. Basel: Birkhäuser. ISBN: 978-3-0348-5979-0. DOI: 10.1007/978-3-0348-5979-0_9 (cit. on p. 79).

Mo, Houjun, Frank van den Bosch, and Simon White (2010). *Galaxy Formation and Evolution*. Cambridge: Cambridge University Press. ISBN: 978-0-521-85793-2. DOI: 10.1017/CBO9780511807244 (cit. on p. 67).

Modern Cosmology (2021). Elsevier. ISBN: 978-0-12-815948-4. DOI: 10.1016/B978-0-12-815948-4.00002-4 (cit. on pp. viii, 1, 15, 18, 23, 25, 26, 31, 67).

Mortonson, Michael J., David H. Weinberg, and Martin White (Dec. 30, 2013). *Dark Energy: A Short Review*. DOI: 10.48550/arXiv.1401.0046. arXiv: 1401.0046 [astro-ph] (cit. on p. 34).

Nakamura, Shintaro et al. (Mar. 27, 2019). "Constraints on Massive Vector Dark Energy Models from Integrated Sachs-Wolfe-galaxy Cross-Correlations". In: *Physical Review D* **99**.6. DOI: 10.1103/PhysRevD.99.063533. arXiv: 1811.07541 [astro-ph, physics:gr-qc, physics:hep-ph, physics:hep-th] (cit. on pp. viii, 72).

Nicolis, Alberto, Riccardo Rattazzi, and Enrico Trincherini (Mar. 31, 2009). "The Galileon as a Local Modification of Gravity". In: *Physical Review D* **79**.6. DOI:

10.1103/PhysRevD.79.064036. arXiv: 0811.2197 [astro-ph, physics:gr-qc, physics:hep-th] (cit. on p. 50).

Palatini, Attilio (Dec. 1, 1919). "Deduzione invariantiva delle equazioni gravitazionali dal principio di Hamilton". In: *Rendiconti del Circolo Matematico di Palermo (1884-1940)* **43**.1. DOI: 10.1007/BF03014670 (cit. on p. 3).

Peebles, P. J. E. (1980). "The Large-Scale Structure of the Universe". In: *Large-Scale Structure of the Universe by Phillip James Edwin Peebles. Princeton University Press* (cit. on p. 72).

Peirone, Simone et al. (Sept. 26, 2019). "Cosmological Data Favor Galileon Ghost Condensate over ΛCDM". In: *Physical Review D* **100**.6. DOI: 10.1103/PhysRevD.100.063540. arXiv: 1905.05166 [astro-ph, physics:gr-qc] (cit. on pp. 52, 85, 86).

Penzias, A. A. and R. W. Wilson (July 1, 1965). "A Measurement of Excess Antenna Temperature at 4080 Mc/s." In: *The Astrophysical Journal* **142**. DOI: 10.1086/148307 (cit. on p. 8).

Pesce, D. W. et al. (Feb. 2020). "The Megamaser Cosmology Project. XIII. Combined Hubble Constant Constraints". In: *The Astrophysical Journal* **891**.1. DOI: 10.3847/2041-8213/ab75f0 (cit. on p. 81).

Piazza, Federico, Heinrich Steigerwald, and Christian Marinoni (May 28, 2014). "Phenomenology of Dark Energy: Exploring the Space of Theories with Future Redshift Surveys". In: *Journal of Cosmology and Astroparticle Physics* **2014**.05. DOI: 10.1088/1475-7516/2014/05/043. arXiv: 1312.6111 [astro-ph, physics:gr-qc, physics:hep-ph, physics:hep-th] (cit. on p. 40).

Pogosian, Levon and Alessandra Silvestri (Nov. 7, 2016). "What Can Cosmology Tell Us about Gravity? Constraining Horndeski Gravity with Σ and μ". In: *Physical Review D* **94**.10. DOI: 10.1103/PhysRevD.94.104014 (cit. on pp. 43, 60).

Pogosian, Levon, Alessandra Silvestri, et al. (May 11, 2010). "How to Optimally Parametrize Deviations from General Relativity in the Evolution of Cosmological Perturbations". In: *Physical Review D* **81**.10. DOI: 10.1103/PhysRevD.81.104023. arXiv: 1002.2382 [astro-ph] (cit. on p. 43).

Pouri, Athina, Spyros Basilakos, and Manolis Plionis (Aug. 19, 2014). "Precision Growth Index Using the Clustering of Cosmic Structures and Growth Data". In: *Journal of Cosmology and Astroparticle Physics* **2014**.08. DOI: 10.1088/1475-7516/2014/08/042. arXiv: 1402.0964 [astro-ph, physics:gr-qc, physics:hep-ph, physics:hep-th] (cit. on p. 73).

Prenter, P. M. and Barrow Mathematics (Jan. 1, 2008). *Splines and Variational Methods*. Courier Corporation. 338 pp. ISBN: 978-0-486-46902-7. Google Books: lZ8lAQAAQBAJ (cit. on p. 79).

Raccanelli, Alvise, Daniele Bertacca, Olivier Dore, et al. (Aug. 11, 2014). "Large-Scale 3D Galaxy Correlation Function and Non-Gaussianity". In: *Journal of Cosmology and Astroparticle Physics* **2014**.08. DOI: 10.1088/1475-7516/2014/08/022. arXiv: 1306.6646 [astro-ph] (cit. on p. 98).

Raccanelli, Alvise, Daniele Bertacca, Donghui Jeong, et al. (Feb. 9, 2016). *Doppler Term in the Galaxy Two-Point Correlation Function: Wide-Angle, Velocity, Doppler Lensing and Cosmic Acceleration Effects*. DOI: 10.48550/arXiv.1602.03186. arXiv: 1602.03186 [astro-ph] (cit. on pp. 97, 98).

Raccanelli, Alvise, Daniele Bertacca, Roy Maartens, et al. (July 2016). "Lensing and Time-Delay Contributions to Galaxy Correlations". In: *General Relativity and Gravitation* **48**.7. DOI: 10.1007/s10714-016-2076-8. arXiv: 1311.6813 [astro-ph] (cit. on p. 98).

Raccanelli, Alvise, Daniele Bertacca, Davide Pietrobon, et al. (Nov. 21, 2013). "Testing Gravity Using Large-Scale Redshift-Space Distortions". In: *Monthly Notices of the Royal Astronomical Society* **436**.1. DOI: 10.1093/mnras/stt1517. arXiv: 1207.0500 [astro-ph] (cit. on pp. 68, 98).

Raveri, Marco et al. (Aug. 15, 2014). "Effective Field Theory of Cosmic Acceleration: Constraining Dark Energy with CMB Data". In: *Physical Review D* **90**.4. DOI: 10.1103/PhysRevD.90.043513. arXiv: 1405.1022 [astro-ph, physics:gr-qc, physics:hep-th] (cit. on p. 47).

Renk, Janina, Miguel Zumalacarregui, and Francesco Montanari (July 25, 2016). "Gravity at the Horizon: On Relativistic Effects, CMB-LSS Correlations and Ultra-Large Scales in Horndeski's Theory". In: *Journal of Cosmology and Astroparticle Physics* **2016**.07. DOI: 10.1088/1475-7516/2016/07/040. arXiv: 1604.03487 [astro-ph, physics:gr-qc] (cit. on p. 98).

Renk, Janina, Miguel Zumalacárregui, et al. (Oct. 17, 2017). "Galileon Gravity in Light of ISW, CMB, BAO and H_0 data". In: *Journal of Cosmology and Astroparticle Physics* **2017**.10. DOI: 10.1088/1475-7516/2017/10/020. arXiv: 1707.02263 [astro-ph, physics:gr-qc, physics:hep-ph, physics:hep-th] (cit. on pp. 54, 55, 84).

Rhodes, J. et al. (Mar. 12, 2014). *Exploiting Cross Correlations and Joint Analyses*. arXiv: 1309.5388 [astro-ph] (cit. on p. 68).

Riess, Adam G., Alexei V. Filippenko, et al. (Sept. 1998). "Observational Evidence from Supernovae for an Accelerating Universe and a Cosmological Constant". In: *The Astronomical Journal* **116**.3. DOI: 10.1086/300499. arXiv: astro-ph/9805201 (cit. on pp. 6, 7).

Riess, Adam G., Wenlong Yuan, et al. (July 1, 2022). "A Comprehensive Measurement of the Local Value of the Hubble Constant with 1 Km/s/Mpc Uncertainty from the Hubble Space Telescope and the SH0ES Team". In: *The Astrophysical Journal Letters* **934**.1. DOI: 10.3847/2041-8213/ac5c5b. arXiv: 2112.04510 [astro-ph] (cit. on pp. 10, 81).

Ross, Ashley J. et al. (May 1, 2015). "The Clustering of the SDSS DR7 Main Galaxy Sample I: A 4 per Cent Distance Measure at Z=0.15". In: *Monthly Notices of the Royal Astronomical Society* **449**.1. DOI: 10.1093/mnras/stv154. arXiv: 1409.3242 [astro-ph] (cit. on p. 81).

Sachs, R. K. and A. M. Wolfe (Jan. 1, 1967). "Perturbations of a Cosmological Model and Angular Variations of the Microwave Background". In: *The Astrophysical Journal* **147**. DOI: 10.1086/148982 (cit. on pp. viii, 30).

Sakstein, Jeremy and Bhuvnesh Jain (Dec. 18, 2017). "Implications of the Neutron Star Merger GW170817 for Cosmological Scalar-Tensor Theories". In: *Physical Review Letters* **119**.25. DOI: 10.1103/PhysRevLett.119.251303. arXiv: 1710.05893 [astro-ph, physics:gr-qc, physics:hep-ph, physics:hep-th] (cit. on p. 51).

Sbisà, Fulvio (Jan. 1, 2015). "Classical and Quantum Ghosts". In: *European Journal of Physics* **36**.1. DOI: 10.1088/0143-0807/36/1/015009. arXiv: 1406.4550 [astro-ph, physics:gr-qc, physics:hep-ph, physics:hep-th] (cit. on p. 42).

Scaramella, R. et al. (June 1, 2022). "Euclid Preparation - I. The Euclid Wide Survey". In: *Astronomy & Astrophysics* **662**. DOI: 10.1051/0004-6361/202141938 (cit. on p. 76).

Schäfer, Björn Malte and Philipp M. Merkel (Sept. 21, 2017). "Angular Spectra of the Intrinsic Galaxy Ellipticity Field, Their Observability and Their Impact on Lensing in Tomographic Surveys". In: *Monthly Notices of the Royal Astronomical Society* **470**.3. DOI: 10.1093/mnras/stx1446 (cit. on p. 86).

Schutz, Bernard F and Rafael Sorkin (Sept. 6, 1977). "Variational Aspects of Relativistic Field Theories, with Application to Perfect Fluids". In: *Annals of Physics* **107**.1. DOI: 10.1016/0003-4916(77)90200-7 (cit. on p. 42).

Scolnic, D. M. et al. (May 29, 2018). "The Complete Light-curve Sample of Spectroscopically Confirmed Type Ia Supernovae from Pan-STARRS1 and Cosmological Constraints from The Combined Pantheon Sample". In: *The Astrophysical Journal* **859**.2. DOI: 10.3847/1538-4357/aab9bb. arXiv: 1710.00845 [astro-ph] (cit. on pp. 7, 81).

Smoot, George F. (1999). "Summary of Results from COBE". In: *Conference on 3K Cosmology*. DOI: 10.1063/1.59326. arXiv: astro-ph/9902027 (cit. on p. 8).

Somerville, Rachel S. et al. (Jan. 10, 2004). "Cosmic Variance in the Great Observatories Origins Deep Survey". In: *The Astrophysical Journal* **600**.2. DOI: 10.1086/378628. arXiv: astro-ph/0309071 (cit. on p. 73).

Sotiriou, Thomas P. and Valerio Faraoni (Mar. 1, 2010). "$f(R)$ theories of gravity". In: *Reviews of Modern Physics* **82**.1. DOI: 10.1103/RevModPhys.82.451 (cit. on p. 35).

Spiegelhalter, David J. et al. (2014). "The Deviance Information Criterion: 12 Years On". In: *Journal of the Royal Statistical Society: Series B (Statistical Methodology)* **76**.3. DOI: 10.1111/rssb.12062 (cit. on p. 85).

Steinhardt, Paul J., Limin Wang, and Ivaylo Zlatev (Dec. 16, 1998). *Cosmological Tracking Solutions*. DOI: 10.1103/PhysRevD.59.123504. arXiv: astro-ph/9812313 (cit. on p. 55).

Stölzner, Benjamin et al. (Mar. 6, 2018). "An Updated Tomographic Analysis of the Integrated Sachs-Wolfe Effect and Implications for Dark Energy". In: *Physical Review D* **97**.6. DOI: 10.1103/PhysRevD.97.063506. arXiv: 1710.03238 [astro-ph] (cit. on pp. 68, 80, 81, 97).

Sunyaev, R. A. and Ia. B. Zeldovich (Jan. 1, 1980). "Microwave Background Radiation as a Probe of the Contemporary Structure and History of the Universe". In: *Annual Review of Astronomy and Astrophysics* **18**. DOI: 10.1146/annurev.aa.18.090180.002541 (cit. on p. 6).

Tsujikawa, Shinji (Oct. 5, 2013). *Quintessence: A Review*. DOI: 10.1088/0264-9381/30/21/214003. arXiv: 1304.1961 [astro-ph, physics:gr-qc, physics:hep-ph, physics:hep-th] (cit. on p. 34).

– (2015). "The Effective Field Theory of Inflation/Dark Energy and the Horndeski Theory". In: vol. 892. DOI: 10.1007/978-3-319-10070-8_4. arXiv:

1404.2684 [astro-ph, physics:gr-qc, physics:hep-ph, physics:hep-th] (cit. on pp. 40, 52).

Tsujikawa, Shinji et al. (Oct. 29, 2009). "The Dispersion of Growth of Matter Perturbations in f(R) Gravity". In: *Physical Review D* **80**.8. DOI: 10.1103/PhysRevD.80.084044. arXiv: 0908.2669 [astro-ph, physics:gr-qc, physics:hep-ph, physics:hep-th] (cit. on p. 73).

Vainshtein, A I (1972). "Institute of Nuclear Physics, Novosibirsk, USSR". In: *PHYSICS LETTERS* **39**.3 (cit. on p. 36).

Verde, Licia (2009). "Statistical Methods in Cosmology". In: (cit. on pp. vii, 97).

Wang, Limin and Paul J. Steinhardt (Dec. 1998). "Cluster Abundance Constraints on Quintessence Models". In: *The Astrophysical Journal* **508**.2. DOI: 10.1086/306436. arXiv: astro-ph/9804015 (cit. on p. 73).

Weinberg, David H. et al. (Sept. 1, 2013). "Observational Probes of Cosmic Acceleration". In: *Physics Reports* **530**. DOI: 10.1016/j.physrep.2013.05.001 (cit. on p. 33).

Weinberg, Steven (Jan. 1, 1989). "The Cosmological Constant Problem". In: *Reviews of Modern Physics* **61**.1. DOI: 10.1103/RevModPhys.61.1 (cit. on pp. viii, 14, 95).

Wick, G. C. (Oct. 15, 1950). "The Evaluation of the Collision Matrix". In: *Physical Review* **80**.2. DOI: 10.1103/PhysRev.80.268 (cit. on p. 74).

Zumalacárregui, Miguel (July 14, 2020). "Gravity in the Era of Equality: Towards Solutions to the Hubble Problem without Fine-Tuned Initial Conditions". In: *Physical Review D* **102**.2. DOI: 10.1103/PhysRevD.102.023523 (cit. on p. 62).